

1995

Wave Diffraction and Refraction Problem and a Block-Wise Band Matrix Solver

Changqing Li

College of William and Mary - Virginia Institute of Marine Science

Follow this and additional works at: <https://scholarworks.wm.edu/etd>



Part of the [Oceanography Commons](#)

Recommended Citation

Li, Changqing, "Wave Diffraction and Refraction Problem and a Block-Wise Band Matrix Solver" (1995). *Dissertations, Theses, and Masters Projects*. Paper 1539617698.
<https://dx.doi.org/doi:10.25773/v5-m2hy-f814>

This Thesis is brought to you for free and open access by the Theses, Dissertations, & Master Projects at W&M ScholarWorks. It has been accepted for inclusion in Dissertations, Theses, and Masters Projects by an authorized administrator of W&M ScholarWorks. For more information, please contact scholarworks@wm.edu.

**WAVE DIFFRACTION AND REFRACTION PROBLEM
AND A BLOCK-WISE BAND MATRIX SOLVER**

A Thesis

Presented to

The Faculty of the school of Marine science
The College of William and Mary in Virginia

In Partial Fulfillment

Of the Requirements for the Degree of
Master of Arts

by

Changqing Li

1995

This thesis is submitted in partial fulfillment of
the requirements for the degree of

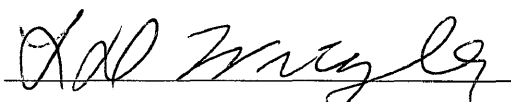
Master of Arts

Changqing Li

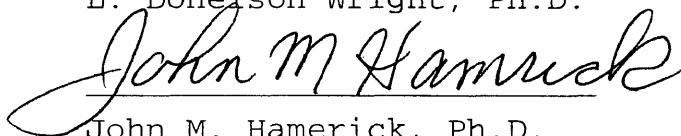
Approved, September 1995



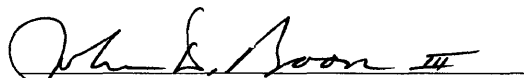
Jerome P.-Y. Maa, Ph.D.
Committee Chairman/Advisor



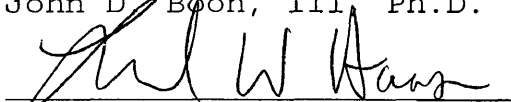
L. Donelson Wright, Ph.D.



John M. Hamerick, Ph.D.



John D. Boon, III, Ph.D.



Leonard W. Haas, Ph.D.

TABLE OF CONTENTS

	Page
ACKNOWLEDGMENTS.....	vi
LIST OF TABLE.....	vii
LIST OF FIGURES.....	viii
NOMENCLATURE.....	x
ABSTRACT.....	xiv
CHAPTERS	
1 INTRODUCTION.....	2
2 GOVERNING EQUATION OF WAVE REFRACTION AND DIFFRACTION.	10
2.1 General equations.....	10
2.2 Two dimensional wave equation.....	12
2.2.1 Derivation of the two dimensional general equation.....	12
2.2.2 Mild slope equation.....	16
2.2.3 Extended refraction-diffraction equation....	17
2.2.4 Massel's extended refraction-diffraction equation.....	19
2.2.5 Comparison of two extended equations.....	19
2.2.6 Comparison of extended equations with mild slope equation.....	21
2.3 Horizontal boundary conditions.....	26
2.3.1 Dirichlet boundary condition.....	27

2.3.2	Radiation boundary condition.....	28
2.3.3	Partial absorption boundary condition.....	38
2.4	A linear system generated from a horizontal two dimensional wave equation and boundary conditions.	40
3	A BLOCK-WISE BANDED MATRIX SOLVER.....	42
3.1	Introduction.....	42
3.2	Storage strategy for band matrix.....	43
3.3	A general band matrix solver.....	44
3.3.1	Factorization of a band matrix by forward elimination.....	45
3.3.2	Back substitution.....	51
3.4	A block-wise band matrix solver.....	53
3.4.1	A property of matrix A_b during elimination	53
3.4.2	Strategy of block-wise band matrix solver.	55
3.4.2.1	Forward elimination.....	56
3.4.2.2	Back substitution.....	58
4	A FINITE DIFFERENCE MODEL FOR THE ELLIPTIC WAVE EQUATION.....	60
4.1	Introduction.....	60
4.2	Band structure of a finite difference model.....	62
4.2.1	Finite difference governing equation.....	62
4.2.2	Finite difference equations of boundary conditions.....	64
4.2.2.1	Dirichlet boundary condition.....	64
4.2.2.2	Partial absorption boundary condition.....	67

4.2.3	Finite difference model with the second order absorption boundary conditions.....	76
4.2.4	Finite difference model with the third order absorption boundary conditions.....	79
4.3	Numerical model organization.....	82
4.3.1	Bathymetric data preparation.....	82
4.3.2	Boundary information.....	84
4.3.3	Sorting different grid points.....	85
4.3.4	Generation of a band matrix.....	85
4.3.5	Interaction with the block-wise band matrix solver.....	88
4.3.6	Model products.....	88
5	MODEL VERIFICATION AND APPLICATION.....	90
5.1	Model verification.....	90
5.1.1	Wave diffraction after a breakwater gap...	91
5.1.2	Wave diffraction after a straight short breakwater	96
5.1.3	Wave diffraction and refraction after an elliptic shoal.....	103
5.2	Model comparison.....	110
6	CONCLUSION AND FURTHER STUDY.....	112
6.1	Conclusion.....	112
6.2	Further study.....	115
	APPENDIX.....	118
	LIST OF REFERENCES.....	127
	VITA.....	131

ACKNOWLEDGMENTS

The support and guidance provided by my major professor, Dr. Jerome P.-Y. Maa, throughout the course of this research are gratefully acknowledged. I also wish to thank my other Advisory Committee members for constructive reviews of this manuscript.

Completion of this project would not have been possible without support by Professors Carl Hobbs, Donelson Wright, and Albert Kuo. Finally, the VIMS library is to be commended for its assistance in the collection of almost all the papers for my model development.

Support from the Department of Interior, Minerals Management Service, contract number 14-35-0001-3074, is gratefully acknowledged.

LIST OF TABLES

Table	Page
1 Storage technique for nonzero elements in matrix A_3 ..	86
2 Parameters of the three study cases and the model performance of each case.....	90
3 Performance of CGM model and present model.....	110

LIST OF FIGURES

Figure	Page
2.1 Coordinate system and major characteristic variables.....	11
2.2 Comparison of the coefficients $R^{(1)}$ and $R^{(2)}$	20
2.3 Rippled bottom topography.....	23
2.4 Reflection coefficient for waves normally approach on a sinusoidal patch.....	25
2.5 Diagram to explain the radiation boundary condition	29
2.6 Comparison of wave reflection coefficients.....	34
3.1 Principle of block-wise forward elimination.....	57
4.1 Layout of a study domain.....	63
4.2 Sketch of four directional boundaries for Dirichlet boundary conditions.....	65
4.3 Sketch of four directional boundaries for the third order partial absorption boundary conditions.....	68
4.4 Sketch of four directional boundaries for the third order partial absorption boundary conditions.....	75
4.5 Flow chart of present numerical model organization.	83
5.1 Layout of the study domain of the breakwater gap case.....	92
5.2a Contours of the wave diffraction coefficient after a breakwater gap.....	93

5.2b	Wave vectors and contours of the wave diffraction coefficient after a breakwater gap.....	94
5.3	Layout of the study domain of the straight short breakwater case.....	98
5.4a	Contours of the wave diffraction coefficient after a straight short breakwater.....	99
5.4b	Wave vectors and contours of the wave diffraction coefficient after a straight short breakwater.....	100
5.5	Layout of the study domain of the elliptic shoal case.....	104
5.6	Calculated contours of the relative wave height after an elliptic shoal.....	105
5.7	Comparisons of the calculated relative wave heights with the laboratory data.....	108
A.1	Schetch of the four corner boundaries.....	119

NOMENCLATURE

$\alpha, \beta, \gamma, \rho$	Reflection coefficients in the positive x, the positive y, the negative x, and the negative y direction at a boundary
ε	$= \sigma\lambda/D$
θ	Approching wave angle
θ_0	Incident wave angle
κ	non-dimensional wave number
λ	$= g/\omega^2$, the deep water wave lenth
ξ	$= (dx/dy)^2$
σ	Mean water depth
Φ	An unknown column matrix represents the total velocity potential
Φ^{ia}	Approching wave potential
ϕ_0^i	A given incident wave potential
ϕ_v	Vertical part of velocity potential
ϕ_h	Horizontal part of velocity potential
ϕ_0, ϕ_1, ϕ_2	Zero, first, and second order horizontal velocity potentials

ϕ	3-dimensional wave potential in Section 2.1-2 = ϕ_0 in Section 2.3 = $(C \cdot C_g)^{0.5} \phi_0$ after Section 2.3
ϕ^i, ϕ^r	Approaching wave and reflected wave
ω	Angular frequency
A	A square matrix
A_b	A rectangular matrix
A₂	A band square matrix from the finite difference model with second order partial absorption boundary condition
A₃	A band square matrix from the finite difference model with third order partial absorption boundary condition
b	Column matrix
x	Unknown column matrix
a_0, a_1, b_1	Coefficients in Kirby's approximation
∂B	Boundary
C	Wave phase velocity
C_g	Wave group velocity
D	Mean water depth
f	A known function
g	Gravitational acceleration
h	Water depth
H	Wave height
i	= $(-1)^{1/2}$

i, j	Indices of grid points
K_r	Reflection coefficient
\mathbf{k}	Wave number vector
k	$= \mathbf{k} $
k_c	Pseudo wave number
k_x, k_y	Wave number in the x and y directions
L_R, L	Ripple wave length and incident wave length
m	Bandwidth of a band matrix
map	The number of unknowns in a study domain
m_b	A grid point index in the x direction
m_l, m_u	Upper half and lower half bandwidth of a band matrix
n	$= 0.5(1+2kh/\sinh(2kh))$
\mathbf{n}	A unit vector normal to the boundary ∂B
n_b	A grid point index in the y direction
p, q	Known functions
R	Reflection coefficient
$R^{(1)}, R^{(2)}$	Coefficient functions of $(\nabla h)^2$ and $\nabla^2 h$
s	Wave phase
T	Wave period
x, y, z	Three coordinates
dx, dy	Step lengths in the x and y directions
∇	$= \mathbf{i}\partial/\partial x + \mathbf{j}\partial/\partial y$, where \mathbf{i} and \mathbf{j} are unit vectors in the x and y directions
∇^2	$= \partial^2/\partial x^2 + \partial^2/\partial y^2$

$l_{i,j}, d_{i,j}$	Coefficients of $\phi_{i-1,j}$ and $\phi_{i,j-1}$ in \mathbf{A}_2
$p_{i,j}, u_{i,j}$	Coefficients of $\phi_{i,j}$ and $\phi_{i,j+1}$ in \mathbf{A}_2
$r_{i,j}$	Coefficient of $\phi_{i+1,j}$ in \mathbf{A}_2
$ld_{i,j}, lc_{i,j}$	Coefficients of $\phi_{i-1,j-1}$ and $\phi_{i-1,j}$ in \mathbf{A}_3
$lu_{i,j}, pd_{i,j}$	Coefficients of $\phi_{i-1,j+1}$ and $\phi_{i,j-1}$ in \mathbf{A}_3
$pc_{i,j}, pu_{i,j}$	Coefficients of $\phi_{i,j}$ and $\phi_{i,j+1}$ in \mathbf{A}_3
$rd_{i,j}, rc_{i,j}$	Coefficients of $\phi_{i+1,j-1}$ and $\phi_{i+1,j}$ in \mathbf{A}_3
$ru_{i,j}$	Coefficient of $\phi_{i+1,j+1}$ in \mathbf{A}_3
\mathbf{a}, \mathbf{ia}	Two column matrices to store the nonzero elements and their positions in \mathbf{A}_3 or \mathbf{A}_2

WAVE DIFFRACTION AND REFRACTION PROBLEM AND A BLOCK-WISE BAND MATRIX SOLVER

ABSTRACT

This thesis presents the results of a study on the wave diffraction and refraction problem, a block-wise band matrix solver, and a finite difference model for solving an elliptic wave equation.

A new extended mild slope equation was derived for wave diffraction and refraction problems in an area with large bottom curvature and steep bottom slope. A numerical experiment was conducted for comparison with laboratory data as well as results from other studies. It was found that inclusion of the bottom curvature and second order bottom slope terms into the classical mild slope equation is necessary when the bottom has a large curvature and a steep local slope.

A block-wise band matrix solver was established for a general band matrix equation. In the process, a 'sandwich' structure in the band area of a band matrix during forward elimination and back substitution was revealed, and an economic storage strategy corresponding to the structure of a

common computer system for solving a band matrix equation was introduced.

Based on the block-wise band matrix solver, a finite difference model for an elliptic wave equation was developed. The model was verified by three well documented cases. With the limited verification, the process of wave diffraction, refraction, and reflection can be studied using this model with reasonable accuracy and efficiency.

Changqing Li

SCHOOL OF MARINE SCIENCE

THE COLLEGE OF WILLIAM AND MARY IN VIRGINIA

**WAVE DIFFRACTION AND REFRACTION PROBLEM
AND A BLOCK-WISE BAND MATRIX SOLVER**

CHAPTER 1

INTRODUCTION

In estuaries and coastal waters, the generation, transformation, and dissipation of water waves are one of the most important processes that affects our living environments. Because of the possible large wave heights, waves can be the greatest destructive forces to the environment, e.g., resuspend and redisturb bottom sediment and the associated pollutants, if any; induce longshore currents after breaking and cause shoreline variation; induce uni-directional residual currents (even a wave itself is a periodic force) that may be responsible for the transport of suspended material, organic or inorganic. All these processes pointed to the need of a better understanding of the wave transformation process.

Water wave transformation includes five major processes: shoaling, refraction, diffraction, reflection, and breaking. It is not easy to process all of them together and simultaneously. The combined effects of these five processes can only be studied by physical model studies. Only after Berkhoff(1972) introduced the mild slope equation, it is possible to use a numerical approach to analyze the first four processes together and simultaneously for engineering and

scientific applications.

The mild slope equation introduced by Berkhoff (1972;1976) is a two dimensional linear wave equation, which can only be applied to an area with a small bottom slope. Recently, this equation has been widely used to simulate wave transformation in coastal areas because it combines the effects from shoaling, diffraction, refraction and reflection, and overcomes the caustics problem by applying traditional wave ray method to a region of complex bathymetry. Using a physical model, Berkhoff *et al.* (1982) verified the equation. The accuracy of the equation was also studied by Booij (1983). It was concluded that the mild slope equation can be used for a bottom with slope up to 1:3 (Booij,1983).

In coastal areas the bottom slope is usually small. Thus, for common cases in the area, Berkhoff's theory is applicable. There are cases, however, in which the mean bottom slope for the entire area is small but the local slope is not because of large scale underwater sandbars, navigational channels, or turning basins. There are also cases with steep mean bottom slope. For example, along the Norwegian coast there are many sea mount like shoals, and water depth on the shoal is usually very small, but it increases rapidly to 50 m and more out of the shoal (Lie and Tøtøm,1991). For the case that has underwater sandbars, Berkhoff's mild slope equation may not be applicable. Since in this case both bottom curvature, $\nabla^2 h$, where h is water depth and $\nabla^2 = \partial^2 / \partial x^2 + \partial^2 / \partial y^2$, and bottom slope,

∇h , where $\nabla = i\partial/\partial x + j\partial/\partial y$, may play a more important role. Therefore, the bottom curvature and the possibly higher orders of bottom slope terms should be taken into account.

Kirby (1986a) developed an extended mild slope equations for ripples on an otherwise mild slope bottom. He introduced an additional term, which accounted for the effect of rapid undulations of the depth, into the mild slope equation. Massel (1993) also developed an general extended mild slope equation. He introduced a bottom slope square term and a bottom curvature term into the mild slope equation. Both Kirby and Massel had the same conclusion: use of the mild slope equation to simulate wave transformation on a ripple bottom underestimates the resonance, and additional terms to include the effects from the rapid bottom undulations are necessary.

In the first part of this study, another general extended mild slope equation was derived by using Berkhoff's power series approach (Berkhoff, 1976). In this extended equation, two additional terms, bottom curvature and second order bottom slope, were introduced. To investigate the importance of these two terms, a numerical experiment was conducted and a comparison with laboratory data and the numerical solutions from Massel's equation and mild slope equation was made.

According to Radder's approach (1979), both Berkhoff's mild slope equation and the extended equations can be transferred to the Helmholtz equation, an elliptic type partial differential equation. This equation can only be

solved numerically if it is applied to a complex area such as a harbor or a coastal water with arbitrary boundaries (Berkhoff,1972;1976; Li and Anastasiou, 1991; Panchang et al., 1991; Chen and Mei, 1974).

Since accuracy and efficiency are two major issues of a numerical method, a perfect numerical model would be good in both. Because of the nature of Helmholtz equation and the possibility of having a large study domain, it is difficult to achieve both goals at the same time. For example, when dealing with a small study domain, accuracy is possible to be achieved, but for a large study domain, one has to give up some accuracy for efficiency. For accuracy, which means a model should be able to simulate wave reflection, refraction, and strong diffraction, researchers solved the elliptic equation directly. They introduced several different methods such as the finite element method (FEM) (Berkhoff, 1972;1976; and Berkhoff et al.,1982), boundary element method (BEM) (Marschall,1993), multigrid finite difference method (MULTI) (Li and Anastasiou,1992), and conjugate gradient method (CGM) (Panchang et al.,1991; Li,1994) to solve the elliptic equation. For efficiency, researchers, however, ignored the wave reflection and changed the original elliptic equation to a parabolic equation (Radder,1979). Hence, they changed the boundary value problem to an initial value problem, which can be solved much more efficiently. Several numerical models to solve the parabolic equation were presented (Kirby,1986b; Tsay

and Liu,1982).

To improve the efficiency as well as keep the reflected wave, researchers also developed a hyperbolic method by introducing a transient term (or time dependent term) into the Helmholtz equation, which changes the elliptic equation into a hyperbolic equation (Copeland,1985; Madsen and Larsen,1987), thus, changing the boundary value problem to an initial value problem, which can be solved by integrating with time until a steady state is reached. Copeland (1985) and Madsen and Larsen (1987) also proposed a numerical method similar to the Numerical Method of Line (Schiesser,1991). The detailed investigation of this method, however, is not included in this study.

Directly solving the elliptic equation has the advantage of accuracy of solution. But it is not always efficient because of either long iterative time (for CGM and MULTI) (Duff et al.,1986) or great computer memory requirements (for FEM and BEM) (Panchang et al., 1991). Considering the computational resource and expenses, scientists and engineers are more concerned with model efficiency than accuracy. The fact that much research has been done using parabolic methods is a good example of this. However, because the parabolic approximation eliminates the reflected waves, it can not describe the wave field if there are structures with high reflection coefficients (e.g., vertical breakwater). Some researchers (Tsay and Lui, 1982; Liu and Tsay, 1983) used an

iteration method to do two directional sweeps solving two parabolic equations to simulate wave reflection by breakwater, but that method could only be applied to simple cases. Another drawback of the parabolic method is that it is not able to simulate the diffracted wave with large wave direction change.

With the rapid development of computer technologies, computer memory has become cheap and computer speed has become fast. The applications of an elliptic model has drawn more attention (Marschall,1993; Li and Anastasiou, 1992; Panchang et al.,1991; Li,1994). Recent solvers for the elliptic equation, however, are all iterative because the huge requirement of the computer memory by a direct method still can not be met.

In the second part of this study, based on the principle of the direct method, a block-wise band matrix solver for the general band matrix equation was developed. This solver solved the problem of huge memory requirement by conventional direct methods. Based on the principle of the block-wise band matrix solver, a new numerical model for the solution of the Helmholtz equation was constructed. The model exploits the feature of the block-wise elimination process of a band matrix and the storage structure of a common computer system to solve the elliptic equation more efficiently.

This paper presents entire study in the following four chapters. Chapter 2 presents the derivation of an extended mild slope equation and boundary conditions for the horizontal

two dimensional wave equation. A comparison of the result from the present model with laboratory data as well as the results from Massel's model and the mild slope equation in an one dimensional wave propagation case is also given in this chapter.

Chapter 3 presents a block-wise band matrix solver. In this chapter, the principle of a general band matrix solver is demonstrated and the block-wise structure of the band matrix solver during elimination is shown using a simple (2,2)-band matrix. The strategy to design a block-wise band matrix solver is discussed.

Chapter 4 presents an finite difference model of the elliptic equation. Through the discussion of finite difference approximation of the governing equation and boundary conditions, the band structure of the large coefficient matrix of a linear system is demonstrated. A special technique of storing non zero elements in the coefficient matrix is presented. The procedures to couple the large coefficient matrix with the block-wise band matrix solver is shown.

Chapter 5 presents the model verification and model comparison results. Three well documented cases: (1) wave diffraction after a breakwater gap; (2) wave diffraction after an short breakwater; and (3) wave refraction and diffraction after an elliptic shoal were selected to verified the present finite difference model. The comparisons of the results from the present model calculation with either laboratory data or

the analytical solution are given in this chapter. A result of the indirect comparison of the performance of the present model with that of the CGM model is also presented in this chapter.

Chapter 6 presents the conclusions obtained from this study and the comments for further study.

CHAPTER 2

GOVERNING EQUATION OF WAVE REFRACTION AND DIFFRACTION

2.1 General equations

Assuming an irrotational and incompressible fluid, and small amplitude waves, the water wave transformation problem can be described by a three dimensional governing equation (eq.2.1a) with the linearized free surface dynamic boundary condition (eq.2.1b), the zero cross flow bottom boundary condition (eq.2.1c), and horizontal boundary conditions to be specified later (Berkhoff, 1976).

$$\frac{\partial^2 \phi}{\partial x^2} + \frac{\partial^2 \phi}{\partial y^2} + \frac{\partial^2 \phi}{\partial z^2} = 0 \quad (2.1a)$$

$$\frac{\partial \phi}{\partial z} - \frac{\omega^2}{g} \phi = 0 \quad \text{at } z=0 \quad (2.1b)$$

$$\frac{\partial \phi}{\partial z} + \frac{\partial \phi}{\partial x} \frac{\partial h}{\partial x} + \frac{\partial \phi}{\partial y} \frac{\partial h}{\partial y} = 0 \quad \text{at } z=-h \quad (2.1c)$$

where $\phi(x,y,z)$ is the complex velocity potential, $h(x,y)$ is the still water depth, ω is angular frequency, g is gravitational acceleration, and x , y , and z are three coordinates shown in Fig.2.1.

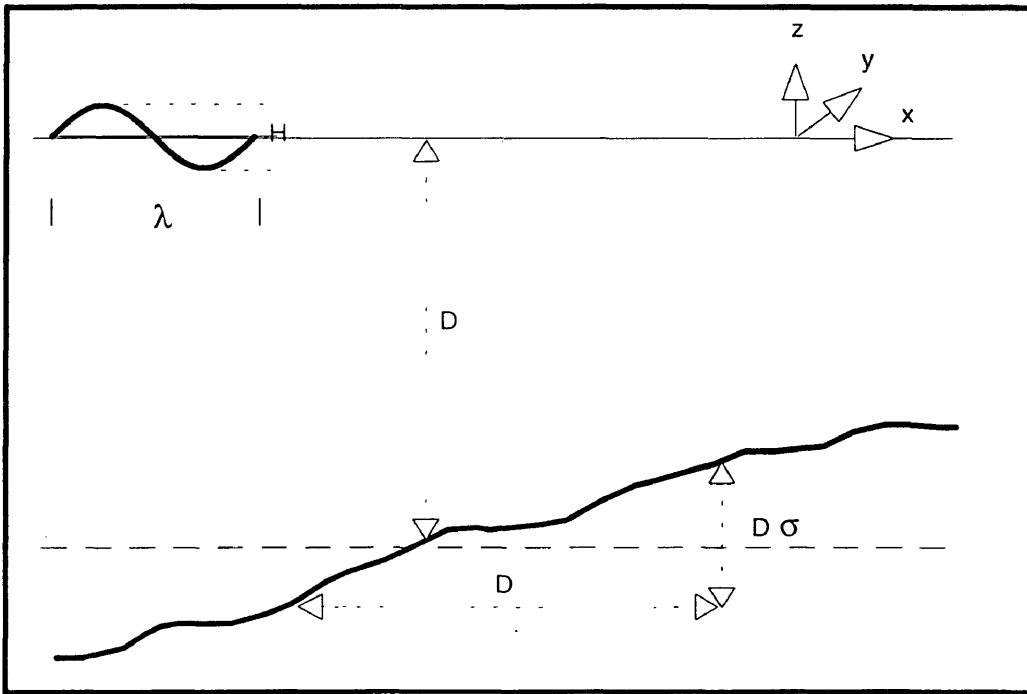


Fig.2.1: Coordinate system and major characteristic variables.

Eq.2.1a is a three dimensional Laplace equation. Because of the difficulty treating the irregular bottom boundary, the free surface boundary, and limited computational resources, it is not easy to apply this system directly. It is much easier to deal with a two dimensional wave model, which can be derived from the three dimensional governing equation (eq.2.1a) by integrating it with depth.

2.2 Two dimensional wave equation

2.2.1 Derivation of the two dimensional general equation

Following Berkhoff (1976), eq.1 can be normalized to

$$\frac{\partial^2 \phi}{\partial x'^2} + \frac{\partial^2 \phi}{\partial y'^2} + \frac{\partial^2 \phi}{\partial z'^2} = 0 \quad (2.2a)$$

$$\frac{\partial \phi}{\partial z'} - \phi = 0 \quad \text{at } z' = 0 \quad (2.2b)$$

$$\frac{\partial \phi}{\partial z'} + \varepsilon \left(\frac{\partial \phi}{\partial x'} \frac{\partial h'}{\partial \bar{x}} + \frac{\partial \phi}{\partial y'} \frac{\partial h'}{\partial \bar{y}} \right) = 0 \quad \text{at } z' = -h' \quad (2.2c)$$

by using the following non-dimensional variables:

$$(x', y', z', h') = \frac{1}{\lambda} (x, y, z, h); \quad (\bar{x}, \bar{y}) = \frac{\sigma}{D} (x, y)$$

where $\lambda = g/\omega^2$ is the deep water wave length, D is the mean water depth, σ is the mean slope over a distance D, $\varepsilon = \sigma\lambda/D$. Fig.2.1 shows the coordinate system and all major characteristic variables.

Analogue to the separation of variable theory, the three

dimensional potential function $\phi(x', y', z')$ is written as the product of two functions (Berkhoff, 1976):

$$\phi(x', y', z') = \phi_v(h', z') \phi_h(x', y', z') \quad (2.3)$$

with

$$\phi_v(h', z') = \frac{\cosh(\kappa(h' + z'))}{\cosh(\kappa h')} \quad (2.4)$$

where κ , non dimensional wave number, is defined by

$$1 = \kappa \tanh(\kappa h') \quad (2.5)$$

In eq.2.3 the function $\phi_h(x', y', z')$ is a weak three dimensional function because the vertical variation has been moved into $\phi_v(h', z')$. Here ϕ_v is also weakly varied with horizontal location because $h' = h'(x', y')$.

Substituting eq.2.3 into eq.2.2, Berkhoff(1976) gave:

$$\begin{aligned} \epsilon^2 \left[\phi_h \left(\frac{\partial^2 \phi_v}{\partial h'^2} (\nabla h' \cdot \nabla h') + \frac{\partial \phi_v}{\partial h'} \nabla^2 h' \right) \right] + \epsilon \left[2 \frac{\partial \phi_v}{\partial h'} (\nabla h' \cdot \nabla \phi_h) \right] \\ + \phi_v \nabla^2 \phi_h + \kappa^2 \phi_v \phi_h + 2 \frac{\partial \phi_h}{\partial z'} \frac{\partial \phi_v}{\partial z'} + \phi_v \frac{\partial^2 \phi_h}{\partial z'^2} = 0 \end{aligned} \quad (2.6a)$$

$$\frac{\partial \phi_h}{\partial z'} = 0 \quad \text{at } z' = 0 \quad (2.6b)$$

$$\epsilon^2 \left[\frac{\partial \phi_v}{\partial h'} (\nabla h' \cdot \nabla h') \phi_h \right] + \epsilon \left[\phi_v (\nabla \phi_h \cdot \nabla h') \right] + \phi_v \frac{\partial \phi_h}{\partial z'} = 0 \quad \text{at } z' = -h' \quad (2.6c)$$

where

$$\bar{\nabla} = i \frac{\partial}{\partial x} + j \frac{\partial}{\partial y}; \quad \bar{\nabla}^2 = \frac{\partial^2}{\partial x^2} + \frac{\partial^2}{\partial y^2}; \quad \nabla' = i \frac{\partial}{\partial x'} + j \frac{\partial}{\partial y'}; \quad \nabla'^2 = \frac{\partial^2}{\partial x'^2} + \frac{\partial^2}{\partial y'^2}.$$

To consider the mean energy flux, eq.2.6 is integrated over the water depth after multiplication with function ϕ_v . Using boundary conditions, eq.2.6b and 2.6c, he obtained:

$$\begin{aligned} & \varepsilon^2 \left[\int_{-h'}^0 \phi_v \left(\frac{\partial^2 \phi_v}{\partial h'^2} (\bar{\nabla} h' \cdot \bar{\nabla} h') + \frac{\partial \phi_v}{\partial h'} \bar{\nabla}^2 h' \right) \phi_h dz' \right] \\ & + \varepsilon \left[\int_{-h'}^0 \frac{\partial \phi_v^2}{\partial h'} (\bar{\nabla} h' \cdot \nabla' \phi_h) dz' \right] + \int_{-h'}^0 \phi_v^2 (\nabla'^2 \phi_h + \kappa^2 \phi_h) dz' \quad (2.7) \\ & + \varepsilon [\phi_v^2 (\bar{\nabla} h' \cdot \nabla' \phi_h)]_{z'=-h'} + \varepsilon^2 \left[\phi_v \frac{\partial \phi_v}{\partial h'} (\bar{\nabla} h' \cdot \bar{\nabla} h') \right]_{z'=-h'} = 0 \end{aligned}$$

Because $\phi_h(x', y', z')$ weakly depends on coordinate z' and a symmetry condition (eq.6b) exists, the function $\phi_h(x', y', z')$ can be expressed with respect to the $\sigma z'$ in the even power series (Berkhoff, 1976):

$$\phi_h(x', y', z') = \phi_0(x', y') + \sigma^2 z'^2 \phi_1(x', y') + \sigma^4 z'^4 \phi_2(x', y') + \dots \quad (2.8)$$

Substituting equation (8) into (7), we get:

$$\begin{aligned}
& \varepsilon^2 \left[\phi_0 \left(\int_{-h'}^0 \phi_v \frac{\partial^2 \phi_v}{\partial h'^2} dz' \right) \langle \bar{\nabla} h' \cdot \bar{\nabla} h' \rangle + \frac{1}{2} \left(\int_{-h'}^0 \frac{\partial \phi_v^2}{\partial h'} dz' \right) \bar{\nabla}^2 h' \right] \\
& + \varepsilon \left[\left(\int_{-h'}^0 \frac{\partial \phi_v^2}{\partial h'} dz' \right) \langle \bar{\nabla} h' \cdot \nabla' \phi_0 \rangle \right] + \left[\left(\int_{-h'}^0 \phi_v^2 dz' \right) \langle \nabla'^2 \phi_0 + \kappa^2 \phi_0 \rangle \right] \\
& + \varepsilon [\phi_v^2|_{z'=-h'} \langle \bar{\nabla} h' \cdot \nabla' \phi_0 \rangle] + \varepsilon^2 \left[\frac{1}{2} \frac{\partial \phi_v^2}{\partial h'} \Big|_{z'=-h'} \langle \bar{\nabla} h' \cdot \bar{\nabla} h' \rangle \phi_0 \right] \\
& + \varepsilon^2 \sigma^2 \left[\phi_1 \left(\int_{-h'}^0 z'^2 \phi_v \frac{\partial^2 \phi_v}{\partial h'^2} dz' \right) \langle \bar{\nabla} h' \cdot \bar{\nabla} h' \rangle + \frac{1}{2} \left(\int_{-h'}^0 z'^2 \frac{\partial \phi_v^2}{\partial h'} dz' \right) \bar{\nabla}^2 h' \right] \\
& + \varepsilon \sigma^2 \left[\left(\int_{-h'}^0 z'^2 \frac{\partial \phi_v^2}{\partial h'} dz' \right) \langle \bar{\nabla} h' \cdot \nabla' \phi_1 \rangle \right] + \sigma^2 \left[\left(\int_{-h'}^0 z'^2 \phi_v^2 dz' \right) \langle \nabla'^2 \phi_1 + \kappa^2 \phi_1 \rangle \right] \\
& + \varepsilon \sigma^2 [z'^2 \phi_v^2|_{z'=-h'} \langle \bar{\nabla} h' \cdot \nabla' \phi_1 \rangle] + \varepsilon^2 \sigma^2 \left[\frac{1}{2} z'^2 \frac{\partial \phi_v^2}{\partial h'} \Big|_{z'=-h'} \langle \bar{\nabla} h' \cdot \bar{\nabla} h' \rangle \phi_1 \right] \\
& + O(\varepsilon^m \sigma^n) = 0 \quad (m \geq 0, n \geq 4)
\end{aligned}$$

(2.9)

Since ϕ_v is a known function, i.e. eq.2.4, all integrals in eq.2.9 can be obtained analytically as follows:

$$\int_{-h'}^0 \phi_v^2 dz' = \frac{1}{2\kappa} \left(1 + \frac{2\kappa h'}{\sinh(2\kappa h')} \right) \quad (2.10a)$$

$$\int_{-h'}^0 \phi_v \frac{\partial^2 \phi_v}{\partial h'^2} dz' = \frac{\kappa^2 h' \sinh^2(\kappa h')}{\cosh^4(\kappa h')} \quad (2.10b)$$

$$\int_{-h'}^0 \frac{\partial \phi_v^2}{\partial h'^2} dz' = -\frac{\kappa h' \sinh(\kappa h')}{\cosh^3(\kappa h')} \quad (2.10c)$$

$$\int_{-h'}^0 z'^2 \phi_v^2 dz' = \frac{1}{2 \cosh^2(\kappa h')} \left(-\frac{h'}{2\kappa^2} \left(1 - \frac{\sinh(2\kappa h')}{2\kappa h'} \right) + \frac{h^3}{3} \right) \quad (2.10d)$$

$$\int_{-h'}^0 z'^2 \phi_v \frac{\partial^2 \phi_v}{\partial h'^2} dz' = \frac{(2\kappa^2 h'^2 - 3) h' \tanh^2(\kappa h')}{6 \cosh^2(\kappa h')} + \frac{\kappa h'^2 \tanh(\kappa h')}{2 \cosh^3(\kappa h')} \quad (2.10e)$$

$$\int_{-h'}^0 z'^2 \frac{\partial \phi_v^2}{\partial h'} dz' = \frac{(3 - 2\kappa^2 h'^2) h' \tanh(\kappa h')}{6 \kappa \cosh^2(\kappa h')} - \frac{h'^2}{2 \cosh^2(\kappa h')} \quad (2.10f)$$

Eq.2.9 is a two dimensional general equation that controls the wave transformation. Because it is an infinite series with respect to $\varepsilon^m \sigma^n$, $m \in [0, \infty)$, and $n \in [0, \infty)$, taking different orders of approximation achieves different wave model equations.

2.2.2 Mild slope equation

If all terms of the order $O(\varepsilon^m \sigma^n)$, $m \geq 2$ and $n \geq 0$, are neglected, eq.9 becomes:

$$\left(\int_{-h'}^0 \phi_v^2 dz' \right) (\nabla'^2 \phi_0 + \kappa^2 \phi_0) + \varepsilon \frac{\partial}{\partial h'} \left(\int_{-h'}^0 \phi_v^2 dz' \right) (\bar{\nabla} h' \cdot \nabla' \phi_0) = 0 \quad (2.11)$$

Using the Chain Rule, Berkhoff (1976) pointed out

$$\nabla' \left(\int_{-h'}^0 \phi_v^2 dz' \right) = \varepsilon \frac{\partial}{\partial h'} \left(\int_{-h'}^0 \phi_v^2 dz' \right) \bar{\nabla} h' \quad (2.12)$$

eq.2.11 becomes:

$$\nabla' \cdot \left[\left(\int_{-h'}^0 \phi_v^2 dz' \right) \nabla' \phi_0 \right] + \kappa^2 \left(\int_{-h'}^0 \phi_v^2 dz' \right) \phi_0 = 0 \quad (2.13)$$

which can be written in dimensional form as:

$$\nabla^2 \phi_0 + \frac{\nabla C C_g}{C C_g} \cdot \nabla \phi_0 + k^2 \phi_0 = 0 \quad (2.14)$$

where C is the wave phase velocity, C_g is the wave group velocity, k is the wave number, and $\nabla^2 = \partial^2 / \partial x^2 + \partial^2 / \partial y^2$.

Eq.2.14 is the mild slope equation given by Berkhoff (1976). The mild bottom slope means σ is small, thus, the terms with order $\varepsilon^m \sigma^n$, where $m \geq 2$ and $n \geq 0$, are all negligible (Berkhoff, 1976). Because both C and C_g are functions of water depth, $h(x, y)$, the wave refraction due to the change of water depth as well as wave diffraction (Penny and Price, 1952) is taken into account by eq.2.14. It is also known as the combined wave refraction and diffraction equation.

2.2.3 Extended refraction-diffraction equation

When Berkhoff (1976) developed the mild slope equation, he did not process any term that contained higher order of $\varepsilon \sigma$. In this study, however, a more general equation (eq.2.9) is presented. If the terms of the order ε^2 in the equation as well as the terms in the mild slope equation are taken into account, we have:

$$\begin{aligned}
& \left(\int_{-h'}^0 \phi_v^2 dz' \right) (\nabla^2 \phi_0 + \kappa^2 \phi_0) + \varepsilon \frac{\partial}{\partial h} \left(\int_{-h'}^0 \phi_v^2 dz' \right) (\nabla h' \cdot \nabla' \phi_0) \\
& + \varepsilon^2 \left[\left(\int_{-h'}^0 \phi_v \frac{\partial^2 \phi_v}{\partial h'^2} dz' \right) (\nabla h' \cdot \nabla h') + \left(\int_{-h'}^0 \phi_v \frac{\partial \phi_v}{\partial h'} dz' \right) \nabla^2 h' \right. \\
& \left. + \phi_v \frac{\partial \phi_v}{\partial h'} \Big|_{z'=-h'} (\nabla h' \cdot \nabla h') \right] \phi_0 = 0 \tag{2.15}
\end{aligned}$$

In dimensional form the equation is written as

$$\nabla^2 \phi_0 + \frac{\nabla C C_g}{C C_g} \cdot \nabla \phi_0 + \left[k^2 + \frac{k^2}{n \cosh^2(kh)} \left((k h \tanh(kh) - 1) (\nabla h)^2 - \frac{h}{2} \nabla^2 h \right) \right] \phi_0 = 0 \tag{2.16}$$

where

$$n = \frac{1}{2} \left(1 + \frac{2kh}{\sinh(2kh)} \right) \tag{2.17}$$

Eq.2.16 is an extended refraction and diffraction equation. Because of the inclusion of ε^2 ($\varepsilon = \sigma\lambda/D$) terms, the restriction of mild bottom slope can be relaxed and the equation can be used to simulate wave transformation in cases having a steep bottom topography.

In fact, the additional two terms in eq.2.16 are $(\nabla h)^2$, a second order bottom gradient term, and $\nabla^2 h$, a bottom curvature term, respectively. It is easy to understand the existence of the second order bottom gradient term for the case that has a steep bottom slope. The curvature term may be important even if the bottom slope is small. For example, Kirby (1986a) showed that large ripples with curvature that is close to a surface wave profile can cause significant wave reflection and even resonance.

2.2.4 Massel's extended refraction-diffraction equation

Using the Galerkin-Eigenfunction Method, Massel (1993) developed another extended refraction and diffraction equation:

$$\nabla^2 \phi_0 + \frac{\nabla C C_g}{C C_g} \cdot \nabla \phi_0 + \left[k^2 + \frac{1}{2nh^2} \frac{kh}{\tanh(kh)} \left(R^{(1)} (\nabla h)^2 + \frac{R^{(2)}}{k \tanh(kh)} \nabla^2 h \right) \right] \phi_0 = 0 \quad (2.18)$$

where $R^{(1)}(kh)$ and $R^{(2)}(kh)$ are coefficients of $(\nabla h)^2$ and $\nabla^2 h$ respectively. Massal (1993) did not give explicit formula for $R^{(1)}(kh)$ and $R^{(2)}(kh)$ but gave a plot for the two coefficients with respect to kh (Fig.2.2a and 2.2b). Like eq.2.17, eq.2.18 also includes the bottom gradient term, $(\nabla h)^2$, and the bottom curvature term, $\nabla^2 h$. The differences between the two equations must be in the coefficients of $(\nabla h)^2$ and $\nabla^2 h$.

2.2.5 Comparison of two extended equations

Changing the format of eq.2.17 into that of eq.2.18 gives:

$$\nabla^2 \phi_0 + \frac{\nabla C C_g}{C C_g} \cdot \nabla \phi_0 + \left[k^2 + \frac{1}{2nh^2} \frac{kh}{\tanh(kh)} \left(R_L^{(1)} (\nabla h)^2 + \frac{R_L^{(2)}}{k \tanh(kh)} \nabla^2 h \right) \right] \phi_0 = 0 \quad (2.19)$$

where

$$R_L^{(1)} = \frac{2kht \tanh(kh) (kht \tanh(kh) - 1)}{\cosh^2(kh)} \quad (2.20)$$

$$R_L^{(2)} = -\frac{k^2 h^2 \tanh^2(kh)}{\cosh^2(kh)} \quad (2.21)$$

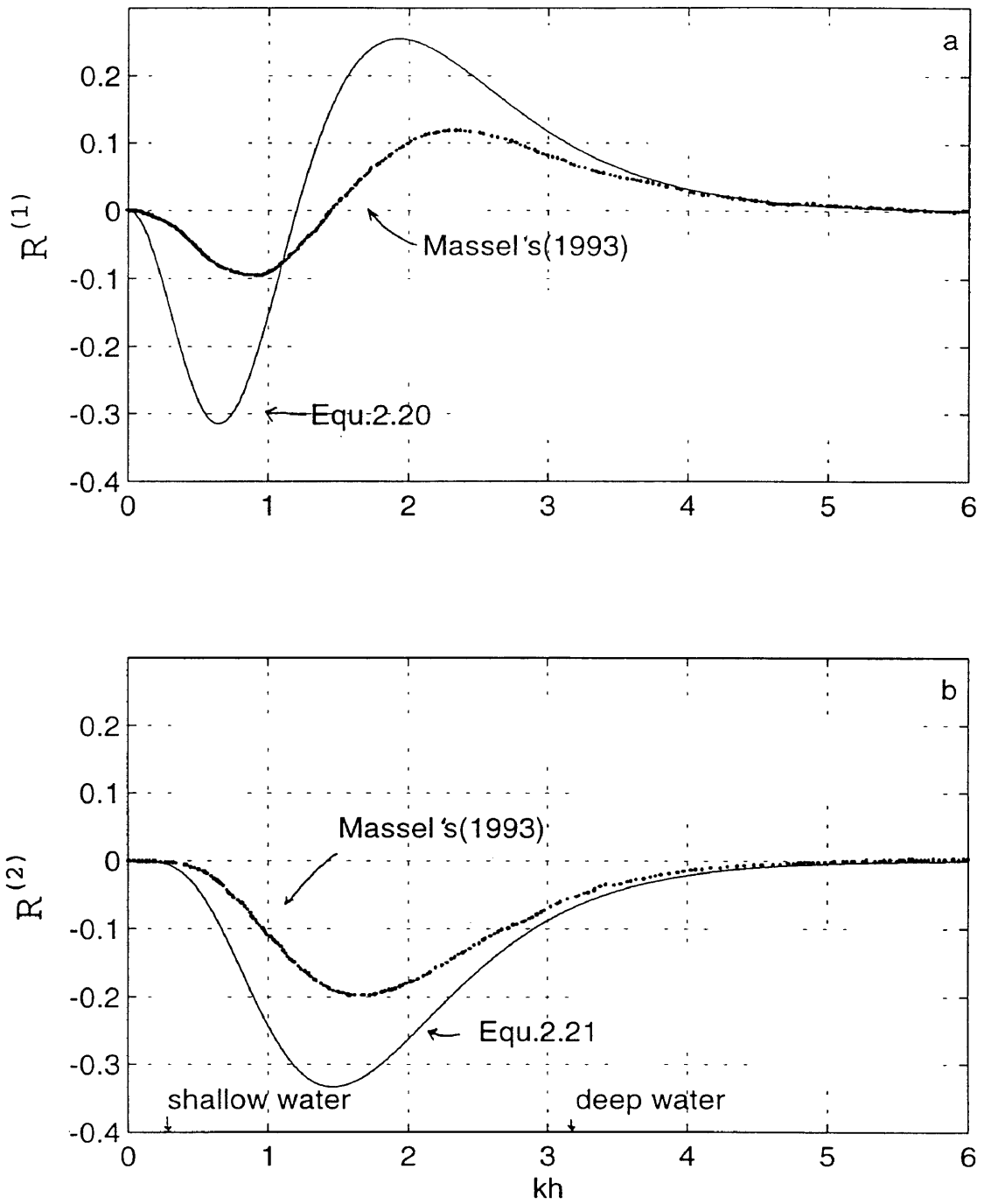


Fig.2.2: Comparison of the coefficients $R^{(1)}$ and $R^{(2)}$.

In eq.2.19,2.20 and 2.21 a subscript 'L' is added to the coefficients $R^{(1)}$ and $R^{(2)}$ to make distinction with Massel's results. The coefficients $R_L^{(1)}$ and $R_L^{(2)}$ are explicitly formulated. Like the coefficients $R^{(1)}$ and $R^{(2)}$ in eq.2.18, both $R_L^{(1)}$ and $R_L^{(2)}$ are functions of kh . For comparison they were plotted in Fig.2.2

It can be seen that the two coefficients in both models are each significant in the intermediate water depth and become trivial in shallow or deep water. Both $R_L^{(1)}$ and $R_L^{(2)}$ are larger than those given by Massel. There are also phase differences between $R_L^{(1)}$ and $R^{(1)}$ as well as $R_L^{(2)}$ and $R^{(2)}$. The method of approximation may be the reason for these discrepancies.

2.2.6 Comparison of extended equations with the mild slope equation

The studies by Davies and Heathershaw (1984), Mei (1985), Kirby (1986a), and Massel (1993) have shown that natural or artificial bed forms of amplitudes which are much smaller than water depth can produce strong reflection of water waves, if the bar spacing is about half of the length of normally incident waves. This kind of resonant reflection is known as Bragg reflection. In particular, Massel (1993) has shown that his extended wave equation (eq.2.18) is able to predict the wave reflection over bed undulations, including the Bragg resonance condition.

In order to make a comparison of Eq.2.19 with Massel's equation as well as the mild slope equation, we studied Bragg reflection. First, we changed eq.2.19 to a one dimensional equation as follows:

$$\frac{\partial^2 \phi_0}{\partial x^2} + \frac{1}{CC_g} \frac{\partial CC_g}{\partial x} \frac{\partial \phi_0}{\partial x} + \left[k^2 + \frac{1}{2nh^2} \frac{kh}{\tanh(kh)} \left(R_L^{(1)} \left(\frac{\partial h}{\partial x} \right)^2 + \frac{R_L^{(2)}}{k \tanh(kh)} \frac{\partial^2 h}{\partial x^2} \right) \right] \phi_0 = 0 \quad (2.22a)$$

then solved eq.2.22a in a region of the following sinusoidal bed topography:

Region 1: $h_1 = 0.156 \text{ m}$

region 2: $h_2 = h_1 - 0.05 \sin\left(\frac{2\pi}{L_R} x\right) \quad 0 \leq x \leq nL_R$

Region 3: $h_3 = 0.156 \text{ m}$

where h_1 , h_2 and h_3 are the water depth in region 1, region 2, and region 3, respectively (see Fig.2.3); $L_R = 1.0\text{m}$ is the bed wave length; and n is the number of bed ripples. For this case, the average slope of the bottom is zero, and the curvature is the dominant term.

The incident wave is from region 1 and propagates across regions 2 and 3. The boundary condition of region 1 is a radiation boundary condition (Booij,1983) as follows:

$$\frac{\partial \phi_0}{\partial x} = -ik\phi_0 + 2ik\phi_0^i \quad \text{on} \quad \partial B_1 \quad (2.22b)$$

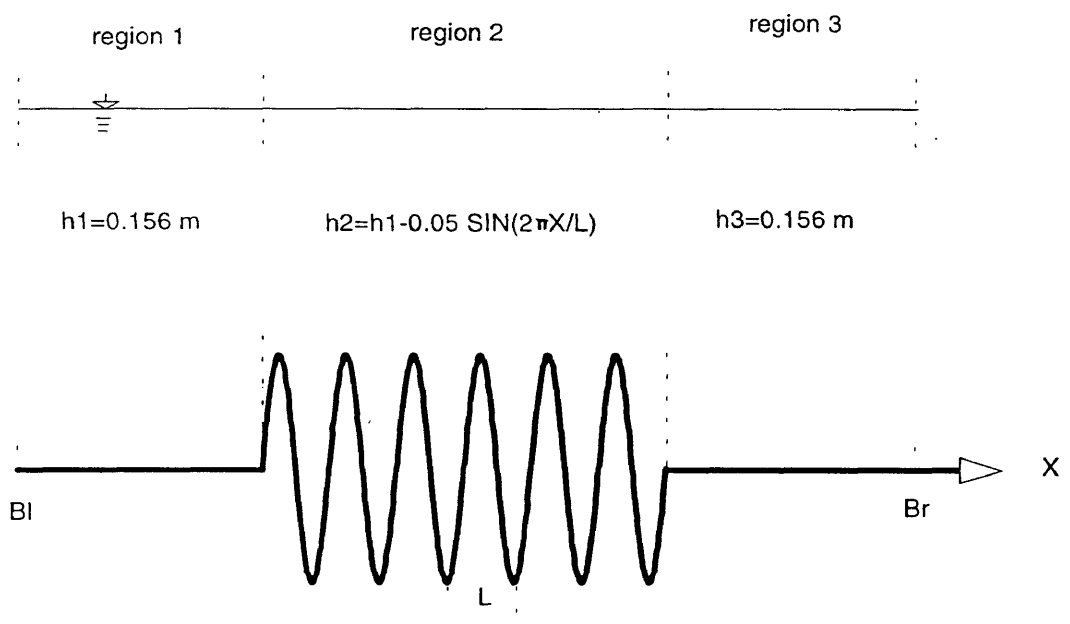


Fig.2.3: Rippled bottom topography.

where ϕ_0^i is a given incident wave potential whose amplitude equals 1, k is the wave number, and ∂B_1 is the boundary of region 1. The boundary condition of region 3 is also a radiation boundary condition (Booij,1983) as follows:

$$\frac{\partial \phi_0}{\partial x} = -ik\phi_0 \quad \text{on } \partial B_r \quad (2.22c)$$

where ∂B_r is the boundary of region 3 (Fig.2.3).

In this study, the finite difference method was used and the differential eq.2.22 was approximated by a system of linear equations as

$$PY=q \quad (2.22d)$$

where Y is a column matrix containing the unknown ϕ on the discrete points along the regions 1, 2, and 3; P is a tridiagonal matrix containing the coefficients of the unknown; and q is a column matrix containing the right side terms of the linear equations. A complex band matrix solver (Dongarra et al., 1979) was used to solve this system.

The reflection coefficient, K_r , is calculated using the following formula:

$$k_r = \left| \frac{\phi_0^i - \phi_0(1)}{\phi_0^i} \right| \quad (2.22e)$$

where $\phi_0(1)$ is the wave potential calculated on the boundary ∂B_1 .

Fig.2.4 demonstrates the calculated reflection coefficients from the present model (eq.2.19), Massel's model

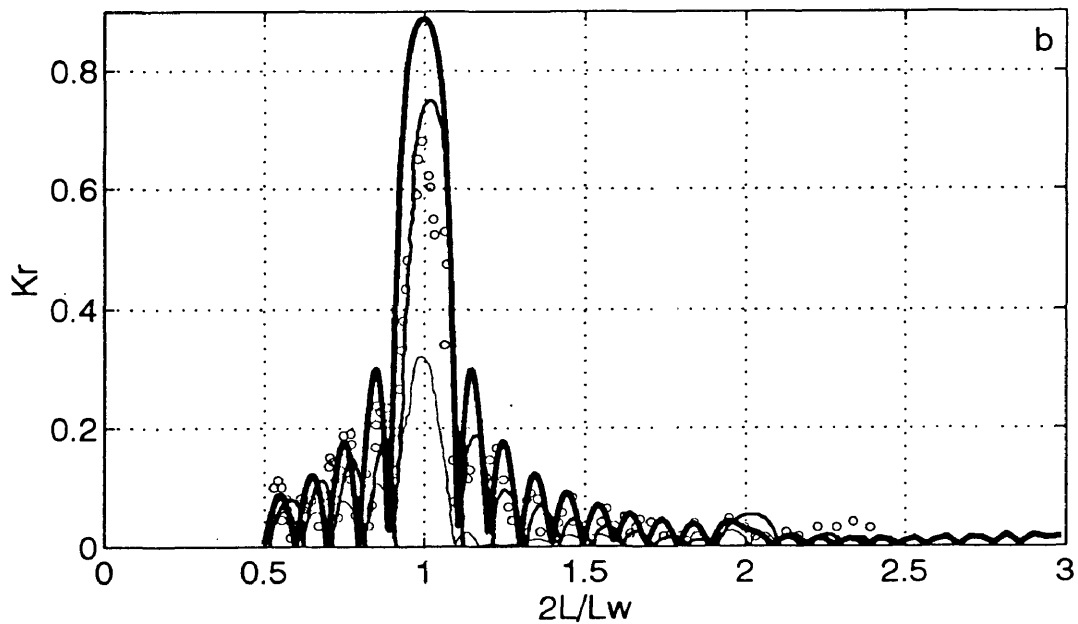
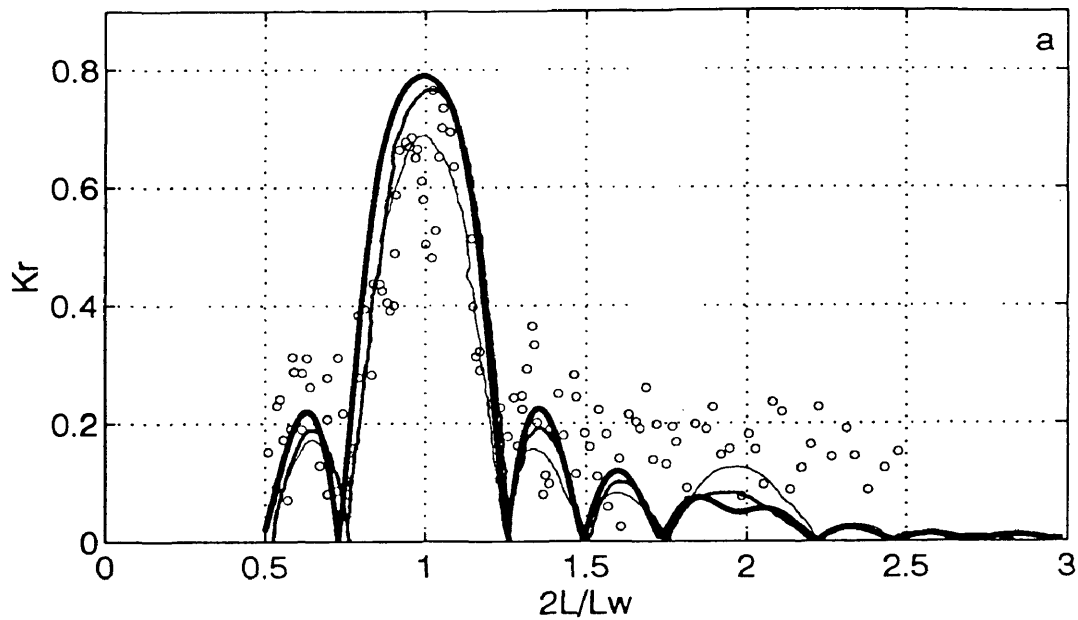


Fig.2.4: Reflection coefficient for waves normally approach on a sinusoidal patch, a. $n=4$ and b. $n=10$. (**—————**) present theory, (**—————**) Massel's solution, (**—————**) classical mild-slope theory (after Massel, 1993), (**o**) laboratory data from Davies and Heathershaw (1984).

(eq.2.18), mild slope equation (eq.2.14), and laboratory data for two cases of rippled bottoms. A strong reflection is shown in all the results when bottom undulations have a wave length (L_R) of one half of the surface wave length (L), i.e. $2L_R/L=1$. When the bottom has four ripples, the mild slope equation slightly underestimates the reflection coefficient, the present model, on the other hand, slightly overestimates the reflection coefficient, and the Massel's model result is closest to the laboratory data. For the case with 10 bottom ripples, the result from the mild slope equation significantly underestimates the reflection coefficient. Both Eq.2.22a and Massel's results overestimate the reflection coefficient. In comparison, however, Massel's result is better (close to the experimental result). It is the curvature term as well as the gradient term in both extended models that make this contribution. The possible reason for the different result of present model from that of Massel's model is the method of approximation.

2.3 Horizontal Boundary conditions

For simplicity, in the following sections the subscript of ϕ_0 in the two dimensional equation (e.g. eq.2.19) and boundary conditions is omitted

In order to solve the two dimensional wave equation (which is an elliptic type partial differential equation given in Section 2.2), the horizontal boundary conditions of the

study domain are needed (Sommerfeld, 1896). For a general elliptic equation there are three kinds of boundary conditions: (1) Dirichlet boundary condition, $\phi|_{\partial B} = \mathbf{f}(\mathbf{x}, \mathbf{y})$; (2) Neumann boundary condition, $\partial\phi/\partial\mathbf{n} = \mathbf{f}(\mathbf{x}, \mathbf{y})$; and (3) mixed or Robin boundary condition, $\mathbf{p}(\mathbf{x}, \mathbf{y})\partial\phi/\partial\mathbf{n} + \mathbf{q}(\mathbf{x}, \mathbf{y})\phi = \mathbf{f}(\mathbf{x}, \mathbf{y})$, where \mathbf{n} is a unit vector that is normal to the boundary, ∂B , and directs toward outside of ∂B , and $\mathbf{p}(\mathbf{x}, \mathbf{y})$, $\mathbf{q}(\mathbf{x}, \mathbf{y})$, and $\mathbf{f}(\mathbf{x}, \mathbf{y})$ are known functions (Sommerfeld, 1896).

In this study wave equations (eq.2.14, eq.2.16, and eq.2.18) are all for linear wave transformation, therefore, they can be applied to an area without the wave breaking. For a water wave transformation problem in this area, the incident wave can be represented by the Dirichlet boundary condition along the offshore boundary of the study domain. The wave conditions along the shoreward boundary and the two lateral boundaries of the study domain can be represented by either Neumann or Robin boundary conditions. For example, the full reflection boundary condition due to a breakwater with vertical wall is a Neumann boundary condition, $\partial\phi/\partial\mathbf{n}=0$, and the radiation boundary condition due to a wave passing through the boundary is a Robin boundary condition.

2.3.1 Dirichlet boundary condition

Along an offshore boundary of the study domain the incident wave can be represented by

$$\phi = |\phi_0^i| e^{i[k_0 \cos(\theta_0)x_0 + k_0 \sin(\theta_0)y_0]} \quad (2.23a)$$

where $|\phi_0^i| = Hg/2\omega$ is the incident wave velocity potential amplitude; θ_0 is the incident wave angle, for a normal incident wave, $\theta_0 = 0$; k_0 is the incident wave number at the boundary; x_0 and y_0 are the coordinates at the boundary. When solving the wave equation (e.g. eq.2.14), the incident wave amplitude, wave angle, wave period, and the water depths in the study domain including all boundaries are each given. Thus, incident wave numbers at the boundary are usually calculated from the dispersion relation equation as follows:

$$\omega = k^2 \tanh(kh) \quad (2.23b)$$

where $\omega = 2\pi/T$ is the wave angular frequency and T is the wave period. In fact, eq.2.23b is a dimensional form of eq.2.5. In eq.2.23b if the wave period is given and the water depth at any point in the study domain is known, the wave number at that point can be calculated.

2.3.2 Radiation boundary condition

The concept of the radiation boundary condition is that a wave train moves across the boundary without any change (Behrendt, 1985). The following is summary from the studies of Behrendt (1985) and Kirby (1989). For simplicity we will use a constant water depth to explain this boundary condition. Assume a wave train, whose amplitude equals 1, approaches the downwave boundary shown in Fig.2.5. In this configuration,

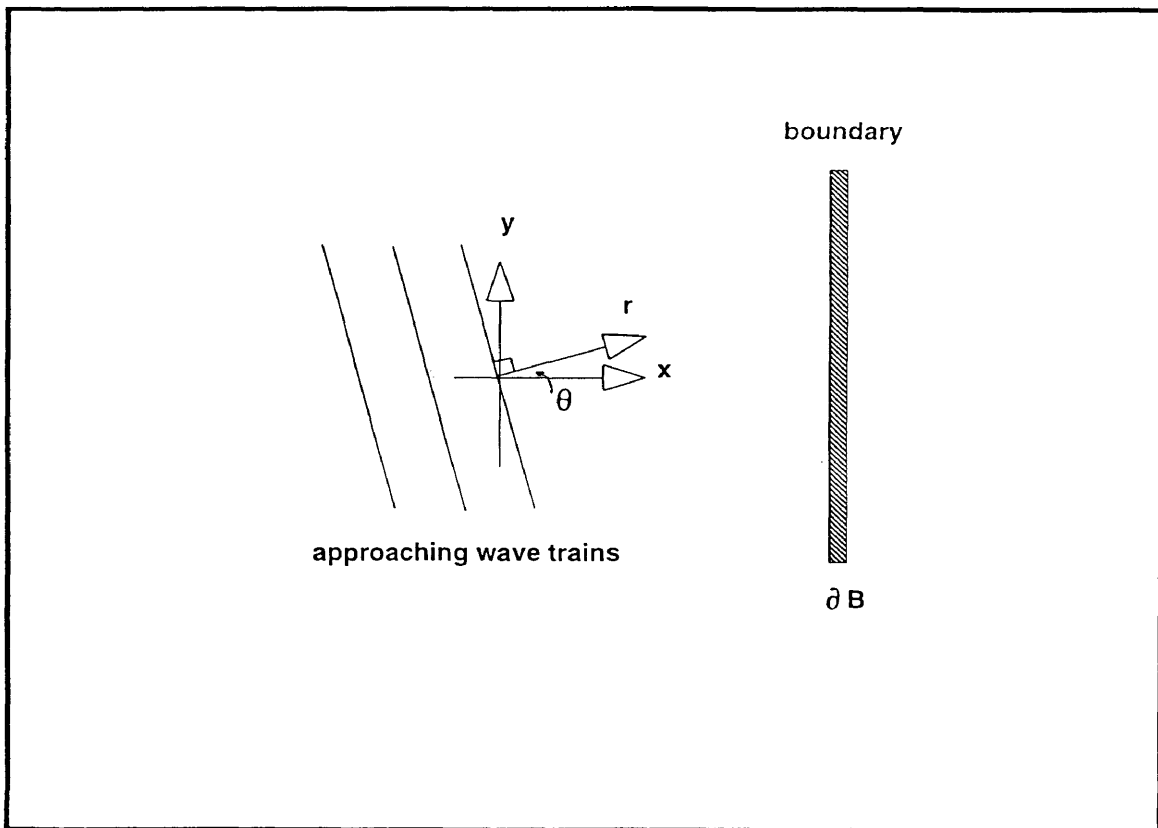


Fig.2.5: Diagram to explain the radiation boundary condition (after Behrendt,1985).

the boundary is perpendicular to the x axis. In mathematical form, the velocity potential of this approaching wave train is

$$\Phi^{ia} = e^{i(k_x x + k_y y - \omega t)} = \Phi \quad (2.24)$$

where Φ is the total wave potential and $\Phi^{ia} = \Phi$ because of the radiation condition; $\mathbf{k} = (k_x, k_y)$ is the wave number vector; ω is the angular frequency; and $i = (-1)^{1/2}$.

Since the radiation boundary condition specifies that there is no change of Φ , Behrendt (1985) gave

$$\frac{d\Phi}{dt} = \frac{\partial\Phi}{\partial t} + C \frac{\partial\Phi}{\partial r} = 0 \quad \text{on } \partial B \quad (2.25)$$

where $C = \omega / |\mathbf{k}| = \omega / k$ is the wave velocity, $r = |\mathbf{r}| = x \cos \theta + y \sin \theta$, and θ is the approaching wave angle (See Fig.2.5).

Because

$$\frac{\partial r}{\partial x} = \cos \theta \quad \frac{\partial r}{\partial y} = \sin \theta \quad (2.26)$$

and

$$\frac{\partial\Phi}{\partial t} = -i\omega\Phi \quad (2.27)$$

therefore, eq.2.25 becomes

$$\frac{\partial\Phi}{\partial x} - ik \cos \theta \Phi = 0 \quad \text{on } \partial B_x \quad (2.28a)$$

where ∂B_x is the boundary. Similarly, for waves approach a radiation boundary, ∂B_y , that is perpendicular to y axis, we obtain:

$$\frac{\partial \Phi}{\partial y} - ik \sin \theta \Phi = 0 \quad \text{on } \partial B_y \quad (2.28b)$$

Assume $\Phi = \phi e^{-i\omega t}$ (i.e. $\phi = e^{i(k_x x + k_y y)}$), and because $k_x = k \cos \theta$ and $k_y = k \sin \theta$ then eq.2.28a and 2.28b becomes

$$\frac{\partial \phi}{\partial x} - ik_x \phi = 0 \quad \text{on } \partial B_x \quad (2.29a)$$

and

$$\frac{\partial \phi}{\partial y} - ik_y \phi = 0 \quad \text{on } \partial B_y \quad (2.29b)$$

In numerical modeling it is impossible to know k_x (or the incident wave angle θ) in advance. Therefore, another way to calculate k_x (or k_y) must be used. Since

$$k_x = \pm k \sqrt{1 - \left(\frac{k_y}{k}\right)^2} \quad (2.30a)$$

$$k_y = \pm k \sqrt{1 - \left(\frac{k_x}{k}\right)^2} \quad (2.30b)$$

the above two equations change the calculation of k_x to k_y and vice versa. It seems no help at all at first glance. However, using eq.2.30, we change the direction of approximation, and this allows us to use the y-directional gradient of ϕ for estimating k_x (or x-directional gradient for estimating k_y).

Further details will be given next in eq.2.35.

From eq.2.28 we know the quadrant of approaching wave angle θ determines the sign of k_x and k_y , therefore, eq.2.29a and 2.29b become:

$$\frac{\partial \phi}{\partial x} - ik \sqrt{1 - \left(\frac{k_y}{k}\right)^2} \phi = 0 \quad \text{on } \partial B_{x+} \quad (2.31a)$$

$$\frac{\partial \phi}{\partial x} + ik \sqrt{1 - \left(\frac{k_y}{k}\right)^2} \phi = 0 \quad \text{on } \partial B_{x-} \quad (2.31b)$$

$$\frac{\partial \phi}{\partial y} - ik \sqrt{1 - \left(\frac{k_x}{k}\right)^2} \phi = 0 \quad \text{on } \partial B_{y+} \quad (2.31c)$$

$$\frac{\partial \phi}{\partial y} + ik \sqrt{1 - \left(\frac{k_x}{k}\right)^2} \phi = 0 \quad \text{on } \partial B_{y-} \quad (2.31d)$$

where ∂B_{x+} , ∂B_{x-} , ∂B_{y+} , and ∂B_{y-} are the boundaries in positive x, negative x, positive y. and negative y direction respectively.

Without losing generality, we will use the radiation boundary condition on positive x direction boundary (eq.2.31a) to proceed further discussion.

The term $(1 - (k_y/k)^2)^{1/2}$ can be expanded, using a Taylor series, as follows:

$$\sqrt{1 - \left(\frac{k_y}{k}\right)^2} = 1 - \frac{1}{2} \left(\frac{k_y}{k}\right)^2 + o\left(\left(\frac{k_y}{k}\right)^4\right) \quad (2.32)$$

If $|k_x| \gg |k_y|$ (or $|k| \gg |k_y|$), which means that the incident wave train almost normally approaches the boundary ∂B_{x+} , or

$\theta \approx 0$, then the approximation $(1 - (k_y/k)^2)^{1/2} = 1$ can be used. Therefore, eq.2.31a becomes

$$\frac{\partial \phi}{\partial x} = ik\phi \quad \text{on } \partial B_{x^+} \quad (2.33)$$

which is first order radiation boundary condition.

If $(1 - (k_y/k)^2)^{1/2}$ is approximated up to the first two terms in eq.2.32, eq. 2.31a becomes:

$$\frac{\partial \phi}{\partial x} - ik \left(1 - \frac{1}{2} \left(\frac{k_y}{k} \right)^2 \right) \phi = 0 \quad \text{on } \partial B_{x^+} \quad (2.34)$$

From $\phi = e^{i(k_x x + k_y y)}$,

$$\frac{\partial^2 \phi}{\partial y^2} = -k_y^2 \phi \quad (2.35)$$

can be derived, therefore, k_y can be expressed as the gradient in the y direction. Thus eq.2.34 becomes:

$$\frac{\partial \phi}{\partial x} = ik \left(\phi + \frac{1}{2k^2} \frac{\partial^2 \phi}{\partial y^2} \right) \quad \text{on } \partial B_{x^+} \quad (2.36)$$

This boundary condition allows the approaching wave angle up to 30 degrees with negligible reflection of wave back to the computational domain (Behrendt, 1985; Kirby, 1989) (See Fig.2.6).

The term $(1 - (k_y/k)^2)^{1/2}$ can also be expanded by the Padé approximation as follows (Behrendt, 1985; Kirby, 1989):

$$\sqrt{1 - \left(\frac{k_y}{k} \right)^2} = 1 - \frac{\left(\frac{k_y}{k} \right)^2}{2 - \frac{1}{2} \left(\frac{k_y}{k} \right)^2} + O \left(\left(\frac{k_y}{k} \right)^6 \right) \quad (2.37)$$

If the first two terms are used, multiplying $2 - 1/2(k_y/k)^2$ on

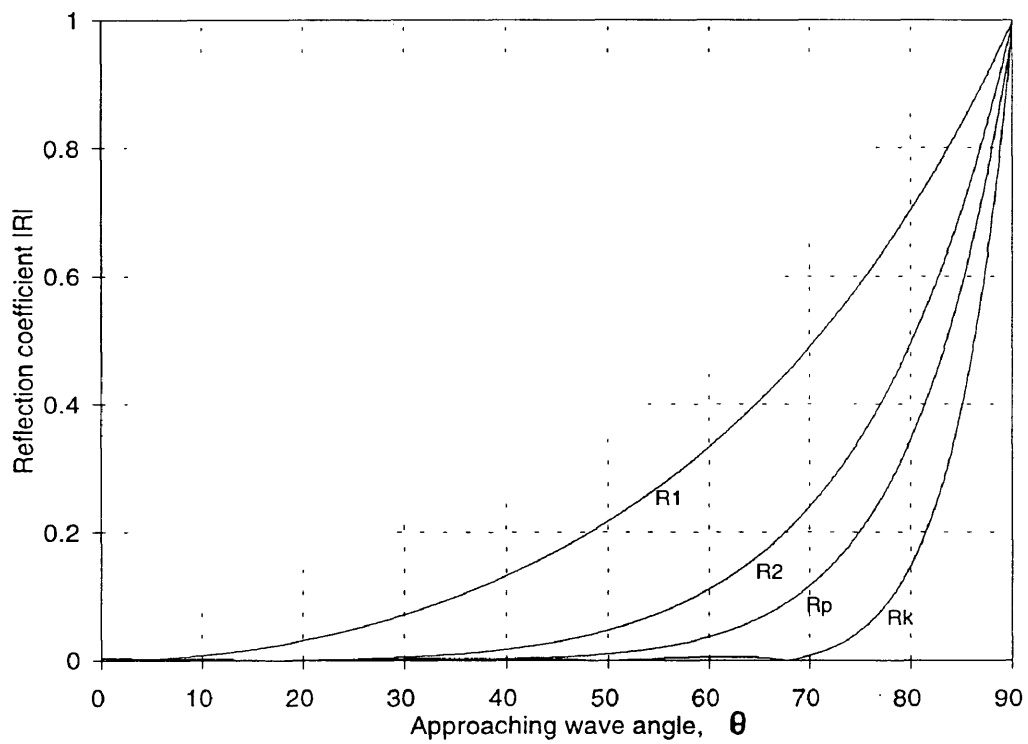


Fig.2.6: Comparison of wave reflection coefficients at a boundary caused by different approximations of the radiation boundary condition. R_1 , R_2 , R_p , and R_k represent the first, second, Padé, and Kirby's approximation, respectively.

both side of eq.2.37, we have

$$\left(2 - \frac{1}{2}\left(\frac{k_y}{k}\right)^2\right) \frac{\partial \phi}{\partial x} - ik \left(2 - \frac{3}{2}\left(\frac{k_y}{k}\right)^2\right) \phi = 0 \quad \text{on } \partial B_{x^+} \quad (2.38)$$

Using eq.2.35 and the following equation

$$\frac{\partial^3 \phi}{\partial y^2 \partial x} = -k_y^2 \frac{\partial \phi}{\partial x} \quad (2.39)$$

we obtain the third order radiation boundary condition:

$$\frac{\partial \phi}{\partial x} + \frac{1}{4k^2} \frac{\partial^3 \phi}{\partial x \partial y^2} = ik \left(\phi + \frac{3}{4k^2} \frac{\partial^2 \phi}{\partial y^2} \right) \quad \text{on } \partial B_{x^+} \quad (2.40)$$

Kirby (1989) introduced another third order approximation for $(1 - (k_y/k)^2)^{1/2}$, which relaxed the condition of exactly zero reflection for small approaching wave angles, but reduced the reflection for large wave angles. The approximation is as follows:

$$\sqrt{1 - \left(\frac{k_y}{k}\right)^2} = \frac{a_0 - a_1 \left(\frac{k_y}{k}\right)^2}{1 - b_1 \left(\frac{k_y}{k}\right)^2} + O\left(\left(\frac{k_y}{k}\right)^6\right) \approx \frac{a_0 - a_1 \left(\frac{k_y}{k}\right)^2}{1 - b_1 \left(\frac{k_y}{k}\right)^2} \quad (3.41)$$

where the parameters a_0 , a_1 and b_1 are determined by the maximum directional aperture, which is the range of θ to be considered and the degree to which the condition of exact transmission at normal approach is to be relaxed. Kirby's third order radiation boundary condition is

$$\frac{\partial \phi}{\partial x} + \frac{b_1}{k^2} \frac{\partial^3 \phi}{\partial x \partial y^2} = ik(a_0 \phi + \frac{a_1}{4k^2} \frac{\partial^2 \phi}{\partial y^2}) \quad \text{on } \partial B_{x^+} \quad (2.42)$$

It is possible to derive forth or higher order approximations for the radiation boundary condition (Behrendt 1985). However, for a numerical scheme used for solving eq.2.14 (or equ 2.16), use of a higher order radiation boundary condition degrades the efficiency of the calculation. This is because the discrete points involved in a higher order boundary condition approximation are more than those in lower order boundary condition, thus, only the radiation boundary conditions of the first order, the second order, and the third order are discussed in this study.

It is no problem to use a first order boundary condition if the wave trains always normally approach the downwave boundary. However, this is not the case in most applications. Thus use of the first order boundary condition leads to wave reflection back into the computational domain if approaching wave angle $\theta > 10^\circ$. In order to reduce such reflection, use of higher order radiation boundary conditions is necessary. The following gives the accuracy of each approximation (Behrendt,1985; Kirby,1989).

Consider that a total wave at the boundary includes an approaching wave and a reflected wave corresponding to the wave back scattering due to the approximations (Behrendt,1985; Kirby,1989), $\phi = \phi^i + \phi^r = e^{i(k_x x + k_y y)} + \text{Re}^{-i(k_x x + k_y y)}$,
Substituting ϕ into the four radiation boundary conditions

respectively gives

$$R_1 = \frac{\cos\theta - 1}{\cos\theta + 1} \quad (2.43)$$

$$R_2 = -\left(\frac{\cos\theta - 1}{\cos\theta + 1}\right)^2 \quad (2.44)$$

$$R_p = \left(\frac{\cos\theta - 1}{\cos\theta + 1}\right)^3 \quad (2.45)$$

$$R_k = \frac{\cos\theta(1 - b_1 \sin^2\theta) - (a_0 - a_1 \sin^2\theta)}{\cos\theta(1 - b_1 \sin^2\theta) + (a_0 - a_1 \sin^2\theta)} \quad (2.46)$$

where R_1 , R_2 , R_p , and R_k represent the reflection coefficients for the first order, the second order, the third order Padé approximation, and the third order Kirby's approximation of the radiation boundary condition. Fig.2.6 shows the relations between the reflection coefficients of different order radiation boundary conditions and the approaching wave angle, θ . It is noticed that with the increase of the approximation order, the range of θ becomes large for the zero reflection coefficient, and the maximum range could be up to 70° if Kirby's approximation (with $a_0=0.9947$, $a_1=0.8901$, $b_1=0.4516$) is used (Kirby 1989). It is also noticed that for $\theta > 80^\circ$, even Kirby's approximation is poor. Under this condition the only suggested approach would be extending the study domain and making the area of interest far away from this boundary.

2.3.3 Partial absorption boundary condition

The fact that a wave train transmits through the downwave boundary without any reflection could be explained as the wave being fully absorbed by the boundary. So the radiation boundary condition is also called the full absorption boundary condition. If a breakwater can only absorb part of the approaching wave energy, a partial absorption boundary condition can be used to cope with this situation. Introducing absorption coefficient α into eq.2.25 gives (Behrendt,1985):

$$\alpha \frac{\partial \Phi}{\partial t} + c \frac{\partial \Phi}{\partial r} = 0 \quad \text{on } \partial B \quad (2.47)$$

Following a similar manipulation previously given, this equation at a positive x boundary becomes:

$$\frac{\partial \phi}{\partial x} - \alpha i k_x \phi = 0 \quad \text{on } \partial B_{x^+} \quad (2.48)$$

Eq.2.48 is the boundary condition with partial absorption or partial reflection. If $\alpha=1$, it becomes a passing through boundary condition; if $\alpha=0$, it becomes the full reflection boundary condition; and if $0<\alpha<1$, it is the partial absorption boundary condition. The value of absorption coefficient α depends on the physical structure at the boundary.

The partial absorption boundary conditions can also be approximated to different orders of boundary conditions as the radiation boundary conditions. For example, the second order partial absorption boundary condition at the positive x

direction boundary is:

$$\frac{\partial \phi}{\partial x} = \alpha ik \left(\phi + \frac{1}{2k^2} \frac{\partial^2 \phi}{\partial y^2} \right) \quad \text{on } \partial B_{x+} \quad (2.49a)$$

Following the same way as that in section 3.2.2 we can also derive the second order boundary conditions on the other boundaries as follows:

$$\frac{\partial \phi}{\partial x} = -\gamma ik \left(\phi + \frac{1}{2k^2} \frac{\partial^2 \phi}{\partial y^2} \right) \quad \text{on } \partial B_{x-} \quad (2.49b)$$

$$\frac{\partial \phi}{\partial y} = \beta ik \left(\phi + \frac{1}{2k^2} \frac{\partial^2 \phi}{\partial x^2} \right) \quad \text{on } \partial B_{y+} \quad (2.49c)$$

$$\frac{\partial \phi}{\partial y} = -\rho ik \left(\phi + \frac{1}{2k^2} \frac{\partial^2 \phi}{\partial x^2} \right) \quad \text{on } \partial B_{y-} \quad (2.49d)$$

where β , γ , and ρ are absorption coefficients on the boundaries of positive y , negative x , and negative y directions respectively. The coefficient α in eq.2.49a is specified for the boundary in the positive x direction.

Similarly, the third order partial absorption boundary conditions of Kirby's approximation on the boundaries in each of the four directions are:

$$\frac{\partial \phi}{\partial x} + \frac{b_1}{k^2} \frac{\partial^3 \phi}{\partial x \partial y^2} = \alpha ik \left(a_0 \phi + \frac{a_1}{4k^2} \frac{\partial^2 \phi}{\partial y^2} \right) \quad \text{on } \partial B_{x+} \quad (2.50a)$$

$$\frac{\partial \phi}{\partial x} + \frac{b_1}{k^2} \frac{\partial^3 \phi}{\partial x \partial y^2} = -\gamma ik \left(a_0 \phi + \frac{a_1}{4k^2} \frac{\partial^2 \phi}{\partial y^2} \right) \quad \text{on } \partial B_{x-} \quad (2.50b)$$

Φ and \mathbf{b} are two column matrices as follows:

$$\Phi = \begin{pmatrix} \phi_{12} \\ \phi_{13} \\ \cdot \\ \cdot \\ \phi_{1m_2(1)} \\ \phi_{22} \\ \phi_{23} \\ \cdot \\ \cdot \\ \phi_{ij-1} \\ \phi_{ij} \\ \phi_{ij+1} \\ \phi_{e_p(d)} \\ \cdot \\ \cdot \\ \cdot \\ \phi_{m_2-1nb(m_2-1)} \\ \phi_{m_2m_2(m_2)} \end{pmatrix}, \quad \mathbf{b} = \begin{pmatrix} b_{12} \\ b_{13} \\ \cdot \\ \cdot \\ b_{1m_2(1)} \\ b_{22} \\ b_{23} \\ \cdot \\ \cdot \\ b_{ij-1} \\ b_{ij} \\ b_{ij+1} \\ b_{e_p(d)} \\ \cdot \\ \cdot \\ \cdot \\ b_{m_2-1nb(m_2-1)} \\ b_{m_2m_2(m_2)} \end{pmatrix}$$

where the elements $l_{i,j}$, $d_{i,j}$, $p_{i,j}$, $u_{i,j}$ and $r_{i,j}$ in matrix \mathbf{A} are the coefficients of elements $\phi_{i-1,j}$, $\phi_{i,j-1}$, $\phi_{i,j}$, $\phi_{i,j+1}$, $\phi_{i+1,j}$ in column matrix Φ , which is an unknown matrix; and the column matrix \mathbf{b} is generated from the right side of each finite difference equation of the partial differential equation. The detailed discretization process of the governing equation and the boundary conditions is given in Chapter 4.

Matrix \mathbf{A} is a band matrix, thus, if using a direct method, the system can be solved by a general band matrix solver with sufficient computer memory available, or a block-wise band matrix solver developed in next chapter.

It is noticed that both the upper bandwidth, μ , and the lower bandwidth, m_l , of \mathbf{A} are 2. The bandwidth of \mathbf{A} is $m = \mu + m_l + 1 = 5$.

A band matrix is one kind of sparse matrix. A sparse matrix, when associated with matrix equations, can usually be solved by special methods, which involve reordering, storing and factoring the matrix (George and Liu, 1981; Duff et al., 1986). Solving a full matrix equation requires dealing with all elements in the matrix. However, it is not necessary to keep all elements in the matrix when solving a sparse matrix equation. A band matrix solver requires only the elements in the band area plus the area reserved for **fill-ins**, which are nonzero elements generated during elimination (Hager, 1988). Therefore, the band matrix solver saves much computer memory. For example, a 10000×10000 matrix equation requires 10^8 storage units, but the same scale band matrix with bandwidth $m=5$ and lower bandwidth $m_l=2$ only requires 7×10^4 storage units (Hager, 1988).

3.2 Storage strategy for band matrix

The required storage of a band matrix depends on the problem being solved. If we solve a band matrix equation and choose a column elimination with the partial pivoting method to solve the matrix equation, the following storage strategy

is more economic (Dongarra et al., 1979). For example,

$$\mathbf{A}_b = \begin{pmatrix} \cdot & & & & & & & & & & \cdot \\ \cdot & & & & & & & & & & \cdot \\ \cdot & & a_{13} & a_{24} & a_{35} & a_{46} & a_{57} & \dots & a_{n-4n-2} & a_{n-3n-1} & a_{n-2n} \\ \cdot & a_{12} & a_{23} & a_{34} & a_{45} & a_{56} & a_{67} & \dots & a_{n-3n-2} & a_{n-2n-1} & a_{n-1n} \\ a_{11} & a_{22} & a_{33} & a_{44} & a_{55} & a_{66} & a_{77} & \dots & a_{n-2n-2} & a_{n-1n-1} & a_{nn} \\ a_{21} & a_{32} & a_{43} & a_{54} & a_{65} & a_{76} & a_{87} & \dots & a_{n-1n-2} & a_{nn-1} & \cdot \\ a_{31} & a_{42} & a_{53} & a_{64} & a_{75} & a_{86} & a_{97} & \dots & a_{nn-2} & \cdot & \cdot \end{pmatrix} \quad (3.2)$$

is a $(m+ml) \times n$ rectangular matrix, which only saves the non-zero elements in matrix \mathbf{A} . In matrix \mathbf{A}_b , the diagonal elements, $a_{k,k}$, $k=1, \dots, n$, of matrix \mathbf{A} are located in row m , the superdiagonal elements, $a_{i,j}$, $0 < j-i \leq \mu$, $i=1, \dots, n-1, j=1, \dots, n$ are located in rows $m-\mu, \dots, m-1$, and the subdiagonal elements $a_{i,j}$, $0 < i-j \leq ml$, $i=1, \dots, n, j=1, \dots, n-1$, are located in rows $m+1, \dots, m+ml$. The elements of superdiagonal and subdiagonal are aligned with the diagonal elements by column in matrix \mathbf{A}_b . A $ml \times n$ spare space from row 1 to row ml in matrix \mathbf{A}_b is reserved for fill-ins. In fact, the dimension of the spare space for this strategy is determined by the lower bandwidth of a band matrix and the matrix dimension. In the above example, the lower bandwidth of the matrix \mathbf{A} is $ml=2$ and the dimension of \mathbf{A} is $n \times n$, thus, the dimension of the spare space is $2 \times n$.

3.3 A general band matrix solver

Like a full matrix solver, a band matrix solver also performs factorization (forward elimination) and back

substitution (Dongarra et al., 1979; Hager, 1988). The only difference is that the band matrix solver uses the band matrix properties to fulfil the task economically in terms of storage. For example, for solving the band matrix \mathbf{A} , a band matrix solver can perform the forward elimination and back substitution in matrix \mathbf{A}_b . In fact, a band matrix solver performs its operations on the full square band matrix (e.g. \mathbf{A}) being solved and saves the relative elements in the full square matrix into a small rectangular matrix (e.g. \mathbf{A}_b). The following sections will show how the band matrix solver works using the full square band matrix \mathbf{A} and the rectangular matrix \mathbf{A}_b as an example.

3.3.1 Factorization of a band matrix by elimination

The forward column elimination with partial pivoting (factorization) includes: (1) Picking the element $a_{L,k}$, which has the largest absolute value among the elements $a_{i,k}$, $i=k, k+1, \dots, k+m_1$ in the current column k , where the subscript L indicates the row number where $a_{L,k}$ stays; (2) Permuting all elements at row L with the elements at row k for the purpose of reducing the truncation errors in the elimination process (Smith, 1985), then elements $a_{k,j}$ (for $j=k+1, \dots, k+m-1$) become the upper triangular elements $u_{k,j}$ and $d_{k,k}=a_{k,k}$ is the diagonal element after permutation; (3) Saving the multipliers of each element after permutation; (4) Calculating the temporary elements as follows:

temporary elements, $t_{i,j}$, $i=2,3$, $j=2,\dots,5$, will change. The first column elimination only reaches the elements up to the third row of matrix **A**, thus, the elements from row 4 to row n , which are $a_{i,j}$, $i=4,5,\dots,n-\mu$, $j=i-1,i-2,\dots,i+\mu$, and $a_{i,j}$, $i=n-\mu+1,\dots,n$, $j=i-1,i-2,\dots,n$, remain inactive.

Using matrix **A_b**, we can save elements of matrix **A** in eq.3.4 as follows

$$\mathbf{A}_b = \begin{pmatrix} . & & & & & u_{15} & & & & & . \\ & & . & u_{14} & t_{25} & . & . & & & & . \\ & & . & u_{13} & t_{24} & t_{35} & a_{46} & a_{57} & \dots & a_{n-4n-2} & a_{n-3n-1} & a_{n-2n} \\ . & u_{12} & t_{23} & t_{34} & a_{45} & a_{56} & a_{67} & \dots & a_{n-3n-2} & a_{n-2n-1} & a_{n-1n} \\ d_{11} & t_{22} & t_{33} & a_{44} & a_{55} & t_{66} & a_{77} & \dots & a_{n-2n-2} & a_{n-1n-1} & a_{nn} \\ m_{21} & t_{32} & a_{43} & a_{54} & a_{65} & a_{76} & a_{87} & \dots & a_{n-1n-2} & a_{nn-1} & . \\ m_{31} & a_{42} & a_{53} & a_{64} & a_{75} & a_{86} & a_{97} & \dots & a_{nn-2} & . & . \end{pmatrix} \quad (3.5)$$

During the second column elimination, the picking-up of the largest elements in column two starts from comparing $t_{2,2}$, $t_{2,3}$ and $a_{4,2}$. After the second column elimination matrix **A** becomes

$$\mathbf{A}_b = \begin{pmatrix} \cdot & & & \cdot & u_{15} & u_{26} & u_{37} & \dots & u_{n-6n-2} & u_{n-5n-1} & u_{n-4n} \\ \cdot & & & u_{14} & u_{25} & u_{36} & u_{47} & \dots & u_{n-5n-2} & u_{n-4n-1} & u_{n-2n} \\ \cdot & & u_{13} & u_{24} & u_{35} & u_{46} & u_{57} & \dots & u_{n-4n-2} & u_{n-3n-1} & u_{n-2n} \\ \cdot & u_{12} & u_{23} & u_{34} & u_{45} & u_{56} & u_{67} & \dots & u_{n-3n-2} & u_{n-2n-1} & u_{n-1n} \\ d_{11} & d_{22} & d_{33} & d_{44} & d_{55} & d_{66} & d_{77} & \dots & d_{n-2n-2} & d_{n-1n-1} & d_{n \ n} \\ m_{21} & m_{32} & m_{43} & m_{54} & m_{65} & m_{76} & m_{87} & \dots & m_{n-1n-2} & m_{n \ n-1} & \cdot \\ m_{31} & m_{42} & m_{53} & m_{64} & m_{75} & m_{86} & m_{97} & \dots & m_{n \ n-2} & \cdot & \cdot \end{pmatrix} \quad (3.11)$$

It is noticed that the elements in the upper triangular submatrix and the elements in diagonal submatrix of matrix \mathbf{A} are saved in the first $m \times n$ rectangular submatrix of \mathbf{A}_b and the elements in the lower triangular submatrix of matrix \mathbf{A} are saved in the last $m_1 \times n$ rectangular submatrix of matrix \mathbf{A}_b .

The next step is the back substitution in which the multiplier submatrix and the upper triangular and diagonal submatrices in matrix \mathbf{A}_b will be used for different purposes to perform the calculation.

3.3.2 back substitution

A matrix equation can be written as

$$\mathbf{Ax}=\mathbf{b} \quad (3.12)$$

where \mathbf{A} is a $n \times n$ band matrix as before, $\mathbf{x} = [x_1, x_2, x_3 \dots x_n]^t$ is an unknown column matrix to be solved, where superscript t represent transpose, and $\mathbf{b}=[b_1, b_2, b_3 \dots b_n]^t$ is the column matrix on the right side of the equation.

Before back substitution, some calculation on \mathbf{b} must be performed similar to those elimination on matrix \mathbf{A} (Dongarra

et al., 1979). These calculations include permuting and modifying elements of \mathbf{b} by the formula

$$b_i = b_i - m_{i,k} b_k \quad (3.13)$$

where $m_{i,k}$, $i=k+1, k+2, \dots, k+m_1$, and $k=1, 2, \dots, n-m_1$, and $m_{i,k}$, $i=k+1, k+2, \dots, n$, and $k=n-m_1+1, \dots, n-1$, are the multipliers stored in matrix \mathbf{A}_p . The calculations must proceed in the forward direction.

Back substitution follows the formula:

$$x_n = \frac{x_n}{d_{n,n}}$$

$$x_i = (x_i - \sum_{k=i+1}^n u_{i,k} x_k) / d_{i,i} \quad \text{for } i=n-1, n-2, \dots, n-m+1 \quad (3.14)$$

$$x_i = (x_i - \sum_{k=i+1}^{i+m-1} u_{i,k} x_k) / d_{i,i} \quad \text{for } i=n-m, n-m-1, \dots, 1$$

To save space, the column matrix \mathbf{b} can be re-used instead of \mathbf{x} . Then the formula becomes

$$b_n = \frac{b_n}{d_{n,n}}$$

$$b_i = (b_i - \sum_{k=i+1}^n u_{i,k} b_k) / d_{i,i} \quad \text{for } i=n-1, n-2, \dots, n-m+1 \quad (3.15)$$

$$b_i = (b_i - \sum_{k=i+1}^{i+m-1} u_{i,k} b_k) / d_{i,i} \quad \text{for } i=n-m, n-m-1, \dots, 1$$

3.4 A block-wise band matrix solver

3.4.1 A Property of matrix \mathbf{A}_b during elimination

A property of the matrix \mathbf{A}_b during elimination is its block structure. The example in the previous discussion demonstrates that during elimination, matrix \mathbf{A}_b contains five submatrix groups, $d_{i,j}$, $u_{i,j}$, $m_{i,j}$, $t_{i,j}$, and $a_{i,j}$. If activity and inactivity are used as criteria to classify the submatrix groups, matrix \mathbf{A}_b in eq.3.9 can be rewritten as:

$$\mathbf{A}_b = \begin{pmatrix} & & & \cdot & V_{15} & V_{26} & V_{37} & & & & \cdot \\ & & & & \cdot & V_{14} & V_{25} & V_{36} & V_{47} & & & \cdot \\ \cdot & \cdot & V_{13} & V_{24} & V_{35} & V_{46} & V_{57} & \cdots & i_{n-4n-2} & i_{n-3n-1} & i_{n-2n} \\ \cdot & V_{12} & V_{23} & V_{34} & V_{45} & V_{56} & i_{67} & \cdots & i_{n-3n-2} & i_{n-2n-1} & i_{n-1n} \\ V_{11} & V_{22} & V_{33} & V_{44} & V_{55} & i_{66} & i_{77} & \cdots & i_{n-2n-2} & i_{n-1n-1} & i_n \ n \\ V_{21} & V_{32} & V_{43} & V_{54} & i_{65} & i_{76} & i_{87} & \cdots & i_{n-1n-2} & i_n \ n-1 & \cdot \\ V_{31} & V_{42} & V_{53} & i_{64} & i_{75} & i_{86} & i_{97} & \cdots & i_n \ n-2 & \cdot & \cdot \end{pmatrix} \quad (3.16)$$

This is the result of grouping elements of $t_{i,j}$, $u_{i,j}$, $m_{i,j}$, and $d_{i,j}$, which have been changed, into an **active submatrix** group, $v_{i,j}$, and changing the name of $a_{i,j}$, which have not participated in the calculation during the previous column elimination, to $i_{i,j}$ to represent an **inactive submatrix** group.

If the submatrices are grouped by another criteria, i.e. grouping $u_{i,j}$, $d_{i,j}$ and $m_{i,j}$ into $h_{i,j}$, the **unchanged elements**; and $t_{i,j}$, and $a_{i,j}$ into $c_{i,j}$, the **changing elements** and the **elements to be changed**, then the matrix \mathbf{A}_b in eq.3.9 becomes:

$$\mathbf{A}_b = \begin{pmatrix} \cdot & & & \cdot & h_{15} & h_{26} & h_{37} & & & & \cdot \\ \cdot & & & \cdot & h_{14} & h_{25} & h_{36} & C_{47} & & \cdot & \cdot & \cdot \\ \cdot & & h_{13} & h_{24} & h_{35} & C_{46} & C_{57} & \cdots & C_{n-4n-2} & C_{n-3n-1} & C_{n-2n} \\ \cdot & h_{12} & h_{23} & h_{34} & C_{45} & C_{56} & C_{67} & \cdots & C_{n-3n-2} & C_{n-2n-1} & C_{n-1n} \\ h_{11} & h_{22} & h_{33} & C_{44} & C_{55} & C_{66} & C_{77} & \cdots & C_{n-2n-2} & C_{n-1n-1} & C_n & n \\ h_{21} & h_{32} & h_{43} & C_{54} & C_{65} & C_{76} & C_{87} & \cdots & C_{n-1n-2} & C_n & n-1 & \cdot \\ h_{31} & h_{42} & h_{53} & C_{64} & C_{75} & C_{86} & C_{97} & \cdots & C_n & n-2 & \cdot & \cdot \end{pmatrix} \quad (3.17)$$

It is noticed that the first three columns of matrix \mathbf{A}_b could be removed without affecting the rest column elimination process.

A sandwich structure in matrix \mathbf{A}_b can be observed if we reorganize the matrix by changing the name of elements in columns containing only unchanged elements, $h_{i,j}$, into $s^{(1)}_{i,j}$, elements from column 11 to column n , which contain only inactive elements, $i_{i,j}$ into $s^{(2)}_{i,j}$, and the rest elements in columns containing $h_{i,j}$, $i_{i,j}$, and $c_{i,j}$ into $w_{i,j}$ as follows:

$$\mathbf{A}_b = \begin{pmatrix} \cdot & & & \cdot & W_{15} & W_{26} & W_{37} & W_{48} & W_{59} & W_{610} & & & \cdot \\ \cdot & & & \cdot & W_{14} & W_{25} & W_{36} & W_{47} & W_{58} & W_{69} & W_{710} & & \cdot \\ & & S_{13}^{(1)} & W_{24} & W_{35} & W_{46} & W_{57} & W_{68} & W_{79} & W_{810} & \cdots & S_{n-4n-2}^{(2)} & S_{n-3n-1}^{(2)} & S_{n-2n}^{(2)} \\ \cdot & S_{12}^{(1)} & S_{23}^{(1)} & W_{34} & W_{45} & W_{56} & W_{67} & W_{78} & W_{89} & W_{910} & \cdots & S_{n-3n-2}^{(2)} & S_{n-2n-1}^{(2)} & S_{n-1n}^{(2)} \\ S_{11}^{(1)} & S_{22}^{(1)} & S_{33}^{(1)} & W_{44} & W_{55} & W_{66} & W_{77} & W_{88} & W_{99} & W_{1010} & \cdots & S_{n-2n-2}^{(2)} & S_{n-1n-1}^{(2)} & S_n^{(2)} \\ S_{21}^{(1)} & S_{32}^{(1)} & S_{43}^{(1)} & W_{54} & W_{65} & W_{76} & W_{87} & W_{98} & W_{109} & W_{1110} & \cdots & S_{n-1n-2}^{(2)} & S_n^{(2)} & \cdot \\ S_{31}^{(1)} & S_{42}^{(1)} & S_{53}^{(1)} & W_{64} & W_{75} & W_{86} & W_{97} & W_{108} & W_{119} & W_{1210} & \cdots & S_n^{(2)} & \cdot & \cdot \\ \cdot & \cdot & \cdot & \cdot & \cdot & \cdot & \cdot & \cdot & \cdot & \cdot & \cdot & \cdot & \cdot & \cdot \end{pmatrix} \quad (2.18)$$

The 'filling' of the 'sandwich' called **working matrix** contains elements $w_{i,j}$, the first slice of 'bread' called **first sleeping matrix** contains $s^{(1)}_{i,j}$, and the second slice of 'bread' called **second sleeping matrix** contains $s^{(2)}_{i,j}$.

3.4.2 Strategy of block-wise band matrix solver

It is possible to utilize the block structure of matrix \mathbf{A}_b during elimination and back substitution to solve the band matrix \mathbf{A} (eq.3.1) without using a large computer memory. In fact, the calculation of elimination can be proceeded in the **working matrix**. Once the calculation completes, part of unchanged elements, $h_{i,j}$, in the working matrix can be transferred into the first sleeping matrix and part of $i_{i,j}$ in the second sleeping matrix can be transferred into the working matrix for further process. Therefore, we can use computer memory to store working matrix only and use hard disk to store the two sleeping matrices. Block by block the elimination of each column of matrix \mathbf{A} can be done in the working matrix.

The working matrix is fixed in size, which is determined by the bandwidth ($m=m_l+m_u+1$) of a band matrix and the size of a submatrix, called **saving matrix**. The saving matrix is a submatrix containing part of unchanged elements $h_{i,j}$. Its size is determined by the number of column of $h_{i,j}$ to be removed from working matrix to the first sleeping matrix. For example, either of the next submatrix,

$$\begin{pmatrix} & & \cdot \\ & & \cdot \\ & \cdot & h_{13} \\ \cdot & h_{12} & h_{23} \\ h_{11} & h_{22} & h_{33} \\ h_{21} & h_{32} & h_{43} \\ h_{31} & h_{42} & h_{53} \end{pmatrix} \quad \text{or} \quad \begin{pmatrix} & & \cdot \\ & & \cdot \\ & \cdot & h_{12} \\ h_{11} & h_{22} & \\ h_{21} & h_{32} & \\ h_{31} & h_{42} & \end{pmatrix} \quad \text{or} \quad \begin{pmatrix} \cdot \\ \cdot \\ \cdot \\ \cdot \\ h_{11} \\ h_{21} \\ h_{31} \end{pmatrix}$$

which can be obtained from in eq.3.17, could be a saving matrix. If the submatrix with three columns is chosen to be a saving matrix, the size of the working matrix will be $(3+m-1) \times (m+m_1) = 7 \times 7$, where, $m=5$ is the bandwidth and $m_1=2$ is the lower bandwidth. In this case, three column eliminations can be proceeded in the working matrix each time after removal of three columns of $h_{i,j}$ to the first sleeping matrix and input of three columns of $i_{i,j}$ from the second sleeping matrix. For example, the working matrix shown in eq.3.18 contains a three column saving matrix.

3.4.2.1 Forward elimination

In the forward elimination process, after column eliminations in the working matrix are complete, the elements in the saving matrix are popped into a hard disk file (the first sleeping matrix), while part of the inactive elements from another hard disk file (the second sleeping matrix) are pushed into the working matrix in computer memory. In the above example, after the first three column eliminations are complete, the first three columns could be popped into a hard disk file while the first three columns in the second sleeping matrix stored in another hard disk file are pushed into the working matrix. This process is shown in Fig.3.1. In Fig.3.1 the left arrow indicates that the elements in the saving matrix are popped into a hard disk file, the middle arrow means that the rest of the elements of the working matrix

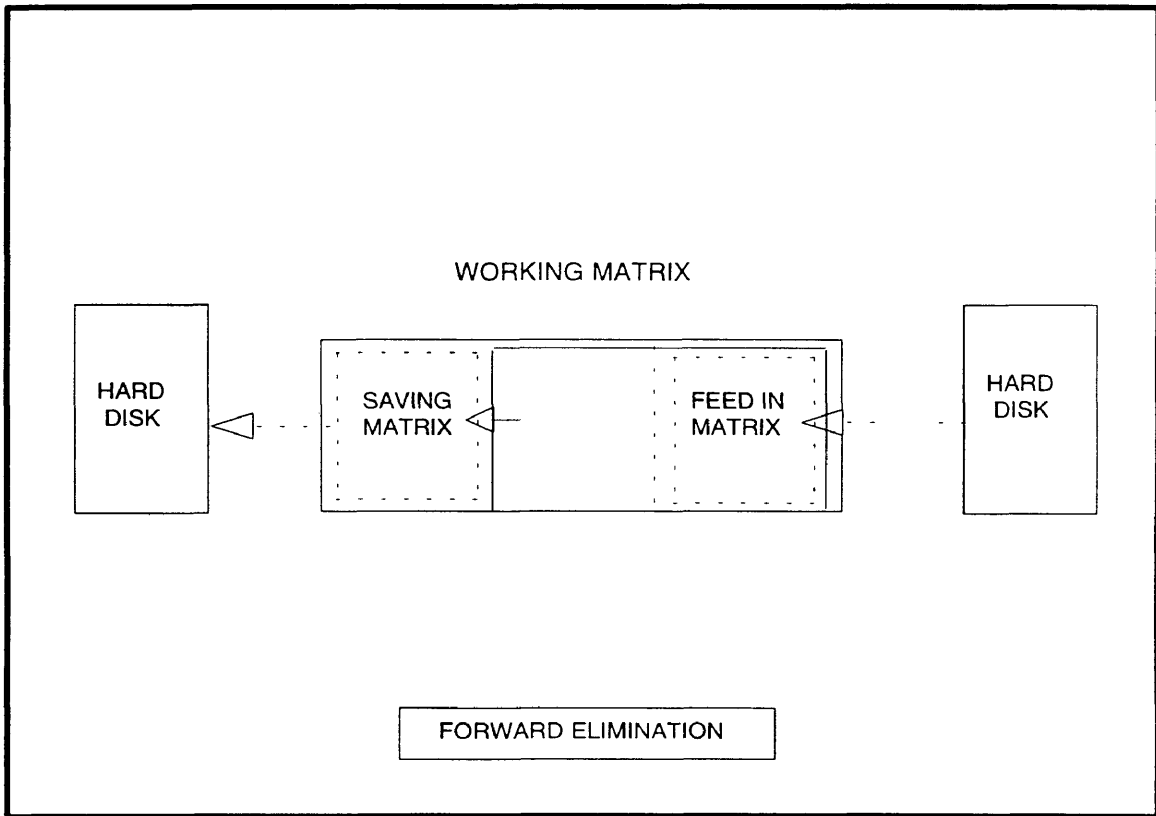


Fig.3.1: Principle of block-wise forward elimination.

are moved forward to the left most bound of the working matrix, and the right arrow indicates that a matrix of the same size as the saving matrix is pushed into the working matrix from another hard disk file (the second sleeping matrix) and concatenated to right end of the working matrix. These transfer processes continue until the last group of inactive elements in the second sleeping matrix are pushed into the working matrix. After completion of the elimination of this last group of elements the whole forward elimination process is complete.

3.4.2.2 Back substitution

As previously discussed, the elements in \mathbf{b} must be permuted and modified by forward elimination before back substitution. This can be done much more economically during forward elimination rather than after. The right column matrix of the matrix equation, $\mathbf{b}=[b_1, b_2, b_3 \dots b_n]^t$ can be treated as diagonal elements $[a_{1,1}, a_{2,2}, a_{3,3} \dots a_{n,n}]^t$ in row m of matrix \mathbf{A}_b when pivoting. The modification of $\mathbf{b}=[b_1, b_2, b_3 \dots b_n]^t$, however, follows the formula given in eq.3.13.

After modification of \mathbf{b} , the remaining step is the back substitutions in which only $u_{i,j}$, $d_{i,j}$, and b_i are involved. The formula of back substitution is same as eq.3.15.

In the substitution process, elements in matrix \mathbf{A}_b still have a block structure. For the example above, after final forward elimination, the working matrix in eq.3.18 becomes:

$$\begin{pmatrix}
 u_{n-6n-2} & u_{n-5n-1} & u_{n-4n} & \cdot & \cdot & \cdot & \cdot \\
 u_{n-5n-2} & u_{n-4n-1} & u_{n-3n} & \cdot & \cdot & \cdot & \cdot \\
 u_{n-4n-2} & u_{n-3n-1} & u_{n-2n} & \cdot & \cdot & \cdot & \cdot \\
 u_{n-3n-2} & u_{n-2n-1} & u_{n-1n} & \cdot & \cdot & \cdot & \cdot \\
 d_{n-2n-2} & d_{n-1n-1} & d_{n \ n} & \cdot & \cdot & \cdot & \cdot \\
 m_{n-1n-2} & m_{n \ n-1} & \cdot & \cdot & \cdot & \cdot & \cdot \\
 m_{n \ n-2} & \cdot & \cdot & \cdot & \cdot & \cdot & \cdot
 \end{pmatrix}$$

Back substitution starts at the right lower corner of the matrix and progresses leftward and upward. This feature may be utilized to proceed the back substitution by retrieving the elements, which were popped out in the forward elimination process, from the hard disk. The back substitution process is exactly inverse of the forward elimination process. Thus it is not presented here in detail.

CHAPTER 4

A FINITE DIFFERENCE MODEL FOR THE ELLIPTIC WAVE EQUATION

4.1 Introduction

The two dimensional linear mild slope wave equation (eq.2.14) can be simplified to (Radder, 1979)

$$\nabla^2\phi+k_c^2\phi=0 \tag{4.1}$$

where $k_c^2=k^2-\nabla^2(C\cdot C_g)^{0.5}/(C\cdot C_g)^{0.5}$ is a pseudo wave number, k is wave number, C is wave phase velocity and C_g is wave group velocity; and $\phi=(C\cdot C_g)^{0.5}\phi_0$ is a pseudo velocity potential. Eq.4.1 is an elliptic partial differential equation. Two kinds of methods are usually used to solved this kind of equation. The first is a direct method including the finite element method (FEM, Berkhoff,1972; 1976; Berkhoff et al., 1982; Chen and Mei, 1974), the boundary element method (BEM, Marschall,1993) and the finite difference method (FDM). The second is an iterative method including the multigrid method (MULTI, Li and Anastasiou,1992), and the conjugate gradient method (CGM, Panchang et al.,1991; Li, 1994). The iteration method has the advantage of saving computer memory (Panchang

et al.,1991) and when dealing with simple boundary problems it is very efficient because of the high convergent rate. However the efficiency of this method can be degraded severely by complexity at either the interior or the exterior boundaries (Panchang *et al.*, 1991). The direct method does not have this drawback because the number of calculations of the direct method only depends on the grid number of the study domain. So to simulate wave climate in an area such as a harbor or near shore zone with structures, the direct method is preferred (FEM, Berkhoff,1972,1976; Berkhoff *et al.*, 1982; Chen and Mei, 1974). The major disadvantages of the direct method usually are the requirement of huge computer memory (Panchang *et al.*, 1991) when dealing with a problem in a large study domain and the associated slow pace of solving a large matrix equation. For example, a rectangular study domain with 1000x1000 grid points requires 10^{12} storage units using a full matrix solver or 10^9 storage units using a band matrix solver for a direct method by a finite difference approximation of eq.4.1, while for an iterative method, e.g., the CGM, only 10^6 storage units are needed. Therefore, prior to this study it is difficult to apply a direct method to a domain with more than 10,000 grid points (Panchang *et al.*, 1991).

In this study, we take the advantage of fixed number of calculations and overcome the shortcoming of large memory requirement of the direct method by use of the block-wise band matrix solver introduced in Chapter 3.

With a direct method, no matter what kind of method (FEM, FDM, or BEM) is applied to discretize the elliptic equation (eq.4.1), the final result is a system of simultaneous linear equations or a matrix equation with a band coefficient matrix. Because of its simplicity, the FDM was selected in this study.

4.2 Band structure of a finite difference model

4.2.1 Finite difference of governing equation

Using a second order finite difference approximation (Fletcher,1988) to discretize the elliptic equation (eq.4.1), gives:

$$\phi_{i-1,j} + \xi\phi_{i,j-1} + (dx^2k_{c_{i,j}}^2 - 2 - 2\xi)\phi_{i,j} + \xi\phi_{i,j+1} + \phi_{i+1,j} = 0 \quad (4.2)$$

where the subscripts i and j are indexes for the grid points in the interior region, which is a water area of interest of a problem, and i and j are in x and y direction, respectively; dx and dy are the space intervals in x and y direction, respectively (see Fig. 4.1); and $\xi = (dx/dy)^2$. It is noticed that the governing equation at point (i,j) can be approximated by the potential values of five grid points, $\phi_{i-1,j}$, $\phi_{i,j-1}$, $\phi_{i,j}$, $\phi_{i,j+1}$, and $\phi_{i+1,j}$. Eq. 4.2 can be written as a matrix form:

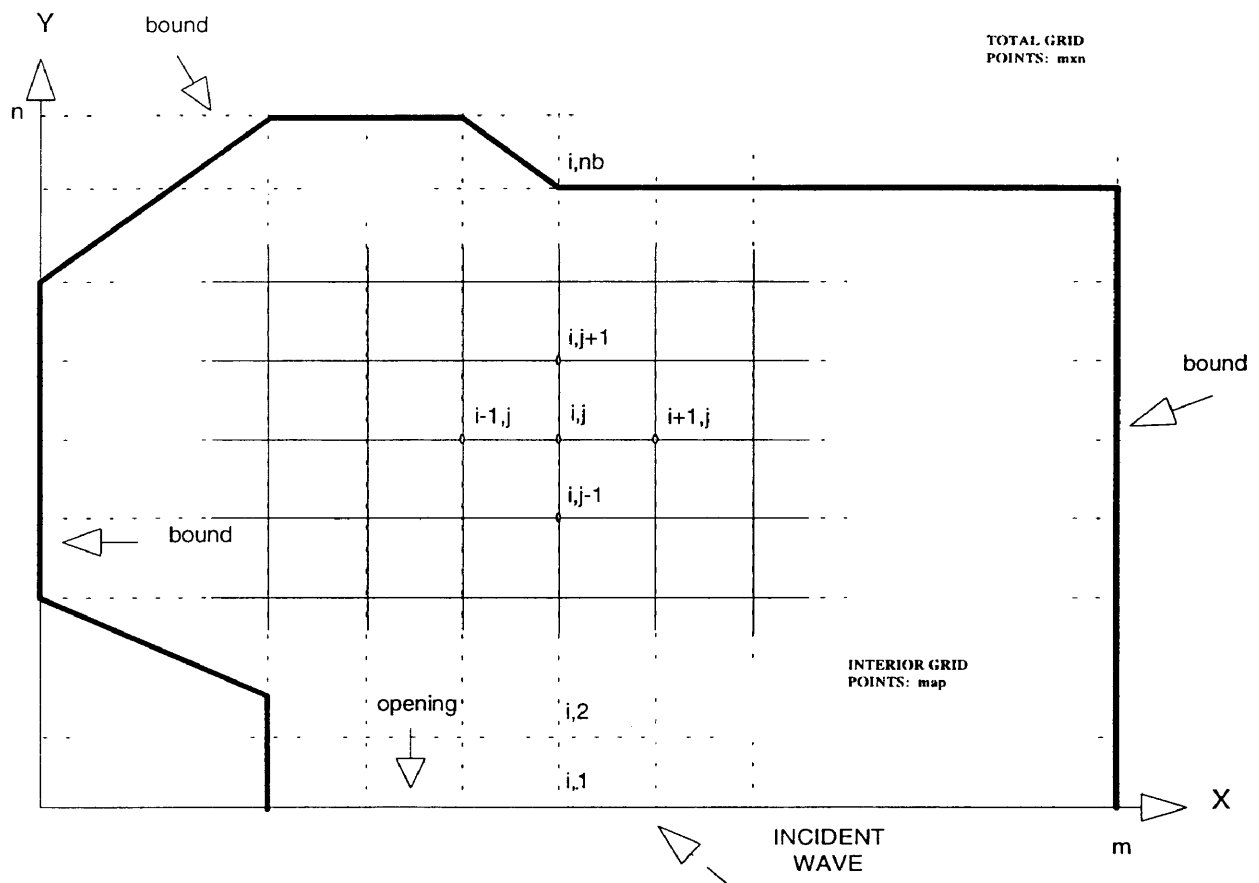
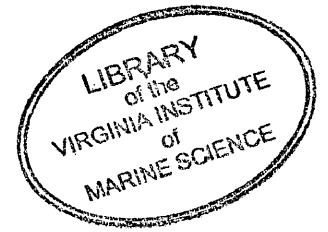


Fig.4.1: Layout of a study domain.

$$(l_{i,j} \quad d_{i,j} \quad p_{i,j} \quad u_{i,j} \quad r_{i,j}) \begin{pmatrix} \phi_{i-1,j} \\ \phi_{i,j-1} \\ \phi_{i,j} \\ \phi_{i,j+1} \\ \phi_{i+1,j} \end{pmatrix} = 0 \quad (4.3)$$

where $l_{i,j}$, $d_{i,j}$, $p_{i,j}$, $u_{i,j}$, and $r_{i,j}$ are the coefficients of $\phi_{i-1,j}$, $\phi_{i,j-1}$, $\phi_{i,j}$, $\phi_{i,j+1}$, and $\phi_{i+1,j}$ in eq.4.2, respectively; the subscript (i,j) of these coefficients indicates the finite difference eq.4.2 is the approximation of the partial differential eq.4.1 at the point (i,j) .

4.2.2 Finite difference equations of boundary conditions

4.2.2.1 Dirichlet boundary condition

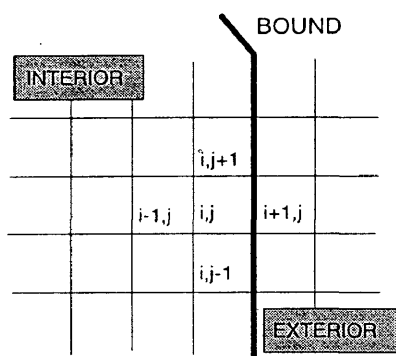
The finite difference equation of the Dirichlet boundary condition (eq.2.23) involves only one grid point. For example in Fig.4.2a,

$$\phi_{i+1,j} = c \quad (4.4a)$$

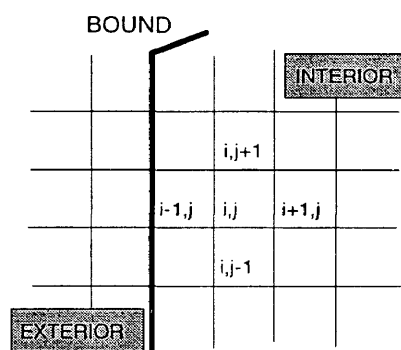
is a Dirichlet boundary condition specified for a point $(i+1,j)$ on a boundary in the positive x direction, and c is a given condition (e.g. for a given wave height, H , wave period, T , and wave angle, θ_0 ,

$$c = \frac{Hg}{2\omega} e^{i[k_0 \cos(\theta_0) dx(i+1) + k_0 \sin(\theta_0) dy(j)]} \quad (4.4b)$$

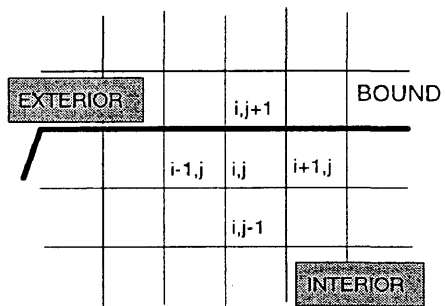
where $\omega = 2\pi/T$ is angular frequency, g is gravitational acceleration, and k_0 can be calculated from the dispersion



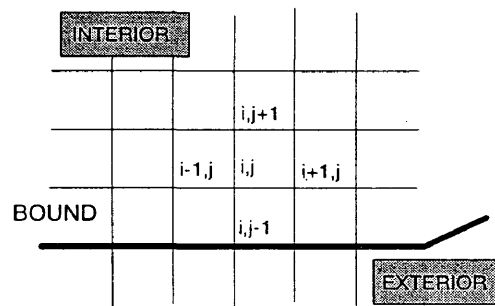
(a)



(b)



(c)



(d)

Fig.4.2: Sketch of four directional boundaries for Dirichlet boundary conditions. a, b, c, and d are for the positive x, negative x, positive y, and negative y directional boundary, respectively.

relation, eq.2.23b, with a given wave period and water depth;

$$\phi_{i-1,j} = c \quad (4.5)$$

is a Dirichlet boundary condition specified for a point $(i-1,j)$ on a boundary in the negative x direction (Fig.4.2b);

$$\phi_{i,j+1} = c \quad (4.6)$$

is a Dirichlet boundary condition specified for a point $(i,j-1)$ on a boundary in the positive y direction (Fig.4.2c);

and

$$\phi_{i,j-1} = c \quad (4.7)$$

is a Dirichlet boundary condition specified for a point $(i,j+1)$ on a boundary in the negative y direction (Fig.4.2d).

When the finite difference governing equation (eq.4.2) is applied to a point (i,j) , which is next to a boundary with a Dirichlet boundary condition, and associated with eq.4.4, it becomes:

$$\phi_{i-1,j} + \xi \phi_{i,j-1} + (dx^2 k_{c_{i,j}}^2 - 2 - 2\xi) \phi_{i,j} + \xi \phi_{i,j+1} = -c$$

In a matrix form:

$$(l_{i,j} \quad d_{i,j} \quad p_{i,j} \quad u_{i,j}) \begin{pmatrix} \phi_{i-1,j} \\ \phi_{i,j-1} \\ \phi_{i,j} \\ \phi_{i,j+1} \end{pmatrix} = -c \quad (4.8)$$

When eq.4.2 is associated with eq.4.5, it becomes:

$$\xi\phi_{i,j-1} + (dx^2 k_{c_{i,j}}^2 - 2 - 2\xi)\phi_{i,j} + \xi\phi_{i,j+1} + \phi_{i+1,j} = -c$$

In a matrix form:

$$(d_{i,j} \quad p_{i,j} \quad u_{i,j} \quad r_{i,j}) \begin{pmatrix} \phi_{i,j-1} \\ \phi_{i,j} \\ \phi_{i,j+1} \\ \phi_{i+1,j} \end{pmatrix} = -c \quad (4.9)$$

When associated with eq.4.6, eq.4.2 becomes:

$$\phi_{i-1,j} + \xi\phi_{i,j-1} + (dx^2 k_{c_{i,j}}^2 - 2 - 2\xi)\phi_{i,j} + \phi_{i+1,j} = -\xi c$$

or

$$(l_{i,j} \quad d_{i,j} \quad p_{i,j} \quad r_{i,j}) \begin{pmatrix} \phi_{i-1,j} \\ \phi_{i,j-1} \\ \phi_{i,j} \\ \phi_{i+1,j} \end{pmatrix} = -\xi c \quad (4.10)$$

When associated with eq.4.7, eq.4.2 becomes:

$$\phi_{i-1,j} + (dx^2 k_{c_{i,j}}^2 - 2 - 2\xi)\phi_{i,j} + \xi\phi_{i,j+1} + \phi_{i+1,j} = -\xi c$$

or

$$(l_{i,j} \quad p_{i,j} \quad u_{i,j} \quad r_{i,j}) \begin{pmatrix} \phi_{i-1,j} \\ \phi_{i,j} \\ \phi_{i,j+1} \\ \phi_{i+1,j} \end{pmatrix} = -\xi c \quad (4.11)$$

Eq.4.8-4.11 are the finite difference equations associated with the Dirichlet boundary conditions at the four direction of boundaries.

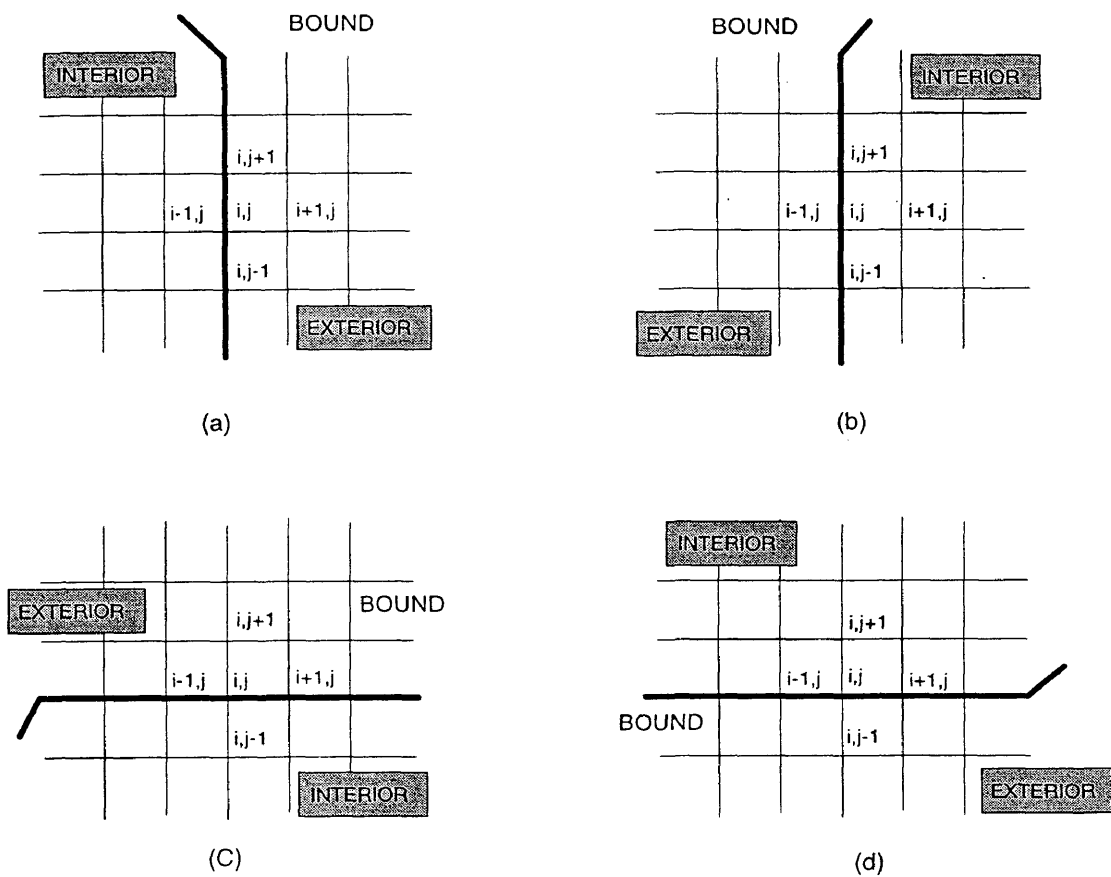


Fig.4.3: Sketch of four directional boundaries for the second order partial absorption boundary conditions. a, b, c, and d are for the positive x, negative x, positive y, and negative y directional boundary, respectively.

4.2.2.2 Partial absorption boundary condition

The finite difference equation of a partial absorption boundary condition, which includes both the radiation boundary condition and the full reflection boundary condition, involves five grid points for the second order (or six grid points for the third order) approximation of the boundary condition. In this study both the second order (eq.2.49) and the third order (eq.2.50) boundary conditions are implemented.

a. The second order boundary condition

The finite difference equation of the second order partial absorption boundary condition (eq.2.49a) with an absorption coefficient α for a positive x directional boundary point (i, j) can be written as

$$\phi_{i-1,j} + \alpha \left(\frac{idx}{k_{i,j} dy^2} \right) \phi_{i,j-1} + \alpha 2ik_{i,j} dx \left(1 - \frac{1}{(k_{i,j} dy)^2} \right) \phi_{i,j} + \alpha \left(\frac{idx}{k_{i,j} dy^2} \right) \phi_{i,j+1} - \phi_{i+1,j} = 0 \quad (4.12)$$

The positive directional boundary means the study domain is on the left side of the boundary (Fig.4.3a). It is noticed that in eq.4.12 point $(i+1, j)$ is out of study domain. Because of this, eq.4.12 alone can not fully describe the boundary condition at point (i, j) . In order to solve this problem, an additional equation is required. The finite difference governing equation (eq.4.2), which can also be used to the boundary point (i, j) , is the additional equation. Using eq.4.2 and eq.4.12 together we can elimination the $\phi_{i+1,j}$ and obtain the following finite difference equation:

$$\begin{aligned}
2\phi_{i-1,j} + \xi \left(1 + \frac{\alpha i}{k_{i,j} dx} \right) \phi_{i,j-1} + \left((dx k_{c_{i,j}})^2 - 2(1+\xi) + i2dx\alpha k_{i,j} \left(1 - \frac{1}{(k_{i,j} dy)^2} \right) \right) \phi_{i,j} \\
+ \xi \left(1 + \frac{\alpha i}{k_{i,j} dx} \right) \phi_{i,j+1} = 0
\end{aligned} \tag{4.13}$$

which can fully describe the boundary condition at point (i,j). In matrix form, eq.4.13 becomes:

$$(l_{i,j} \quad d_{i,j} \quad p_{i,j} \quad u_{i,j}) \begin{pmatrix} \phi_{i-1,j} \\ \phi_{i,j-1} \\ \phi_{i,j} \\ \phi_{i,j+1} \end{pmatrix} = 0 \tag{4.14}$$

Similar to equ 4.12 the following equations are the finite difference equation of partial absorption boundary conditions (equ 2.49b, 2.49c, and 2.49d) on the boundary points (i,j) in the negative x, positive y, and negative y directional boundaries, respectively (see Fig.4.3b, 4.3c, and 4.3d):

$$-\phi_{i-1,j} + \gamma \left(\frac{idx}{k_{i,j} dy^2} \right) \phi_{i,j-1} + \gamma 2ik_{i,j} dx \left(1 - \frac{1}{(k_{i,j} dy)^2} \right) \phi_{i,j} + \gamma \left(\frac{idx}{k_{i,j} dy^2} \right) \phi_{i,j+1} + \phi_{i+1,j} = 0 \tag{4.15}$$

$$\beta \left(\frac{id y}{k_{i,j} dx^2} \right) \phi_{i-1,j} + \phi_{i,j-1} + \beta 2ik_{i,j} dy \left(1 - \frac{1}{(k_{i,j} dx)^2} \right) \phi_{i,j} - \phi_{i,j+1} + \beta \left(\frac{id y}{k_{i,j} dx^2} \right) \phi_{i+1,j} = 0 \tag{4.16}$$

$$\rho \left(\frac{id y}{k_{i,j} dx^2} \right) \phi_{i-1,j} - \phi_{i,j-1} + \rho 2ik_{i,j} dy \left(1 - \frac{1}{(k_{i,j} dx)^2} \right) \phi_{i,j} + \phi_{i,j+1} + \rho \left(\frac{id y}{k_{i,j} dx^2} \right) \phi_{i+1,j} = 0 \tag{4.17}$$

where β , γ , and ρ are the absorption coefficients on the negative x, positive y and negative y directional boundaries, respectively.

Eliminating $\phi_{i-1,j}$ in eq.4.15 with eq.4.2 we have

$$\begin{aligned} \xi \left(1 + \frac{\gamma i}{k_{i,j} dx} \right) \phi_{i,j-1} + \left((dx k_{c_{i,j}})^2 - 2(1+\xi) + i 2 dx \gamma k_{i,j} \left(1 - \frac{1}{(k_{i,j} dy)^2} \right) \right) \phi_{i,j} \\ + \xi \left(1 + \frac{\gamma i}{k_{i,j} dx} \right) \phi_{i,j+1} + 2\phi_{i+1,j} = 0 \end{aligned}$$

or

$$(d_{i,j} \ p_{i,j} \ u_{i,j} \ r_{i,j}) \begin{pmatrix} \phi_{i,j-1} \\ \phi_{i,j} \\ \phi_{i,j+1} \\ \phi_{i-1,j} \end{pmatrix} = 0 \quad (4.18)$$

Eq.4.18 describes the partial absorption boundary condition at a negative x directional boundary point (i,j).

Eliminating $\phi_{i,j+1}$ in eq.4.16 with eq.4.2 we have

$$\begin{aligned} \left(1 + \frac{\beta i}{k_{i,j} dy} \right) \phi_{i-1,j} + 2\xi \phi_{i,j-1} + \left((dx k_{c_{i,j}})^2 - 2(1+\xi) + \xi i 2 dy \beta k_{i,j} \left(1 - \frac{1}{(k_{i,j} dx)^2} \right) \right) \phi_{i,j} \\ + \left(1 + \frac{\beta i}{k_{i,j} dy} \right) \phi_{i+1,j} = 0 \end{aligned}$$

or

$$(l_{i,j} \ d_{i,j} \ p_{i,j} \ r_{i,j}) \begin{pmatrix} \phi_{i-1,j} \\ \phi_{i,j-1} \\ \phi_{i,j} \\ \phi_{i+1,j} \end{pmatrix} = 0 \quad (4.19)$$

Eq.4.19 describes the partial absorption boundary condition at a positive y directional boundary point (i,j).

Eliminating $\phi_{i,j+1}$ in eq.4.17 with eq.4.2 we have

$$\left(1 + \frac{\rho i}{k_{i,j} dy}\right) \phi_{i-1,j} + \left((dx k_{c_{i,j}})^2 - 2(1+\xi) + \xi i 2 dy \rho k_{i,j} \left(1 - \frac{1}{(k_{i,j} dx)^2}\right) \right) \phi_{i,j} \\ + 2\xi \phi_{i,j+1} + \left(1 + \frac{\rho i}{k_{i,j} dy}\right) \phi_{i+1,j} = 0$$

or

$$(l_{i,j} \quad p_{i,j} \quad u_{i,j} \quad r_{i,j}) \begin{pmatrix} \phi_{i-1,j} \\ \phi_{i,j} \\ \phi_{i,j+1} \\ \phi_{i-1,j} \end{pmatrix} = 0 \quad (4.20)$$

eq.4.20 describes the partial absorption boundary condition at a negative y directional boundary point (i,j).

b. The third order boundary conditions

The finite difference equation of the third order partial absorption boundary condition, eq.2.50a, with an absorption coefficient α for a positive x directional boundary point (i,j) (Fig.4.4a), is

$$\left(-\frac{b_1}{k_{i,j}^2 dy^2}\right) \phi_{i-1,j-1} + \left(-1 + \frac{2b_1}{k_{i,j}^2 dy^2}\right) \phi_{i-1,j} + \left(-\frac{b_1}{k_{i,j}^2 dy^2}\right) \phi_{i-1,j+1} + \left(\frac{b_1}{k_{i,j}^2 dy^2} - \alpha \frac{ia_1 dx}{k_{i,j} dy^2}\right) \phi_{i,j-1} \\ + \left(1 - \frac{2b_1}{k_{i,j}^2 dy^2} - \alpha i k_{i,j} a_0 dx + \alpha \frac{ia_1 dx}{k_{i,j} dy^2}\right) \phi_{i,j} + \left(\frac{b_1}{k_{i,j}^2 dy^2} - \alpha \frac{ia_1 dx}{k_{i,j} dy^2}\right) \phi_{i,j+1} = 0 \quad (4.21)$$

In eq. 4.21, six grid points $\phi_{i-1,j-1}, \phi_{i-1,j}, \phi_{i-1,j+1}, \phi_{i,j-1}, \phi_{i,j},$ and $\phi_{i,j+1}$ are all in the interior region thus eq.4.21 alone can describe the boundary condition at point (i,j). In matrix form eq.4.21 becomes:

$$(ld_{i,j} \quad lc_{i,j} \quad lu_{i,j} \quad pd_{i,j} \quad pc_{i,j} \quad pu_{i,j}) \begin{pmatrix} \phi_{i-1,j-1} \\ \phi_{i-1,j} \\ \phi_{i-1,j+1} \\ \phi_{i,j-1} \\ \phi_{i,j} \\ \phi_{i,j+1} \end{pmatrix} = 0 \quad (4.22)$$

where $ld_{i,j}$, $lc_{i,j}$, $lu_{i,j}$, $pd_{i,j}$, $pc_{i,j}$, and $pu_{i,j}$ are the coefficients of $\phi_{i-1,j-1}$, $\phi_{i-1,j}$, $\phi_{i-1,j+1}$, $\phi_{i,j-1}$, $\phi_{i,j}$, and $\phi_{i,j+1}$ respectively.

Similarly the finite difference equations of partial absorption boundary conditions (equ 2.50b, 2.50c, and 2.50d) on the boundary points (i,j) in the negative x, positive y, and negative y directional boundary, respectively (see Fig.4.4b, 4.4c and 4.4d) are as follows.

In the negative x directional boundary:

$$\begin{aligned} & \left(-\frac{b_1}{k_{i,j}^2 dy^2} + \gamma \frac{ia_1 dx}{k_{i,j} dy^2} \right) \phi_{i,j-1} + \left(-1 + \frac{2b_1}{k_{i,j}^2 dy^2} + \gamma ik_{i,j} a_0 dx - \gamma \frac{ia_1 dx}{k_{i,j} dy^2} \right) \phi_{i,j} + \\ & \left(-\frac{b_1}{k_{i,j}^2 dy^2} + \gamma \frac{ia_1 dx}{k_{i,j} dy^2} \right) \phi_{i,j+1} + \left(\frac{b_1}{k_{i,j}^2 dy^2} \right) \phi_{i+1,j-1} + \left(1 - \frac{2b_1}{k_{i,j}^2 dy^2} \right) \phi_{i+1,j} + \left(\frac{b_1}{k_{i,j}^2 dy^2} \right) \phi_{i+1,j+1} = 0 \end{aligned} \quad (4.23)$$

or

$$(pd_{i,j} \quad pc_{i,j} \quad pu_{i,j} \quad rd_{i,j} \quad rc_{i,j} \quad ru_{i,j}) \begin{pmatrix} \phi_{i,j-1} \\ \phi_{i,j} \\ \phi_{i,j+1} \\ \phi_{i+1,j-1} \\ \phi_{i+1,j} \\ \phi_{i+1,j+1} \end{pmatrix} = 0 \quad (4.24)$$

where $rd_{i,j}$, $rc_{i,j}$, and $ru_{i,j}$ are the coefficients of $\phi_{i+1,j-1}$, $\phi_{i+1,j}$, and $\phi_{i+1,j+1}$ respectively;

In the positive y directional boundary:

$$\begin{aligned}
& \left(-\frac{b_1}{k_{i,j}^2 dx^2} \right) \phi_{i-1,j-1} + \left(\frac{b_1}{k_{i,j}^2 dx^2} - \beta \frac{ia_1 dy}{k_{i,j} dx^2} \right) \phi_{i-1,j} + \left(-1 + \frac{2b_1}{k_{i,j}^2 dx^2} \right) \phi_{i,j-1} + \\
& \left(1 - \frac{2b_1}{k_{i,j}^2 dx^2} - \beta ik_{i,j} a_0 dy + \beta \frac{ia_1 dy}{k_{i,j} dx^2} \right) \phi_{i,j} + \left(-\frac{b_1}{k_{i,j}^2 dx^2} \right) \phi_{i+1,j-1} + \\
& \left(\frac{b_1}{k_{i,j}^2 dx^2} - \beta \frac{ia_1 dy}{k_{i,j} dx^2} \right) \phi_{i+1,j} = 0
\end{aligned} \tag{4.25}$$

or

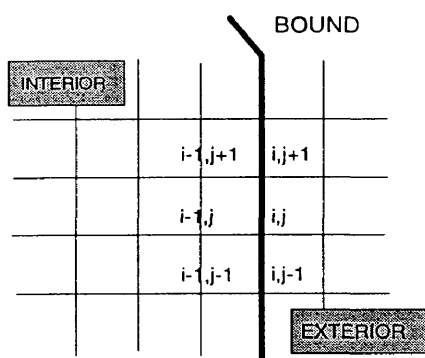
$$\begin{pmatrix} \phi_{i-1,j-1} \\ \phi_{i-1,j} \\ \phi_{i,j-1} \\ \phi_{i,j} \\ \phi_{i+1,j-1} \\ \phi_{i+1,j} \end{pmatrix} = 0 \tag{4.26}$$

In the negative y directional boundary:

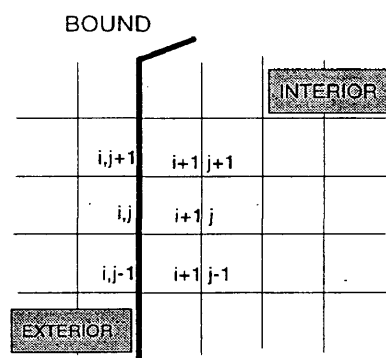
$$\begin{aligned}
& \left(-\frac{b_1}{k_{i,j}^2 dx^2} + \rho \frac{ia_1 dy}{k_{i,j} dx^2} \right) \phi_{i-1,j} + \left(\frac{b_1}{k_{i,j}^2 dx^2} \right) \phi_{i-1,j+1} + \\
& \left(-1 + \frac{2b_1}{k_{i,j}^2 dx^2} + \rho ik_{i,j} a_0 dy - \rho \frac{ia_1 dy}{k_{i,j} dx^2} \right) \phi_{i,j} + \left(1 - \frac{2b_1}{k_{i,j}^2 dx^2} \right) \phi_{i,j+1} + \\
& \left(-\frac{b_1}{k_{i,j}^2 dx^2} + \rho \frac{ia_1 dy}{k_{i,j} dx^2} \right) \phi_{i+1,j} + \left(\frac{b_1}{k_{i,j}^2 dx^2} \right) \phi_{i+1,j+1} = 0
\end{aligned} \tag{4.27}$$

or

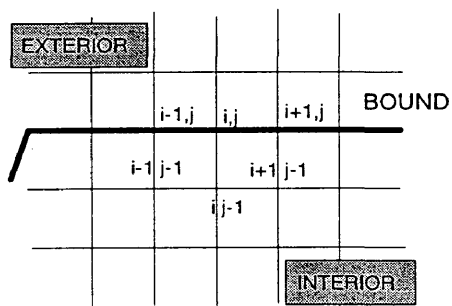
$$\begin{pmatrix} \phi_{i-1,j} \\ \phi_{i-1,j+1} \\ \phi_{i,j} \\ \phi_{i,j+1} \\ \phi_{i+1,j} \\ \phi_{i+1,j+1} \end{pmatrix} = 0 \tag{4.28}$$



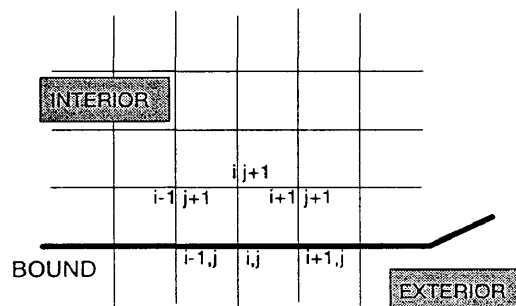
(a)



(b)



(c)



(d)

Fig.4.4: Sketch of four directional boundaries for the third order partial absorption boundary conditions. a, b, c, and d are for the positive x, negative x, positive y, and negative y directional boundary, respectively.

4.2.3 finite difference model with the second order absorption boundary conditions

The finite difference governing equation (eq.4.2), Dirichlet boundary conditions (eq.4.6-4.11), and the second order partial absorption boundary conditions (eq.4.14,4.18-4.20) construct a finite difference model with the second order partial absorption boundary condition. Applying eq.4.2 (governing equation), eq.4.11 (Dirichlet boundary condition), and eq.4.19 (absorption boundary) to the grid points $(i,2), (i,3), \dots, (i,n_b-1)$, and (i,n_b) (see Fig.4.1), in which n_b is the number of grid number in y direction in interior region, we have a system of linear equations. In matrix form they can be written as follows:

$$\begin{pmatrix}
 \overline{1_{i2}} & 0 & \dots & 0 & 0 & p_{i2} & u_{i2} & 0 & \dots & 0 & r_{i2} \\
 & \overline{1_{i3}} & 0 & \dots & 0 & d_{i3} & p_{i3} & u_{i3} & 0 & \dots & 0 & r_{i3} \\
 & & & & & & \dots & \dots & & & & \\
 \overline{0} & & & & & & & & & & & \\
 & \overline{1_{in_b-1}} & 0 & \dots & 0 & d_{in_b-1} & p_{in_b-1} & u_{in_b-1} & 0 & \dots & 0 & r_{in_b-1} \\
 & & \overline{1_{in_b}} & 0 & \dots & 0 & d_{in_b} & p_{in_b} & 0 & 0 & \dots & 0 & r_{in_b} \\
 & & & & & & & & & & \overline{n_b-1} & & \overline{r_{in_b}}
 \end{pmatrix}
 \begin{pmatrix}
 \phi_{i-1,2} \\
 \phi_{i-1,3} \\
 \vdots \\
 \phi_{i-1,n_b-1} \\
 \phi_{i-1,n_b} \\
 \phi_{i2} \\
 \phi_{i3} \\
 \phi_{i4} \\
 \vdots \\
 \phi_{in_b-2} \\
 \phi_{in_b-1} \\
 \phi_{in_b} \\
 \phi_{i+1,2} \\
 \phi_{i+1,3} \\
 \vdots \\
 \phi_{i+1,n_b-1} \\
 \phi_{i+1,n_b}
 \end{pmatrix}
 =
 \begin{pmatrix}
 -\xi C \\
 0 \\
 \cdot \\
 \cdot \\
 0 \\
 0 \\
 0
 \end{pmatrix}
 \tag{4.29}$$

Because of the space limit, the subscript 'ij' of each elements in matrices of eq.4.29 represents 'i,j', e.g. ϕ_{ij+1} represents $\phi_{i,j+1}$. It is noticed that the above $(n_b-1) \times 3(n_b-1)$ coefficient matrix is a band matrix with bandwidth of $2n_b-1$. Both upper bandwidth and lower bandwidth of the matrix are n_b-1 . The unknown column matrix has length of $3(n_b-1)$ because the left and right neighbor points $(i-1,j)$ and $(i+1,j)$ are involved in the finite difference equation of point (i,j) . For the grid points $(i,2), (i,3), \dots, (i,n_b-1),$ and (i,n_b) , there are n_b-1 finite difference equations, therefore, the right side column matrix has a length of n_b-1 .

Expanding eq.4.29 to the whole interior region in Fig.4.1, with the Dirichlet boundary conditions (eq.4.6-4.11), and the partial absorption boundary conditions (eq.4.14,4.18-4.20) for the boundaries and eq.A.1-eq.A.4 (see Appendix) for the corners of the boundaries, we have a system of equations as follows:

or

$$\mathbf{A}_2 \Phi = \mathbf{b} \quad (4.31)$$

where i and j are indices in the x and y direction; $n_b(i)$ is the number of grid points in y direction for the i -th x directional grid location; m_b is the maximum grid number in the x direction; Φ is the unknown column matrix to be solved; \mathbf{b} is a column matrix; and the \mathbf{A}_2 is a square matrix containing the coefficients of the unknowns $\phi_{i,j}$. Also Because of the space limit, the subscript 'ij' of each elements in matrices of eq.4.30 represents 'i,j', e.g. ϕ_{ij+1} represents $\phi_{i,j+1}$.

The number of grid points in the interior region (Fig.4.1) determines the dimension of the matrix \mathbf{A}_2 . The following formula is used to calculate this number (map):

$$map = \sum_{i=1}^{m_b} n_b(i)$$

and the dimension of matrix \mathbf{A}_2 is $map \times map$.

Matrix \mathbf{A}_2 is a band matrix. The upper bandwidth of matrix \mathbf{A}_2 is the maximum 'distance' between $\phi_{i,j}$ and $\phi_{i+1,j}$, and the lower bandwidth is the maximum 'distance' $\phi_{i,j}$ and $\phi_{i-1,j}$. The 'distance' is defined as the location number difference of one element, i.e. $\phi_{i,j}$, in the unknown column matrix Φ to the left (or right) element, i.e. $\phi_{i-1,j}$ (or $\phi_{i+1,j}$) in the same matrix Φ . for this reason, the bandwidth of \mathbf{A}_2 is actually depend on the way we align the grid and the study domain.

4.2.4 *finite difference model with
the third order absorption boundary condition*

If the third partial absorption boundary conditions (eq.4.22, 4.24, 4.26, and 4.28) is used instead of the second order ones, a finite difference model with the third order partial absorption boundary conditions can be obtained. Like derivation of the model with the second order absorption boundary condition, applying the eq.4.3,4.6-4.11, 4.22, 4.24, 4.26, and 4.28 to the whole domain in Fig.4.1, we can obtain a system of equation as follows:

or

$$\mathbf{A}_3 \Phi = \mathbf{b} \quad (4.33)$$

For the same reason as eq.4.29, the subscript 'ij' of each elements in matrices of eq.4.32 represents 'i,j', e.g. ϕ_{ij+1} represents $\phi_{i,j+1}$. The coefficient matrix \mathbf{A}_3 in eq.4.33 has exactly the same size as matrix \mathbf{A}_2 . The bandwidth of matrix \mathbf{A}_3 , however, is larger than that of matrix \mathbf{A}_2 . The reason is that the boundary conditions (eq.4.22, 4.24, 4.26 and 4.28) involves six grid points, thus, the upper bandwidth is determined by the maximum 'distance' between $\phi_{i,j}$ and $\phi_{i+1,j+1}$ rather than between $\phi_{i,j}$ and $\phi_{i+1,j}$ in matrix Φ , and the lower bandwidth is determined by the maximum 'distance' between $\phi_{i-1,j-1}$ and $\phi_{i,j}$ rather than between $\phi_{i-1,j}$ and $\phi_{i,j}$. For the same study domain and grid alignment, the bandwidth of matrix \mathbf{A}_3 is two more than that of matrix \mathbf{A}_2 . The column matrices Φ and \mathbf{b} are identical to those given in eq.4.31.

4.3 Numerical model organization

Fig.4.5 shows the flow chart of the model. Procedures include inputting bathymetric data and boundary information, sorting the different grid points and generating a band matrix, and interacting with the band matrix solver.

4.3.1 bathymetric data preparation

Bathymetric data can be generated through digitizing and

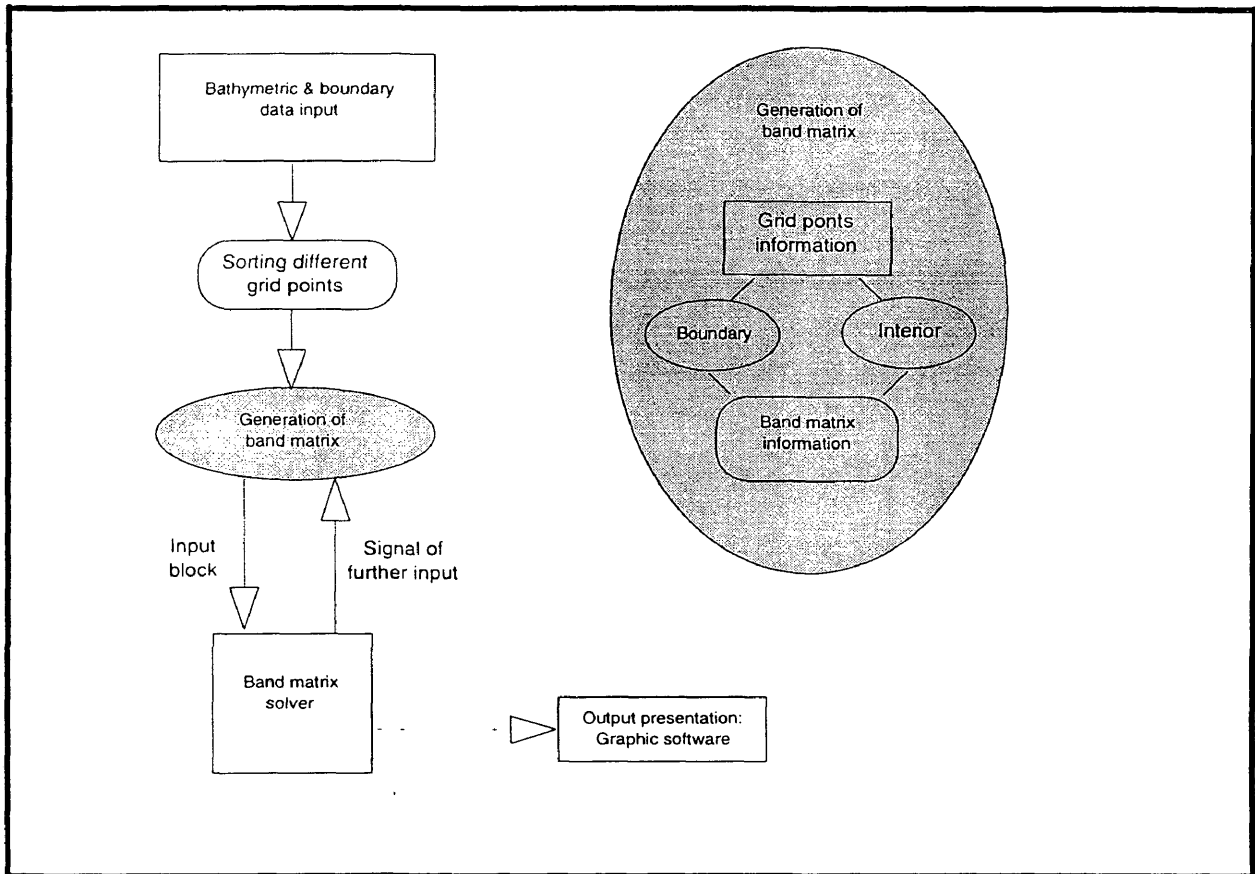


Fig.4.5: Flow chart of the present numerical model organization.

gridding processes. **Digitizing** converts the continuous contour lines and supplemental depth information from a given bathymetric chart to a series of discrete data points. **Gridding** changes the discrete data points, which are non-uniformly spaced, to even spaced grid points that cover the computational domain. There are several commercial software packages (e.g. SURFER and MATLAB) available to perform gridding, therefore, the gridding will not be further discussed here.

The bathymetric data after gridding includes depth information on all grid points (both the interior and exterior region). In order to let a computer separate the grid points in the interior region and the exterior region automatically, the depths at all grid points in the exterior region are assigned to be 999.9, the depths of all points at the boundaries with a partial absorption boundary condition are assigned to be 101.0, and the depths of all points at the boundaries with a Dirichlet boundary condition are assigned to be 103.0.

4.3.2 *Boundary information*

In addition to the simple boundary conditions specified by depth = 101.0 for the Dirichlet boundary condition and depth = 103.0 for the partial absorption boundary condition, more information is required for the radiation, reflection and partial reflection boundary conditions (see Chapter 2) on the

boundaries of depth = 103.0. This information is given by four absorption coefficients $\alpha^0_{i,j}$, $\beta^0_{i,j}$, $\gamma^0_{i,j}$, and $\rho^0_{i,j}$ in four directions at any point (i,j) of boundaries. At any point (i,j) of interior region all four absorption coefficients are assigned to be zero. Because boundary conditions do not apply to the grid points of the interior region, the zero reflection coefficients of these points will not be used.

4.3.3 *sorting different grid points*

Based on the bathymetric data the grid points at interior region and the boundaries are sorted out. Each of these grid points is then associated with an individual equation (eq.4.2, 4.6-4.11, 4.22, 4.24, 4.26, or 4.28) as well as an absorption coefficient $\alpha^0_{i,j}$, $\beta^0_{i,j}$, $\gamma^0_{i,j}$, or $\rho^0_{i,j}$ for band matrix generation.

4.3.4 *Generation of a band matrix*

As discussed previously, the coefficient matrices \mathbf{A}_2 and \mathbf{A}_3 (eq.4.31 and eq.4.33) are both band matrices. Moreover even in the band area there are still many zero elements. In fact, in matrix \mathbf{A}_2 there are at most only five nonzero elements in each row and in matrix \mathbf{A}_3 there are at most six nonzero elements in each row. The position of each nonzero element in each of the matrix is determined by the alignment of x-y coordinates and the location of each unknown in the study domain.

If we only save the nonzero elements as well as its position in the matrix, the requirement of storage for the matrix will be intensively reduced. The following table shows the storage required for one row of matrix \mathbf{A}_3 :

Table 1. Storage technique for nonzero elements in matrix \mathbf{A}_3

Array storing elements in \mathbf{A}_3	Corresponding unknowns in Φ	Array storing element locations in \mathbf{A}_3
$\mathbf{a}(k, 1)$	$\phi_{i-1, j-1}$	$\mathbf{ia}(k, 1)$
$\mathbf{a}(k, 2)$	$\phi_{i-1, j}$	$\mathbf{ia}(k, 2)$
$\mathbf{a}(k, 3)$	$\phi_{i-1, j+1}$	$\mathbf{ia}(k, 3)$
$\mathbf{a}(k, 4)$	$\phi_{i, j-1}$	$\mathbf{ia}(k, 4)$
$\mathbf{a}(k, 5)$	$\phi_{i, j}$	$\mathbf{ia}(k, 5)$
$\mathbf{a}(k, 6)$	$\phi_{i, j+1}$	$\mathbf{ia}(k, 6)$
$\mathbf{a}(k, 7)$	$\phi_{i+1, j-1}$	$\mathbf{ia}(k, 7)$
$\mathbf{a}(k, 8)$	$\phi_{i+1, j}$	$\mathbf{ia}(k, 8)$
$\mathbf{a}(k, 9)$	$\phi_{i+1, j+1}$	$\mathbf{ia}(k, 9)$

In table 1 $\phi_{i-1, j-1}$, $\phi_{i-1, j}$, $\phi_{i, j+1}$, $\phi_{i, j-1}$, $\phi_{i, j}$, $\phi_{i, j+1}$, $\phi_{i-1, j-1}$, $\phi_{i-1, j}$, and $\phi_{i-1, j+1}$ are unknowns for an individual finite difference equation of either the governing equation or the boundary conditions (i.e. eq.4.3, 4.6-4.11, 4.22, 4.24, 4.26,

or 4.28); $\mathbf{a}(k,\text{num})$ and $\mathbf{ia}(k,\text{num})$ are elements of two column matrices for storing the coefficients of unknowns and their relative locations in \mathbf{A}_3 , k is a row index ranged from 1 to map , and $\text{num}=1,\dots,9$. It is noticed that besides the coefficients of unknowns in matrix \mathbf{A}_3 , all other elements are zero, and the coefficients of unknowns are the elements located in the diagonal, the four superdiagonal, and the four subdiagonal of matrix \mathbf{A}_3 . Therefore, array $\mathbf{a}(\text{map},9)$ only stores the elements of these diagonal, superdiagonal, and subdiagonal, and $\mathbf{ia}(\text{map},9)$ stores the locations of the corresponding elements in matrix \mathbf{A}_3 .

The reason of using nine storage units ($\text{num}=1,\dots,9$) for the coefficients and their locations respectively, instead of six storage units required by the maximum number of unknowns in eq.4.22, 4.24, 4.26, or 4.28, is that the range of the unknown locations in the study domain is from grid point $(i-1,j-1)$ to $(i+1,j+1)$, and it is easy to book-keep the unknown coefficient locations in the matrix \mathbf{A}_3 by nine storage units. Because of this, some elements in $\mathbf{a}(k,\text{num})$ and $\mathbf{ia}(k,\text{num})$ are not used. But, compared with storing full band area elements in the \mathbf{A}_3 , this technique is still much economic.

A similar technique can be used for the nonzero elements and their positions in \mathbf{A}_2 . The storage units are $\mathbf{a}(\text{map},5)$ and $\mathbf{ia}(\text{map},5)$.

By the completion of storing all coefficients and their position information respectively into $\mathbf{a}(\text{map},9)$ and $\mathbf{ia}(\text{map},9)$,

the job of band matrix generation is done. The two matrix $\mathbf{a}(\text{map},9)$ and $\mathbf{ia}(\text{map},9)$ for the \mathbf{A}_3 , can be saved into a hard disk file for the block-wise band matrix solver presented in Chapter 3. If $\mathbf{a}(\text{map},9)$ and $\mathbf{ia}(\text{map},9)$ are small because of the small number of grid points in study domain, we can keep them in the computer memory.

4.3.5 interaction with the block-wise band matrix solver

Because the block-wise band matrix solver requires full information (both nonzero and zero elements) in a block of band area for solution, the information stored in $\mathbf{a}(\text{map},9)$ and $\mathbf{ia}(\text{map},9)$ must first be converted to a full block of elements in band area, and then this block of elements is pushed into the working matrix in the solver. The sequence of block by block conversion is same as that of block by block pushing-in of a new matrix into the working matrix from the second sleeping matrix defined in Chapter 3. The conversion is in conjunction with the whole elimination process of the solver.

4.3.6 model products

The output of the model is the complex velocity potential $\phi_{i,j}$ on each grid point of the interior region in the study domain. Wave height, surface water particle velocity and wave phase can be calculated from $\phi_{i,j}$ by the following formulas:

$$H_{i,j} = \frac{2\omega}{g} |\phi_{i,j}| \quad (4.34)$$

$$u_{i,j} = -Re\left(\frac{\phi_{i+1,j} - \phi_{i-1,j}}{dx}\right) \quad (4.35)$$

$$v_{i,j} = -Re\left(\frac{\phi_{i,j+1} - \phi_{i,j-1}}{dy}\right) \quad (4.36)$$

$$s_{i,j} = \tan^{-1}\left(\frac{Im(\phi_{i,j})}{Re(\phi_{i,j})}\right) \quad (4.37)$$

where $H_{i,j}$ is wave height; $u_{i,j}$ and $v_{i,j}$ are the surface water particle velocity in the x direction and the y direction respectively, this is because the horizontal function $\phi(x,y)$ in this case is the first order approximation of function $\phi_h(x,y,z)$ (eq.2.8) and, therefore, denotes the surface velocity potential; $s_{i,j}$ is the wave phase; $Re(f)$ and $Im(f)$ are the real and imaginary part of a complex value f .

From the definition of the wave number vector:

$$\mathbf{k} = \nabla s \quad (4.38)$$

where s is wave phase, $\mathbf{k} = (k\cos\theta, k\sin\theta)$ is the wave number vector, $k = |\mathbf{k}|$, and θ is the wave angle, we can calculate the wave angle as follows:

$$\theta_{i,j} = \tan^{-1}\left[\left(\frac{s_{i+1,j} - s_{i-1,j}}{s_{i,j+1} - s_{i,j-1}}\right) \frac{\Delta x}{\Delta y}\right] \quad (4.39)$$

CHAPTER 5

MODEL VERIFICATION AND COMPARISON

5.1 Model verification

Three well documented cases were used to verify the numerical model. They are wave diffraction after a breakwater gap (BWG), wave diffraction after a straight short breakwater (SSB), and wave refraction and diffraction after an elliptic shoal (ELS). The model runs for case BWG and SSB were made on IBM 486DX 33MHZ 4MB RAM PC, and model run for case ELS was made on IBM 486DX 33MHZ 16MB RAM PC. The parameters specified for each case run are shown in Table 2 and the model

Table 2. Parameters of the three study cases and the model performance of each case.

Case	Grid number	dx(m)	dy(m)	Incident wave length (m)	Wave Period (sec)	Incident wave height (cm)	CPU time* (min)
BWG	80×200	0.156	0.156	1.56	1.0	1.0	11
SSB	200×60	0.120	0.120	1.20	0.9	4.1	8
ELS	160×200	0.125	0.115	1.22	1.0	1.01	50

*CPU time is based on a IBM 486DX 33MHZ 4MB RAM PC for case BWG and SSB and a IBM 486DX 33MHZ 16MB RAM PC for case ELS.

performance for each case is also given in Table 2.

5.1.1 Wave diffraction after a breakwater gap (BWG)

This case is well documented in the Shore Protection Manual (1972). In this case, only wave diffraction is considered because of constant water depth. The study domain is a rectangular basin measuring 12.48m×15.6m (see Fig.5.1). On the bottom of the domain, there is a breakwater, 9.36m long, with a gap of 3.12m in the middle. The other three sides of the domain have passing through boundary conditions. The water depth is 0.9m in the entire domain. An incident wave with period of 1.0s and a wave height of 0.01m approaches normally to the breakwater. Therefore, the wave length is 1.56m, the domain has a size of 8 wave length × 10 wave length, and the gap of the breakwater has a size of 2 wave length.

Fig.5.2a shows the experimental and calculated results of contours of the wave diffraction coefficient in the domain. It is noticed that the two results are almost the same except (1) the calculated result underestimates the diffraction coefficient by a maximum of 6% near the point (0,5), and (2) the calculated curves are not smooth.

The experimental results shown in Fig.5.2a are from the Shore Protection Manual. The experimental data came from Johnson (1953). It was mentioned in the Shore Protection

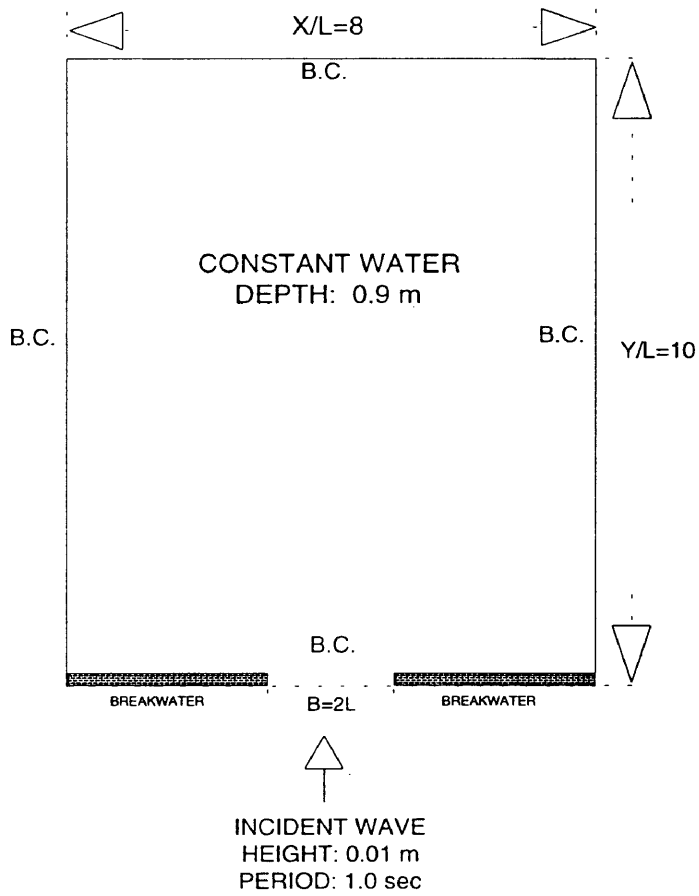


Fig.5.1: Layout of the study domain of breakwater gap case.

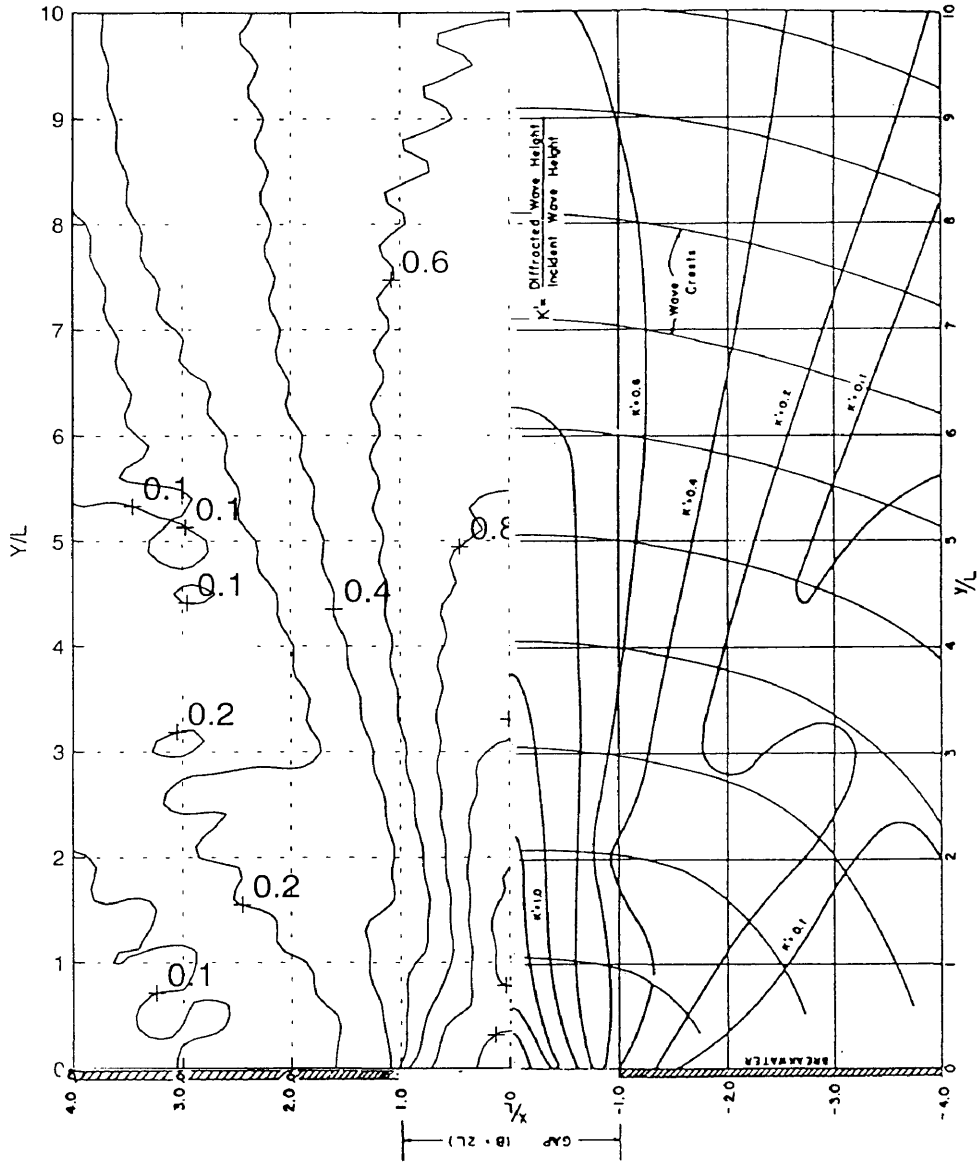


Fig.5.2a: Contours of the wave diffraction coefficient after a breakwater gap. Left side is the calculated result; Right side is the experimental result (after Shore Protection Manual, 1972).

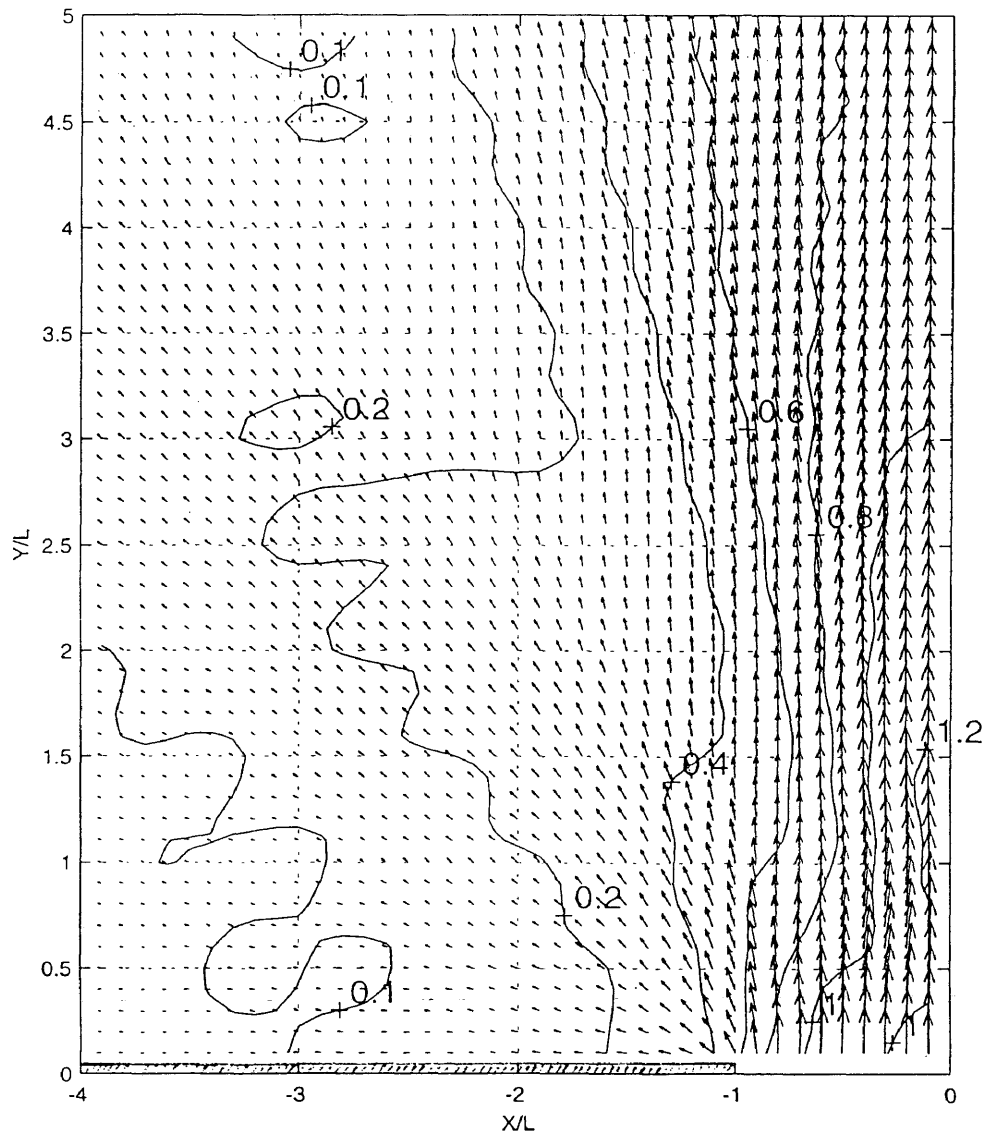


Fig.5.2b: Wave vectors and contours of the wave diffraction coefficient after a breakwater gap.

Manual that contours were drawn conservatively. This means the actual diffraction coefficient was slightly smaller than that shown in the diagram.

The reason for having a smaller calculated result near the opening is not clear. The schemes of discretization of partial differential equations (e.g. eq.4.1) may be a possible reason. For example, in this study a second order finite difference approximation is used to discretize the governing equation (eq. 4.1). If a higher order approximation is used, the result may be improved, because the high order approximation, in other word, higher order accuracy is needed where the wave height gradient, $\partial H/\partial s$, is large, where H is the wave height and s represents the path. Another possible reason is that the experimental data may include some nonlinear effects from the tips of breakwater, and the nonlinear effects, however, are not included in the linear model presented here (eq.4.1).

The contour plot was generated using MATLAB software. There is no control of the smoothness. This may be one of the reasons for the rough curves. Another possible reason for the rough curves may be the computational error. Decrease of grid size may smooth out the roughness.

The wave vectors shown in Fig.5.2b indicate that they bend after the breakwater. The change of wave angle depends on the location, and a maximum of nearly 90° can be found near the breakwater but away from the opening. This demonstrates

the capability of the mild slope equation to handle wave diffraction. The parabolic approximation of the mild slope equation does improve the computing speed, but it fails to simulate strong wave diffraction similar to what is presented in Fig.5.2b.

From Fig.5.2b, It can also be seen that along the left boundary, from $Y/L=0$ to $Y/L=5$, the approaching wave angles increased from zero to almost 60° . However, there was no significant reflection observed around the boundary because of large approaching wave angles (see Fig.2.5). This is because the wave energy along the boundary is much smaller than that near the region of the gap. Thus, even with a high reflection coefficient, the outcomes from the model with second order approximation of radiation boundary condition were still reasonable.

5.1.2 *Wave diffraction after a straight short breakwater (SSB)*

Goda (1971) reported the following case in his study: An incident wave with period of 0.9s and wave height of 0.041m approaches normally to a straight short breakwater located in the middle of one side of a rectangular domain. The three other sides of the domain are open boundaries where the radiation boundary condition was applied. The water depth of the entire domain is a constant, 0.4m. The length of the breakwater is two wave lengths.

In fact, using a series of Mathieu functions, Goda solved the governing equation (eq.4.1) analytically for wave reflection and diffraction by a vertical elliptical cylinder and then derived the exact general solution for a straight short breakwater case by deforming the elliptical cylinder into a plate of infinitesimal thickness. Using his general solution for the straight short breakwater, Goda gave the solution of the above case in a 5 wave length \times 6 wave length domain (see Fig.5.4) in which only wave diffraction was concerned.

For model verification, we set up a computational domain as shown in Fig.5.3. Because the study domain is symmetric, Goda only gave the results in one half of the domain (left half of Fig.5.4). The present calculation was done in the whole domain because of the negligence of using this symmetric feature. Actually, if the symmetric feature is used by specifying a total reflection boundary condition at the center of the domain (i.e., eq.2.48, with $\alpha=0$) the calculation can be made more economically. It is noticed that in the x direction, the computational domain specified in this study was twice as large as Goda's domain. The reason for this is discussed later.

Fig.5.4 compares the analytic and calculated contours of the wave diffraction coefficient. The two results are almost identical except for some roughness in the calculated curves for the same reason discussed in the previous section. The

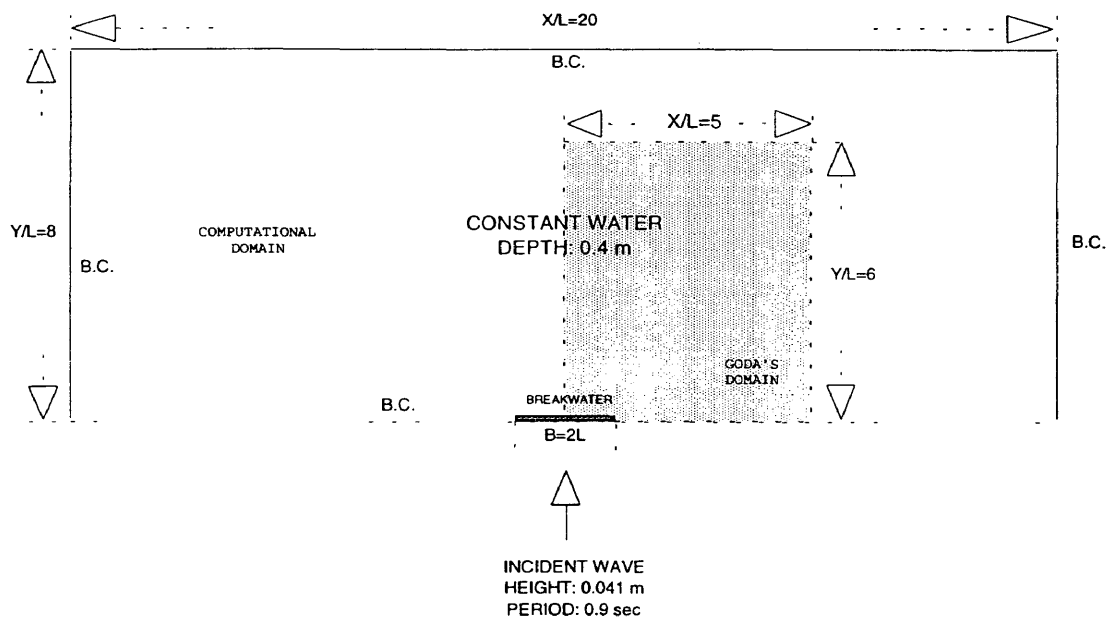


Fig.5.3: Layout of the study domain of the straight short breakwater case.

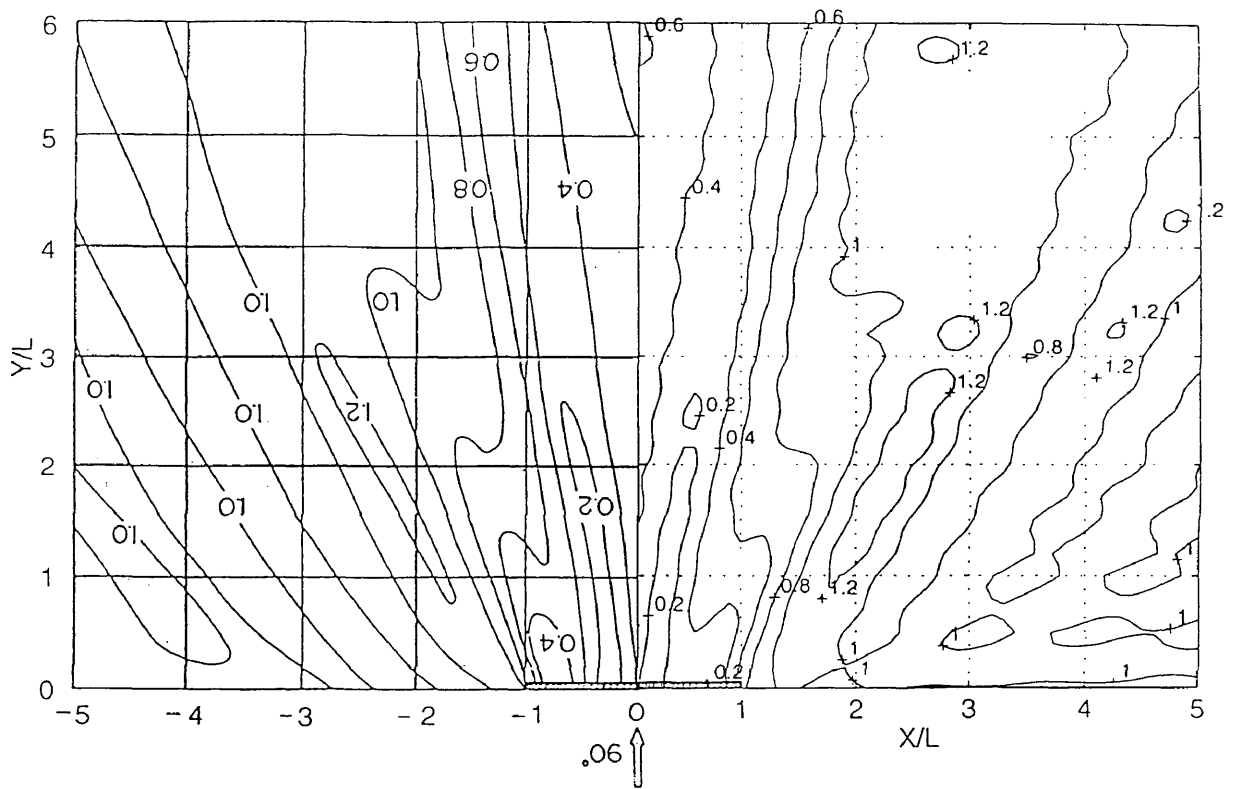


Fig.5.4a: Contours of the wave diffraction coefficient after a straight short breakwater. Left side is the analytical solution (after Goda, 1971) and right side is the calculated result.

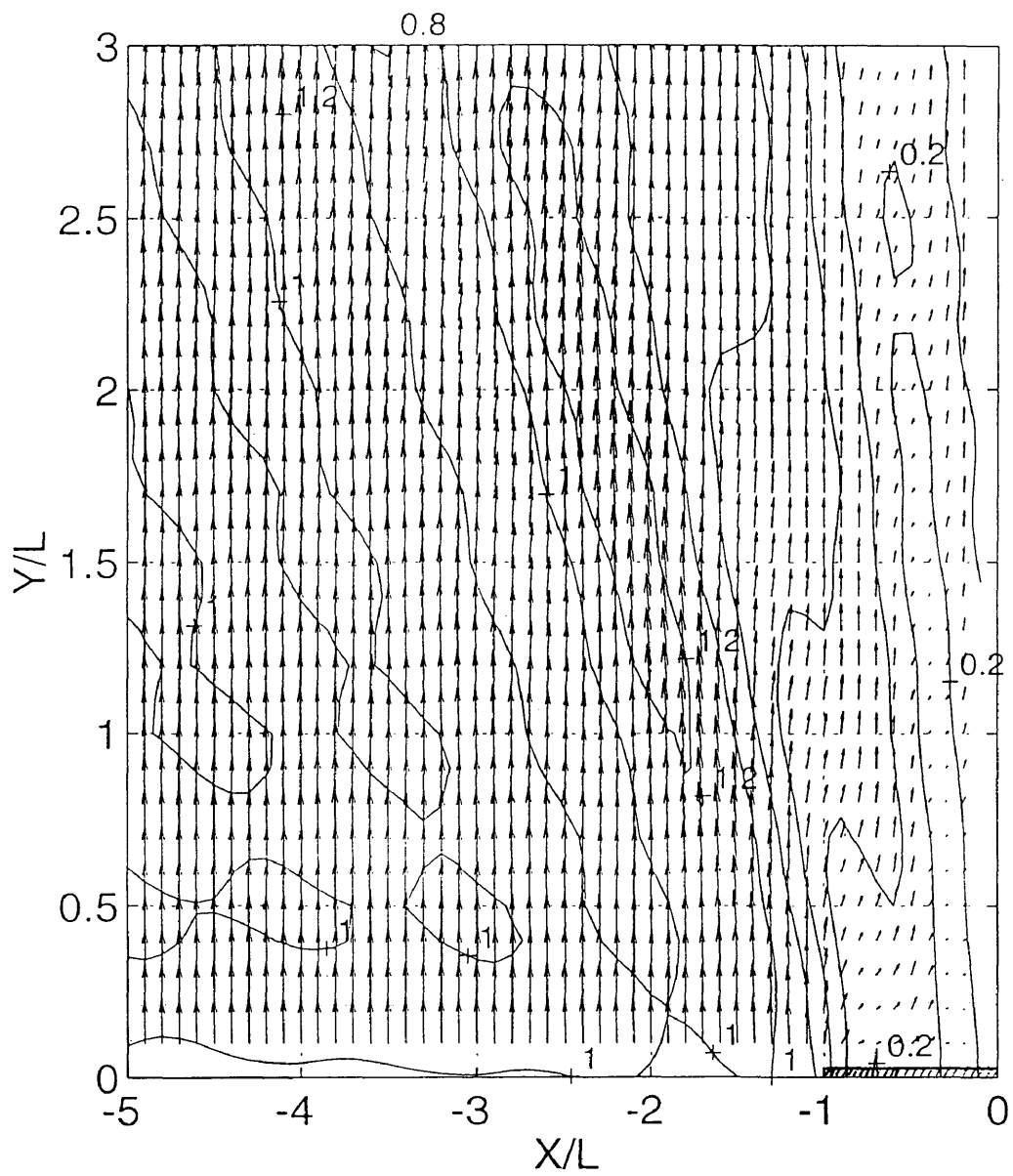


Fig.5.4b: Wave vectors and contours of the wave diffraction coefficient after a straight short breakwater.

wavv vectors shown in Fig.5.4b provide two type of information: (1) The wave vectors near the left side bound are parallel to the bound. This means the approaching wave angle specified in Fig.2.5 is close to 90° . Further discussion about this is given next; (2) The wave vectors show that when a wave approaches the center right behind the breakwater ($-1 < X/L < 0$, $Y/L=0.1$) the wave height decreases and the wave angle turns gradually to 0° . The wave heights along $Y/L=0.1$ seem to be modulated by another wave. In fact, there is another wave train coming from the other side of the domain because of the diffraction from the other side of the breakwater ($X/L > 1$). The wave heights displayed in Fig.5.4b are actually a combination of two wave trains: One propagates from left to right with its wave height decreasing along a line from $X/L=-1$ to 1, and the other is opposite to the first. The wave vectors show the directions and heights of the combined waves.

It seems that we used two similar diffraction cases to verify the numerical model. In fact, the two cases are quite different in respect to the breakwater and the treatment of the side boundaries. In case BWG (Fig.5.2a), waves can only enter the domain through the gap of breakwater which actually extends to infinity in both the positive and negative x directions. Because of this, the energy behind the breakwater is only from diffraction of the waves. Therefore, the waves approaching the two sides of the domain possess much less energy than those near the gap, and the angles of the

approaching waves are always small (Fig.5.2b). However, in the SSB case (Fig.5.4a), since the breakwater is finite length, the waves near the side boundaries are almost not affected by the breakwater, thus, the angles of approaching waves are close to 90° (Fig.5.4b). As discussed in Chapter 2, for any approximation of a radiation boundary condition, a large approaching wave angle to the boundary leads to wave reflection back to the computational domain. Thus, for the BWG case, there is almost no reflection because of the small approaching wave angle. For the SSB case, however, there is significant reflection even for Kirby's approximation, because the approaching wave angle, θ , is larger than 80° . For the above reason, we used both cases to test the approximation of boundary conditions and tried to find an alternative to treat the boundaries with a large approaching wave angle to avoid the reflection back into the domain of interest. When using a second order approximation of the radiation boundary condition, eq.2.36, an angle of more than 30° is considered large. When using Kirby's approximation, eq.2.42, an angle of more than 80° is considered large.

By numerical experiment, one alternative way was found to treat a boundary with a large approaching wave angle. That is to move the boundary far away from the domain of interest, in another words, to enlarge the computational domain. In the SSB case, doubling the domain given by Goda in x-direction, we obtained a good result from the second order approximation of

radiation boundary condition.

5.1.3 *Wave diffraction and refraction after an elliptic shoal (ELS)*

Berkhoff *et al.* (1982) published measurements obtained from a physical model study on wave refraction and diffraction after an elliptic shoal to verify his mild slope equation (eq.2.14). The physical model had a bottom bathymetry shown in Fig.5.5. It consisted of an elliptic shoal situated on a slope beach (1:50). At one end of the model, $y=10$ m, waves were generated and at the other end, $y=-15$ m, the wave energy was nearly totally dissipated by breaking on a gravel beach. For a large number of points (minimal grid size $0.25\text{m} \times 0.25\text{m}$) of the study domain the wave height and the wave phase had been recorded.

In this study the present numerical model was used to simulate the wave transformation in the domain specified by Berkhoff *et al.* (1982). The incident wave with period 1.0s and wave height of 0.0106m was given at the top of the domain. The radiation boundary conditions were given to the two lateral boundaries. Since the purpose of solving this case was model verification, we were only interested in the area just behind the elliptic shoal, where the combined wave diffraction and refraction phenomenon was important. Although the wave breaking was expected to occur near the shoreline, it was not of interest for this study because the present linear model

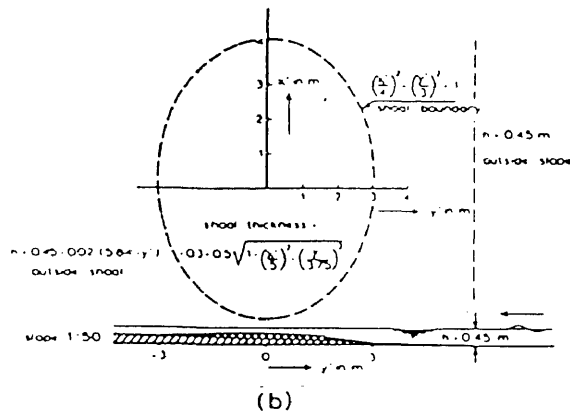
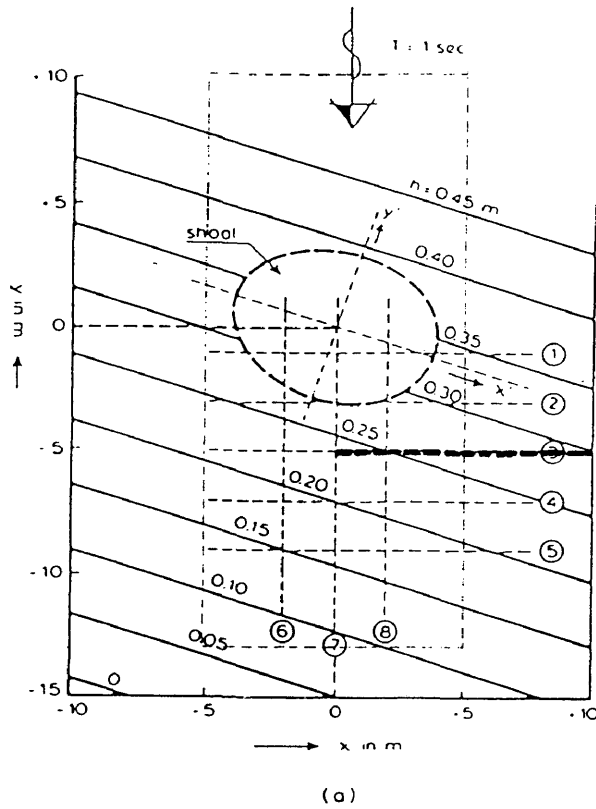


Fig.5.5: Layout of the study domain of the elliptic shoal case (after Berkhoff *et al.*, 1982). The additional thick dashed line represents a breakwater specified by Panchang *et al.* (1991).

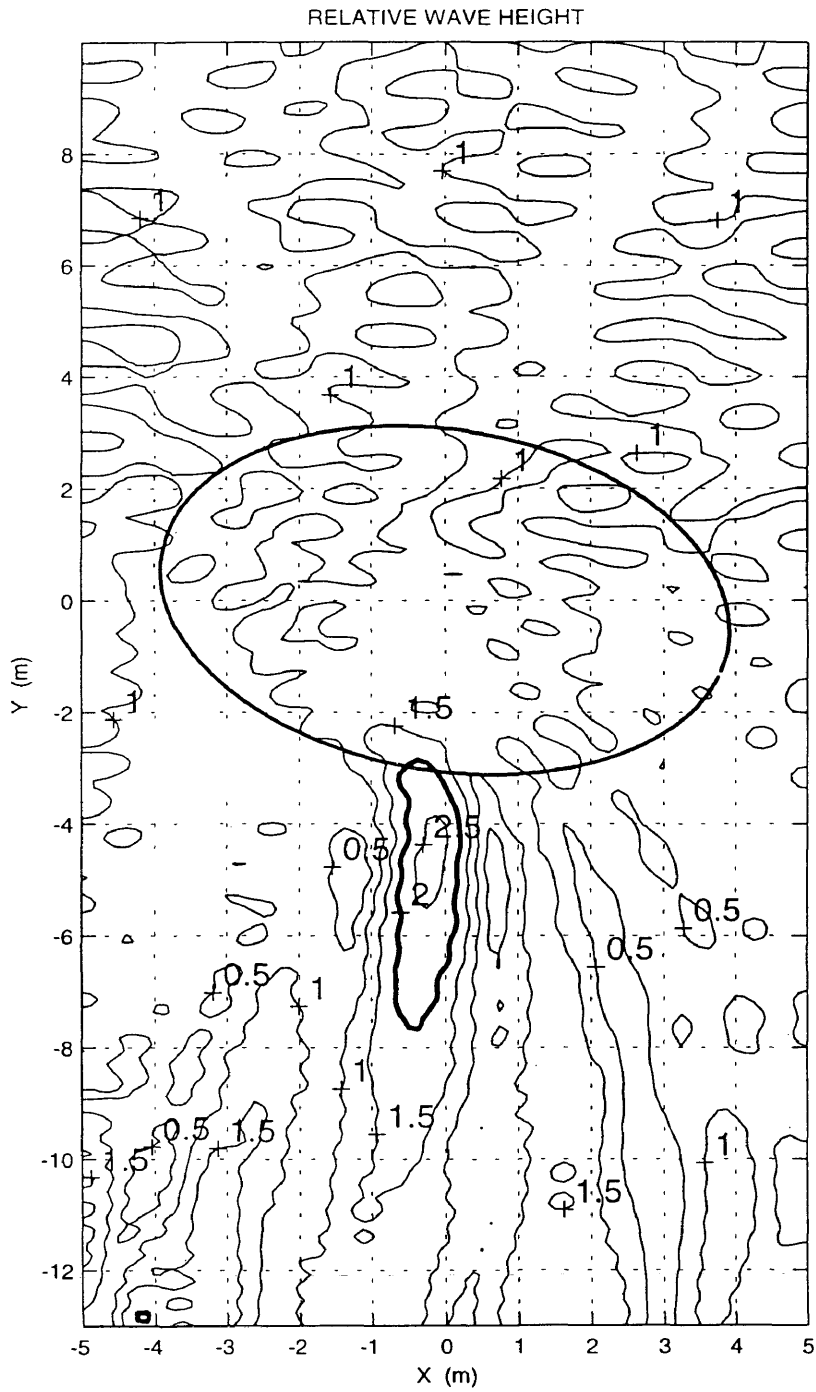
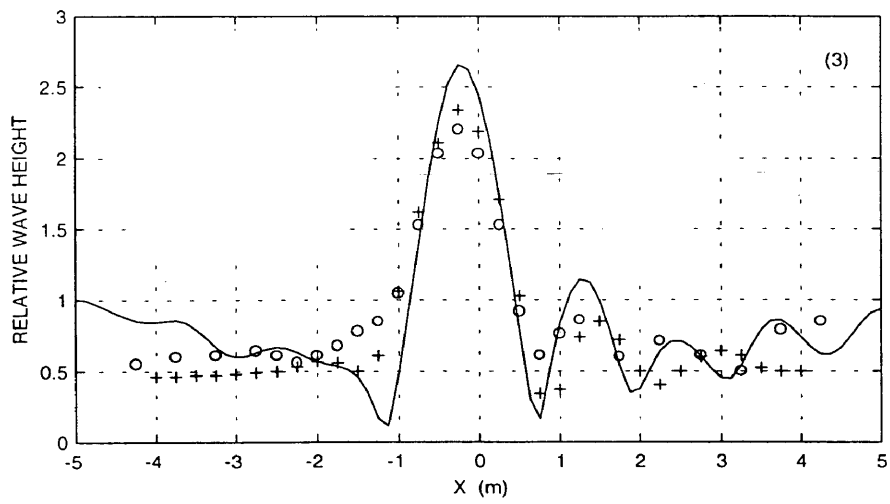
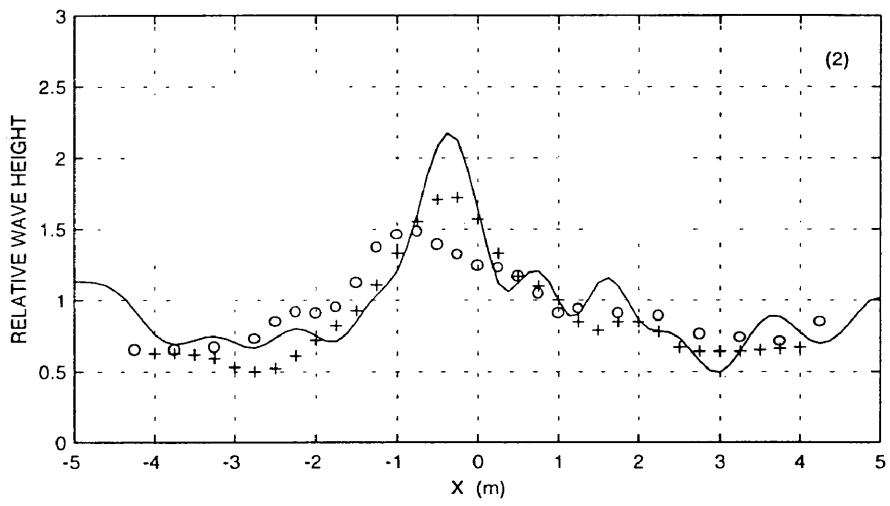
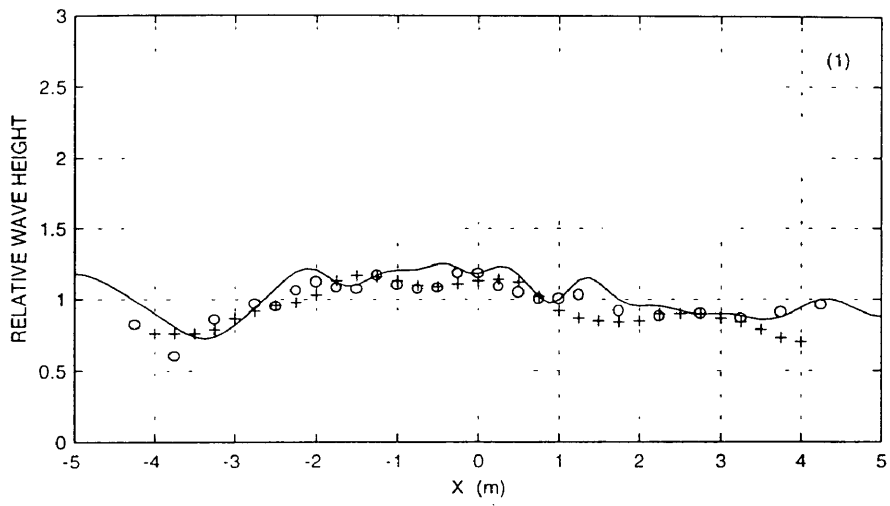
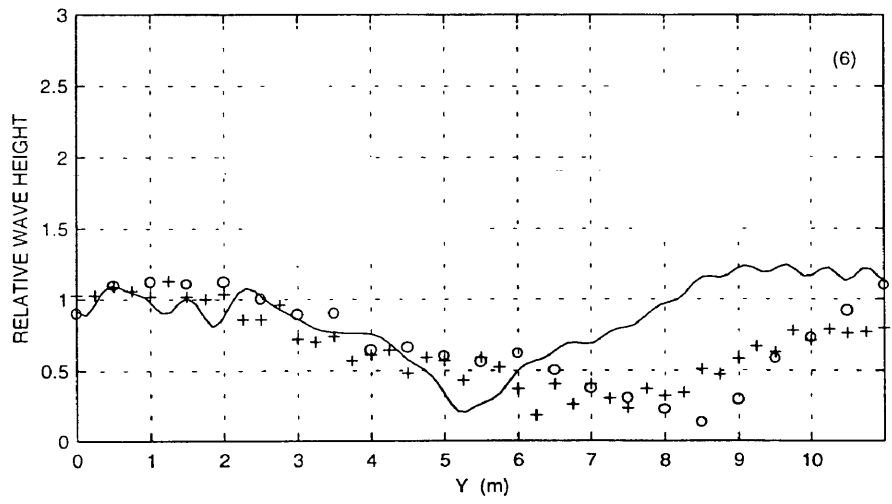
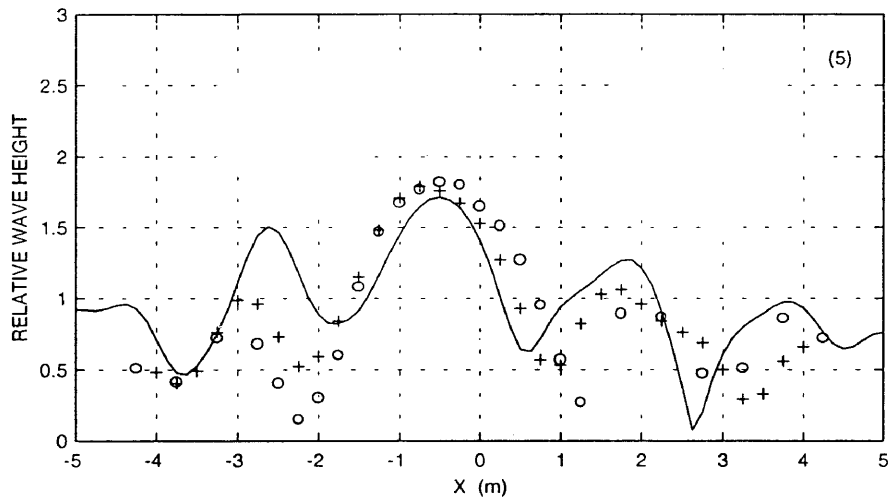
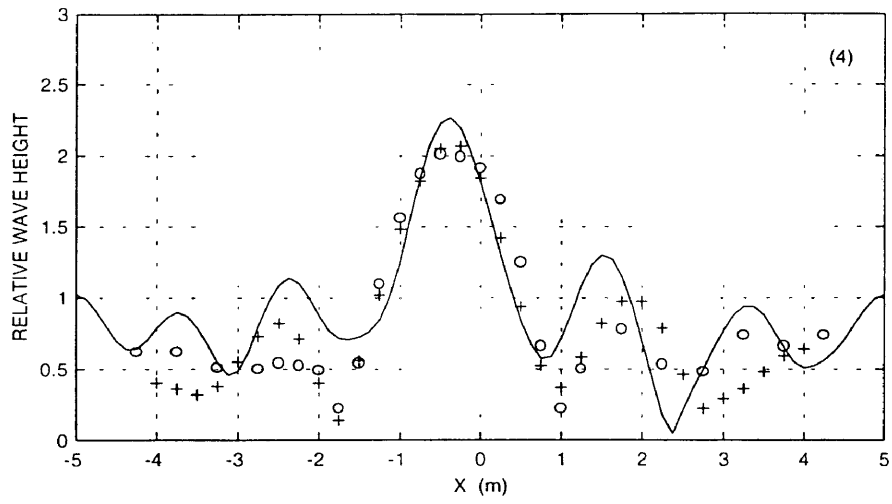


Fig.5.6: Calculated contours of the relative wave height after an elliptic shoal.





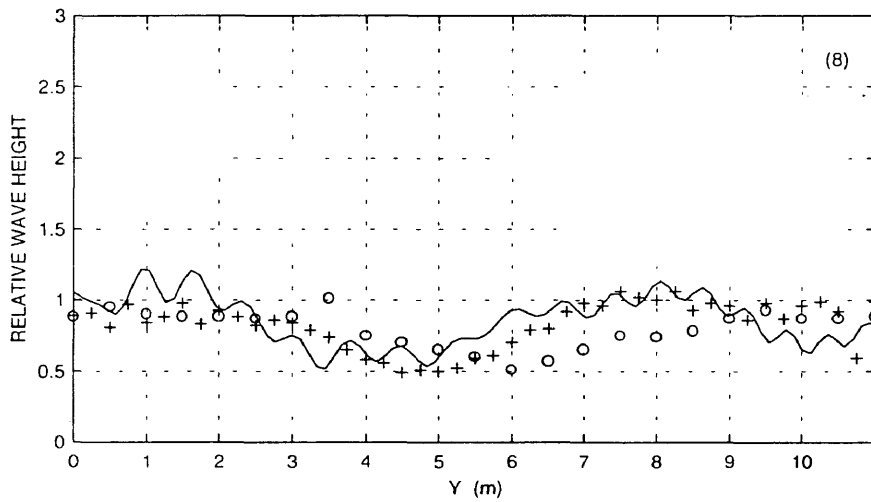
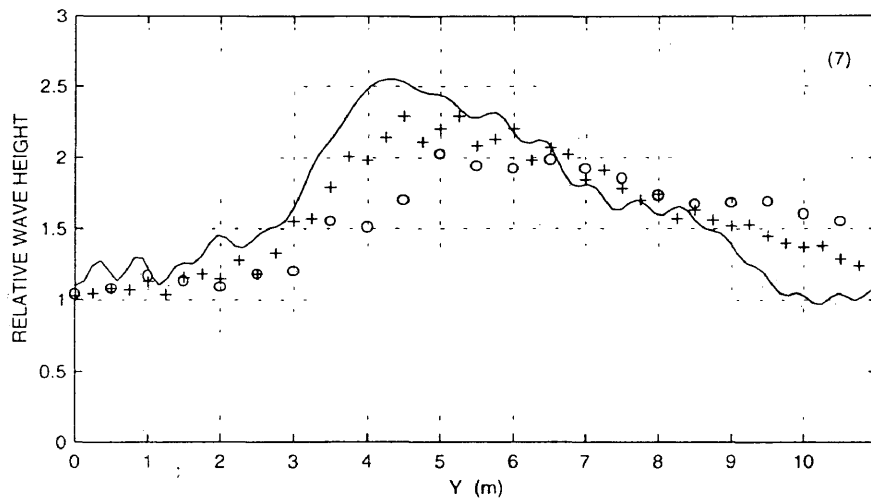


Fig.5.7: Comparisons of the calculated relative wave heights with the laboratory data (after Berkhoff et al,1982) in eight cross sections specified in Fig.5.5. (—) solution from present model, (+) Berkhoff et al.'s finite element model (1982), (o) laboratory measurements.

was not capable of predicting the nonlinear wave breaking phenomenon. At $y=-13\text{m}$, another radiation boundary condition was given, thus, the wave breaking problem was avoided. However, because of this, a small portion of reflected waves, which is generated by the beach from $y=-13\text{m}$ to -15m , was lost in the model results.

Fig.5.6 shows the calculated results of relative wave height (calculated wave height divide by incident wave height) in a domain of $10\text{m} \times 23\text{m}$ defined by the dashed box in Fig.5.5. The maximum relative wave height (2.5) behind the elliptic shoal indicates the area of energy convergence. Another high energy area near the lower-left corner is the result of wave shoal and wave close to breaking.

Fig.5.7 compares the calculated relative wave height profiles with measurements as well as the numerical results from Berkhoff *et al.* (1982) in the eight cross sections specified in Fig.5.5. The circles in Fig.5.7 are the measurements, pluses (+) are the numerical results from the finite element model of Berkhoff *et al.*(1982), and solid curves are from the present model. The agreement between numerical models and the measurements of the relative wave height in all cross sections is reasonably good. But the discrepancy between the numerical results and measurements exists, especially around the peak of the wave height. However, this discrepancy is within the range of contemporary linear wave models (Panchang *et al.*,1991). The nonlinearity of

the wave around the shoal is the main reason of the discrepancy. The inclusion of the nonlinear effects can lead to a better fit (Kirby and Dalrymple, 1984; 1986).

5.2 Model comparison

Using the conjugate gradient method (CGM), Panchang *et al.* (1991) developed an iterative model. The study of model performance was done by solving two problems: (1) the elliptic shoal problem specified by Berkhoff *et al.*'s physical model, and (2) the same problem as (1) except a breakwater half-way across the domain was added at the location $y = -5$ m (see

Table 3. Performance of the CGM model and present model

	layout	number of iteration	tolerance	CPUtime* (min)
CGM model	without breakwater	2,000	0.71×10^{-7}	21.1
CGM model	with breakwater	5,500	0.96×10^{-7}	60
present model	without breakwater	-	-	240
present model	with breakwater	-	-	240

*CPU time for the CGM model was from IBM3090 machines and the CPU time for the present model was from an IBM 486DX 33MHZ 16MB RAM PC.

Fig.5.5). The CGM model runs were made on the IBM3090 machines at the University of Maine and the Cornell Theory Center. The computational domain covered with $220 \times 200 = 44,000$ grid points. The performances of CGM model for bathymetry without and with breakwater are shown in Table 3. It is noticed that the number of iteration of the model increased almost three times because of inserting a simple straight breakwater.

In order to compare the speed of present model with that of the CGM model, present model runs for problem (1) and (2) described above were made on IBM 486DX 33MHZ PC with 16MB RAM at the Virginia Institute of Marine Science. The computational domain was also covered with 44,000 grid points. The performances is also shown in Table 3. It is noticed that the present model speeds of two cases were the same. The reason is that the speed of present model is determined only by the number of unknowns in the computational domain and in both cases the number of unknowns was all 44,000.

Because the two model runs were made on different machine the comparison is indirect. However, based on the comperison of this section and the present model performance shown in previous section, two conclusions were still reached: The first is that the present model speed is acceptable; Another is that unlike the CGM model, the performance of present model does not degrade because of interior structures or irregular exterior boundary.

CHAPTER 6

CONCLUSION AND FURTHER STUDY

6.1 Conclusion

This paper presents the results of a study on the combined wave refraction and diffraction problem, a matrix equation solver, and a numerical model for solving an elliptic wave equation. The major works and conclusions from this study are summarized as follows:

(1) An extended mild slope equation was developed. This equation is different from the Massel's extended equation in the coefficient functions of bottom curvature and second order bottom slope terms. A numerical experiment based on the present extended equation was conducted to show the importance of both bottom curvature and second order bottom slope terms. The results were compared with laboratory data, results from the mild slope equation and Massel's extended mild slope equation. It was found that the inclusion of the bottom curvature term in the classical mild slope equation is reasonable when solving a wave problem in a region with a rapid undulation bottom and the inclusion of the second order bottom slope term is not determined by the mean bottom slope

but rather by the local bottom slope.

(2) A block-wise band matrix solver was developed. It was found that during both forward elimination and back substitution when solving a band matrix equation, a block structure (or sandwich structure) was presented in the band area of the matrix. Using this feature as well as the storage structure of a common computer system, we established the block-wise matrix solver by keeping the 'filling' of the 'sandwich' in the computer memory in which all calculations proceed, and storing the two slices of 'bread' in two hard disk files. In this way, a large band matrix equation can be solved without a huge computer memory requirement.

In computational fluid dynamics, most of the problems are finally discretized to be a large linear system of equations and most of the linear system are band matrix equations. Thus, the block-wise matrix solver presented here can also be used to solve any of these systems.

(3) Based on the principle of the block-wise band matrix solver, a numerical model for solving the mild slope equation was constructed. Panchang et al. (1991) indicated that one disadvantage of the mild slope equation is that until 1991 it could be solved only for small coastal domains and before 1991, the largest wave problem only contained 10,000 grid points. For a square domain this translates to 100 grid points in each direction. Because 10 grid points are required to describe one wave, 10,000 grid points can only describe 10

waves in each direction. The difficulty stems from the exorbitant storage requirement (in fact, the computer memory space requirement) associated with solution of the mild slope equation by direct methods, which, until 1991, were only way to solve a non-diagonally dominant coefficient matrix of a linear system generated from the mild slope equation. In the model of this study, because of using a block-wise band matrix solver, the computer memory space requirement is intensively reduced. Therefore, a wave problem in an area of 44,000 grid points can be solved even on a computer with 16MB memory and 100MB hard disk space.

(4) The indirect comparison of the present model with the CGM model indicates that the speed of the present model is acceptable. The efficiency (or speed) of a model is determined by the number of calculations. The present model has an advantage of solving a problem with complex interior and exterior boundaries by a fixed number of calculations. This is because the model is constructed from a direct method of which the number of calculations is determined by the number of unknowns of a linear system (or the number of grid points in the computational domain). For an iterative method such as CGM and MULTI, the complex interior and exterior boundaries as well as bottom topography may make a tremendous increase of the number of calculations because the number of calculations in an iterative method is determined not only by the number of unknowns but also by the features of the coefficients of the

unknowns and these features are, in fact, determined by complexity of interior and exterior boundaries as well as the bottom topography. For example, if a point (i,j) is in the interior domain, the coefficient of the unknown $\phi_{i,j}$ will be $(dx kc_{i,j})^2 - 2(1+\xi)$ (eq.4.2); if the point is at the positive x directional boundary with a radiation boundary condition, the coefficient of $\phi_{i,j}$ will be $(dxkc_{i,j})^2 - 2(1+\xi) + i2dxk_{i,j}(1 - 1/(k_{i,j}dy)^2)$ (eq.4.13). This change of the coefficient of $\phi_{i,j}$ due to the position of the point in an domain will definitely affect the speed of iterative model. Panchang *et al.* (1991) gave an example showing that inserting a simple straight breakwater into the study domain of Berkhoff *et al.*'s case made the CGM three time slower.

It should be clarified that the present model, CGM model, and MULTI model were all designed to deal with the non-diagonally dominant large matrix equation system, For a diagonally dominant matrix equation system the conventional iteration methods (e.g., Gauss-Seidel method) are very efficient.

6.2 Further study

Although a numerical experiment for the extended mild slope equation derived in this study demonstrated the importance of the two additional terms, the discrepancies of the result from present equation and that from Massel's equation were also shown. The reason of the discrepancies is

not clear. For further study, other case runs are necessary to clarify the reason and find which is more effective.

During derivation of the present extended mild slope equation, the high order terms in the Taylor series of the two dimensional equation were ignored, When solving a case of a wave traveling over a trench or a turning basin, these terms representing non-propagating waves may play an important role in describing the energy trapped in the complex bottom. Thus, it is interesting to pursue further study on these high order terms, because the understanding of the wave energy trapped in the complex bottom will benefit the study of sediment transport and coastal structure design.

The present finite difference model was constructed to solve the Helmholtz equation (eq.4.1) in which the pseudo wave number was specified as $k_c^2 = k^2 - \nabla^2(C \cdot C_g)^{0.5} / (C \cdot C_g)^{0.5}$. However, if we use Kirby and Dalrymple's surf zone wave equation (Kirby and Dalrymple, 1985), which also can be transferred into a Helmholtz equation, we will be able to simulate the wave transformation in the surf zone. In fact, the only difference between the surf zone Helmholtz equation and the non-surf zone Helmholtz equation (present model) is the pseudo wave numbers. There is an additional term, which accounts for a dissipation due to a turbulent bottom boundary in the surf zone pseudo wave number (Kirby and Dalrymple, 1985). Therefore, the surf zone wave model can be easily built.

Further study on how to establish a model that could

determine the wave breaking line first and then solve the non-surf zone and surf zone wave equation, respectively is needed. It is possible to implement this model based on the present model. The idea (Yu *et al.*,1992) is: first to find the wave breaking line by running the present non-surf zone model in a whole computational domain and using the criteria of wave breaking to locate each wave breaking point; second to construct the boundary between the surf zone and non-surf zone; and third to run two models, a surf zone model and non-surf zone model to obtain the final solution.

APPENDIX

THE SECOND ORDER FINITE DIFFERENCE APPROXIMATIONS OF BOUNDARY CONDITIONS AT THE FOUR BOUNDARY CORNERS

A.1 Boundary conditions at a corner formed by the boundaries ∂B_{x-} and ∂B_{y-}

Second order finite difference approximations of boundary conditions at the corner point (i, j) , formed by the boundaries ∂B_{x-} and ∂B_{y-} (Fig.A.1a), are as follows:

If each of ∂B_{x-} and ∂B_{y-} has a Dirichlet boundary conditions, inserting eq.4.5 and eq.4.7 into eq.4.2 gives the corner boundary condition as

$$(dx^2 k_{c_{i,j}}^2 - 2 - 2\xi) \phi_{i,j} + \xi \phi_{i,j+1} + \phi_{i+1,j} = -c_{x-} - \xi c_{y-} \quad (\text{A.1a})$$

where c_{x-} and c_{y-} can be calculated from eq.4.4b.

if ∂B_{x-} has a Dirichlet boundary condition and ∂B_{y-} has a partial absorption boundary condition, using eq.4.2 and eq.4.17, we can eliminate the $\phi_{i,j-1}$ and then with eq.4.5 obtain the following finite difference equation:

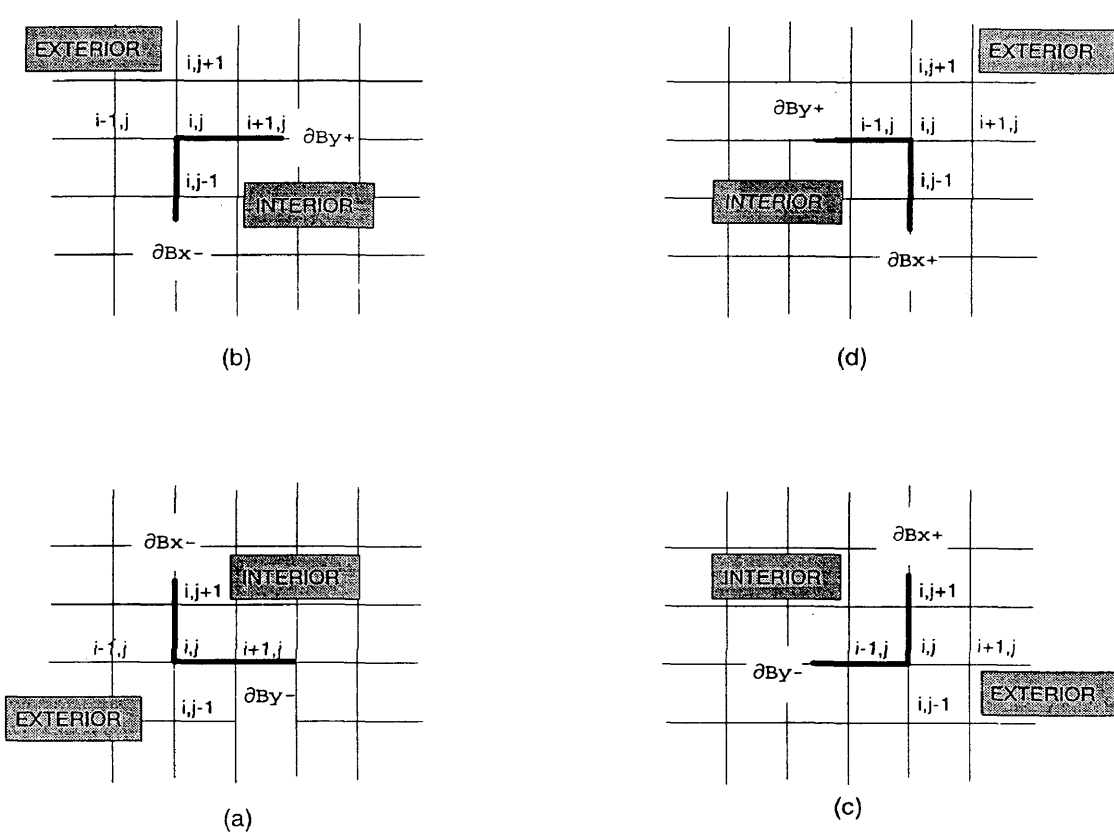


Fig.A.1: Schetch of the four corner boundaries. a. is for the corner formed by boundaries $\partial Bx-$ and $\partial By-$; b. is for the corner formed by boundaries $\partial Bx-$ and $\partial By+$; c. is for the corner formed by boundaries $\partial Bx+$ and $\partial By-$; and d. is for the corner formed by boundaries $\partial Bx+$ and $\partial By+$.

$$\begin{aligned} & \left((dxk_{c_{i,j}})^2 - 2(1+\xi) + \xi i 2 dy \rho k_{i,j} \left(1 - \frac{1}{(k_{i,j} dx)^2}\right) \right) \phi_{i,j} \\ & + 2\xi \phi_{i,j+1} + \left(1 + \frac{\rho i}{k_{i,j} dy}\right) \phi_{i+1,j} = - \left(1 + \frac{\rho i}{k_{i,j} dy}\right) c_{x-} \end{aligned} \quad (\text{A.1b})$$

if ∂B_{x-} has a partial absorption boundary condition and ∂B_{y-} has a Dirichlet boundary condition, using eq.4.2 and eq.4.15, we can eliminate the $\phi_{i-1,j}$ and then with eq.4.7 obtain the following finite difference equation:

$$\begin{aligned} & \left((dxk_{c_{i,j}})^2 - 2(1+\xi) + i 2 dx \gamma k_{i,j} \left(1 - \frac{1}{(k_{i,j} dy)^2}\right) \right) \phi_{i,j} \\ & + \xi \left(1 + \frac{\gamma i}{k_{i,j} dx}\right) \phi_{i,j+1} + 2\phi_{i+1,j} = -\xi \left(1 + \frac{\gamma i}{k_{i,j} dx}\right) c_{y-} \end{aligned} \quad (\text{A.1c})$$

if each of ∂B_{x-} and ∂B_{y-} has a partial absorption boundary condition, using eq.4.2, eq.4.17, and eq.4.15, we can eliminate the $\phi_{i-1,j}$ and $\phi_{i,j-1}$ and then obtain the following finite difference equation:

$$\begin{aligned} & \left[\frac{(dxk_{c_{i,j}})^2 - 2(1+\xi) + \xi \frac{i 2 dy \rho k_{i,j} \left(1 - \frac{1}{(k_{i,j} dx)^2}\right) - \gamma \rho \frac{2 dy}{dx} \left(1 - \frac{1}{(k_{i,j} dy)^2}\right)}{1 + \frac{\gamma \rho}{k_{i,j}^2 dx dy}} \right] \phi_{i,j+} \\ & \left[\frac{i 2 dx \gamma k_{i,j} \left(1 - \frac{1}{(k_{i,j} dy)^2}\right) - \gamma \rho \frac{2 dx}{dy} \left(1 - \frac{1}{(k_{i,j} dx)^2}\right)}{1 + \frac{\gamma \rho}{k_{i,j}^2 dx dy}} \right] \phi_{i,j+} \\ & \left[2\xi \frac{1 + \frac{\gamma i}{k_{i,j} dx}}{1 + \frac{\gamma \rho}{k_{i,j}^2 dx dy}} \right] \phi_{i,j+1} + \left[2 \frac{1 + \frac{\rho i}{k_{i,j} dy}}{1 + \frac{\gamma \rho}{k_{i,j}^2 dx dy}} \right] \phi_{i+1,j} = 0 \end{aligned} \quad (\text{A.1d})$$

**A.2 Boundary conditions at a corner formed by
the boundaries ∂B_{x^-} and ∂B_{y^+}**

Second order finite difference approximations of boundary conditions at the corner point (i, j) , formed by the boundaries ∂B_{x^-} and ∂B_{y^+} (Fig.A.1b), are as follows:

If each of ∂B_{x^-} and ∂B_{y^+} has a Dirichlet boundary conditions, inserting eq.4.5 and eq.4.6 into eq.4.2 gives the corner boundary condition as

$$\xi\phi_{i,j-1} + (dx^2 k_{c_{i,j}}^2 - 2 - 2\xi)\phi_{i,j} + \phi_{i+1,j} = -c_{x^-} - \xi c_{y^+} \quad (\text{A.2a})$$

where c_{x^-} and c_{y^+} can be calculated from eq.4.4b.

if ∂B_{x^-} has a Dirichlet boundary condition and ∂B_{y^+} has a partial absorption boundary condition, using eq.4.2 and eq.4.16, we can eliminate the $\phi_{i,j+1}$ and then with eq.4.5 obtain the following finite difference equation:

$$2\xi\phi_{i,j-1} + \left((dx k_{c_{i,j}})^2 - 2(1+\xi) + \xi i 2 dy \beta k_{i,j} \left(1 - \frac{1}{(k_{i,j} dx)^2} \right) \right) \phi_{i,j} + \left(1 + \frac{\beta i}{k_{i,j} dy} \right) \phi_{i+1,j} = - \left(1 + \frac{\beta i}{k_{i,j} dy} \right) c_{x^-} \quad (\text{A.2b})$$

if ∂B_{x^-} has a partial absorption boundary condition and ∂B_{y^+} has a Dirichlet boundary condition, using eq.4.2 and eq.4.15, we can eliminate the $\phi_{i-1,j}$ and then with eq.4.6 obtain the following finite difference equation:

$$\begin{aligned} \xi \left(1 + \frac{\gamma i}{k_{i,j} dx} \right) \phi_{i,j-1} + \left((dx k_{c_{i,j}})^2 - 2(1+\xi) + i 2 dx \gamma k_{i,j} \left(1 - \frac{1}{(k_{i,j} dy)^2} \right) \right) \phi_{i,j} \\ + 2 \phi_{i+1,j} = -\xi \left(1 + \frac{\gamma i}{k_{i,j} dx} \right) c_{y+} \end{aligned} \quad (\text{A.2c})$$

if each of ∂B_{x-} and ∂B_{y+} has a partial absorption boundary condition, using eq.4.2, eq.4.15, and eq.4.16, we can eliminate the $\phi_{i-1,j}$ and $\phi_{i,j+1}$ and then obtain the following finite difference equation:

$$\begin{aligned} \left[2\xi \frac{1 + \frac{\gamma i}{k_{i,j} dx}}{1 + \frac{\gamma \beta}{k_{i,j}^2 dx dy}} \right] \phi_{i,j-1} \\ \left[\frac{(dx k_{c_{i,j}})^2 - 2(1+\xi) + \xi \frac{i 2 dy \beta k_{i,j} \left(1 - \frac{1}{(k_{i,j} dx)^2} \right) - \gamma \beta \frac{2 dy}{dx} \left(1 - \frac{1}{(k_{i,j} dy)^2} \right)}{1 + \frac{\gamma \beta}{k_{i,j}^2 dx dy}} \right] \phi_{i,j+} \\ \left[\frac{i 2 dx \gamma k_{i,j} \left(1 - \frac{1}{(k_{i,j} dy)^2} \right) - \gamma \beta \frac{2 dx}{dy} \left(1 - \frac{1}{(k_{i,j} dx)^2} \right)}{1 + \frac{\gamma \beta}{k_{i,j}^2 dx dy}} \right] \phi_{i,j+} \\ \left[2 \frac{1 + \frac{\beta i}{k_{i,j} dy}}{1 + \frac{\gamma \beta}{k_{i,j}^2 dx dy}} \right] \phi_{i+1,j} = 0 \end{aligned} \quad (\text{A.2d})$$

A.3 Boundary conditions at a corner formed by the boundaries ∂B_{x+} and ∂B_{y-}

Second order finite difference approximations of boundary conditions at the corner point (i,j) , formed by the boundaries

∂B_{x-} and ∂B_{y-} (Fig.A.1c), are as follows:

If each of ∂B_{x+} and ∂B_{y-} has a Dirichlet boundary conditions, inserting eq.4.4a and eq.4.7 into eq.4.2 gives the corner boundary conditon as

$$\phi_{i-1,j} + (dx^2 k_{i,j}^2 - 2 - 2\xi) \phi_{i,j} + \xi \phi_{i,j+1} = -c_{x+} - \xi c_{y-} \quad (\text{A.3a})$$

where c_{x+} and c_{y-} can be calculated from eq.4.4b.

if ∂B_{x+} has a Dirichlet boundary condtion and ∂B_{y-} has a partial absorpction boundary condition, using eq.4.2 and eq.4.17, we can eliminate the $\phi_{i,j-1}$ and then with eq.4.4a obtain the following finite difference equation:

$$\begin{aligned} & \left(1 + \frac{\rho i}{k_{i,j} dy}\right) \phi_{i-1,j} + \\ & \left((dx k_{i,j})^2 - 2(1+\xi) + \xi i 2 dy \rho k_{i,j} \left(1 - \frac{1}{(k_{i,j} dx)^2}\right) \right) \phi_{i,j} \\ & + 2\xi \phi_{i,j+1} = - \left(1 + \frac{\rho i}{k_{i,j} dy}\right) c_{x+} \end{aligned} \quad (\text{A.3b})$$

if ∂B_{x+} has a partial absorpction boundary condition and ∂B_{y-} has a Dirichlet boundary condtion, using eq.4.2 and eq.4.13, we can eliminate the $\phi_{i+1,j}$ and then with eq.4.7 obtain the following finite difference equation:

$$\begin{aligned} & 2\phi_{i-1,j} + \left((dx k_{i,j})^2 - 2(1+\xi) + i 2 dx \alpha k_{i,j} \left(1 - \frac{1}{(k_{i,j} dy)^2}\right) \right) \phi_{i,j} \\ & + \xi \left(1 + \frac{\alpha i}{k_{i,j} dx}\right) \phi_{i,j+1} = -\xi \left(1 + \frac{\alpha i}{k_{i,j} dx}\right) c_{y-} \end{aligned} \quad (\text{A.3c})$$

if each of ∂B_{x+} and ∂B_{y-} has a partial absorption boundary condition, using eq.4.2, eq.4.13, and eq.4.17, we can eliminate the $\phi_{i+1,j}$ and $\phi_{i,j-1}$ and then obtain the following finite difference equation:

$$\begin{aligned}
 & \left[2 \frac{1 + \frac{\rho i}{k_{i,j} dy}}{1 + \frac{\alpha \rho}{k_{i,j}^2 dx dy}} \right] \phi_{i-1,j^+} \\
 & \left[\frac{(dx k_{c_{i,j}})^2 - 2(1+\xi) + \xi \frac{i 2 dy \rho k_{i,j} \left(1 - \frac{1}{(k_{i,j} dx)^2}\right) - \alpha \rho \frac{2 dy}{dx} \left(1 - \frac{1}{(k_{i,j} dy)^2}\right)}{1 + \frac{\alpha \rho}{k_{i,j}^2 dx dy}} \right] \phi_{i,j^+} \\
 & \left[\frac{i 2 dx \alpha k_{i,j} \left(1 - \frac{1}{(k_{i,j} dy)^2}\right) - \alpha \rho \frac{2 dx}{dy} \left(1 - \frac{1}{(k_{i,j} dx)^2}\right)}{1 + \frac{\alpha \rho}{k_{i,j}^2 dx dy}} \right] \phi_{i,j^+} \\
 & \left[2 \xi \frac{1 + \frac{\alpha i}{k_{i,j} dx}}{1 + \frac{\alpha \rho}{k_{i,j}^2 dx dy}} \right] \phi_{i,j+1} = 0
 \end{aligned} \tag{A.3d}$$

A.4 Boundary conditions at a corner formed by the boundaries ∂B_{x+} and ∂B_{y+}

Second order finite difference approximations of boundary conditions at the corner point (i,j) , formed by the boundaries ∂B_{x-} and ∂B_{y+} (Fig.A.1d), are as follows:

If each of ∂B_{x+} and ∂B_{y+} has a Dirichlet boundary conditions, inserting eq.4.4a and eq.4.6 into eq.4.2 gives the corner boundary condition as

$$\phi_{i-1,j} + \xi \phi_{i,j-1} + (dx^2 k_{c_{i,j}}^2 - 2 - 2\xi) \phi_{i,j} = -c_{x^+} - \xi c_{y^+} \quad (\text{A.4a})$$

where c_{x^+} and c_{y^-} can be calculated from eq.4.4b.

if ∂B_{x^+} has a Dirichlet boundary condition and ∂B_{y^+} has a partial absorption boundary condition, using eq.4.2 and eq.4.16, we can eliminate the $\phi_{i,j+1}$ and then with eq.4.4a obtain the following finite difference equation:

$$\begin{aligned} & \left(1 + \frac{\beta i}{k_{i,j} dy}\right) \phi_{i-1,j} + 2\xi \phi_{i,j-1} + \\ & \left((dx k_{c_{i,j}})^2 - 2(1+\xi) + \xi i 2 dy \beta k_{i,j} \left(1 - \frac{1}{(k_{i,j} dx)^2}\right) \right) \phi_{i,j} \\ & = - \left(1 + \frac{\beta i}{k_{i,j} dy}\right) c_{x^+} \end{aligned} \quad (\text{A.4b})$$

if ∂B_{x^+} has a partial absorption boundary condition and ∂B_{y^+} has a Dirichlet boundary condition, using eq.4.2 and eq.4.13, we can eliminate the $\phi_{i+1,j}$ and then with eq.4.6 obtain the following finite difference equation:

$$\begin{aligned} & 2\phi_{i-1,j} + \xi \left(1 + \frac{\alpha i}{k_{i,j} dx}\right) \phi_{i,j-1} + \\ & \left((dx k_{c_{i,j}})^2 - 2(1+\xi) + i 2 dx \alpha k_{i,j} \left(1 - \frac{1}{(k_{i,j} dy)^2}\right) \right) \phi_{i,j} \\ & = -\xi \left(1 + \frac{\alpha i}{k_{i,j} dx}\right) c_{y^+} \end{aligned} \quad (\text{A.4c})$$

if each of ∂B_{x^+} and ∂B_{y^+} has a partial absorption boundary condition, using eq.4.2, eq.4.13, and eq.4.16, we can eliminate the $\phi_{i+1,j}$ and $\phi_{i,j+1}$ and then obtain the following

finite difference equation:

$$\begin{aligned}
 & \left[\frac{1 + \frac{\beta i}{k_{i,j} dy}}{1 + \frac{\alpha \beta}{k_{i,j}^2 dx dy}} \right] \phi_{i-1,j} + \left[\frac{1 + \frac{\alpha i}{k_{i,j} dx}}{1 + \frac{\alpha \beta}{k_{i,j}^2 dx dy}} \right] \phi_{i,j-1} \\
 & \left[\frac{(dx k_{c_{i,j}})^2 - 2(1+\xi) + \xi}{1 + \frac{\alpha \beta}{k_{i,j}^2 dx dy}} \frac{i 2 dy \beta k_{i,j} \left(1 - \frac{1}{(k_{i,j} dx)^2}\right) - \alpha \beta \frac{2 dy}{dx} \left(1 - \frac{1}{(k_{i,j} dy)^2}\right)}{1 + \frac{\alpha \beta}{k_{i,j}^2 dx dy}} \right] \phi_{i,j} \\
 & \left[\frac{i 2 dx \alpha k_{i,j} \left(1 - \frac{1}{(k_{i,j} dy)^2}\right) - \alpha \beta \frac{2 dx}{dy} \left(1 - \frac{1}{(k_{i,j} dx)^2}\right)}{1 + \frac{\alpha \beta}{k_{i,j}^2 dx dy}} \right] \phi_{i,j} = 0 \tag{A.4d}
 \end{aligned}$$

LIST OF REFERENCES

- Behrendt, L., 1985. A finite element Model for water wave diffraction including boundary absorption and bottom friction. Series Paper 37, Institute of Hydrodynamic and Hydraulic Engineering, Tech. University of Denmark.
- Berkhoff, J.C.W., 1972. Computation of combined refraction-diffraction. Proc. 13th Coastal Eng. Conf., ASCE., Vancouver, Canada.
- Berkhoff, J.C.W., 1976. Mathematical models for simple harmonic linear water waves, wave diffraction and refraction. Publication 163, Delf Hydraulics Laboratory.
- Berkhoff, J.C.W., Booij, N. and Radder, A.C., 1982. Verification of numerical wave propagation models for simple harmonic water waves. Coastal Eng.. 6: 255-279.
- Booij, N., 1983. A note on the accuracy of the mild-slope equation. Coastal Eng., 7: 191-203.
- Chen, H.S. and Mei, C.C., 1974. Oscillation and wave forces in an offshore harbor. Rep: 190, Ralphm Parsons Lab. for Water Resource and Hydrodynamics, MIT.
- Copeland, G.J.M., 1985. A practical alternative to the "mild-slope" wave equation. Coastal Eng., 9: 125-149.
- Davies, A.G. and Heathershaw, A. D., 1984. Surface-wave propagation over sinusoidally varying topography. J. Fluid

- Mech., 192:33-50.
- Dongarra, J.J., Bunch, J.R., Moler, C.B. and Stewart, G.W., 1979, Linpack Users Guide, SIAM.
- Duff, I.S., Erisman, A.M. and Reid, J.K., 1986, Direct Methods for Sparse Matrices, Oxford University Press.
- Goda, Y., Yoshimura, T. and Ito, M., 1971. Reflection and diffraction of water wave by an insular breakwater. Report of the Port and Harbor Research Institute, 10(2):4-51.
- George, A. and Liu, J.W.H., 1981, Computer Solution of Large Sparse Positive Definite system, Prentice-Hall, Englewood Cliffs, N.J..
- Hager, W.W., 1988, Applied Numerical Linear Algebra, Prentice-Hall, Englewood Cliffs, N.J..
- Johnson, J.W., 1953. Engineering aspects of diffraction and refraction. Transactions of the American Society of Civil Engineers, 118(2556):617-652.
- Kirby, J.T. and Dalrymple, R.A., 1984. Verification of a parabolic equation for propagation of weakly-nonlinear waves. Coastal Eng., 8:219-232.
- Kirby, J.T. and Dalrymple, R.A., 1985. Modeling waves in surfzones and around island. J. Waterway, Port, Coastal and Ocean, Engng., 112(1):78-93.
- Kirby, J.T., 1986a. A general wave equation for waves over rippled beds. J. Fluid Mech., 162:171-186.
- Kirby, T.J., 1986b. Higher-order approximation in the parabolic equation method for water waves, J. Geophys. Res., 91(C1):

933-952.

- Kirby, J.T. and Dalrymple, R.A., 1986. An approximate model for nonlinear dispersion in monochromatic wave propagation models, *Coastal Eng.*, 9:545-561.
- Kirby, J.T., 1989. A note on parabolic radiation boundary conditions for elliptic wave calculations. *Coastal Eng.*, 13:211-218.
- Li, B. and Anastasiou, K., 1992. Efficient elliptic solvers for mild-slope equation using the multigrid technique. *Coastal Eng.*, 16: 245-266.
- Li, B., 1994. A generalized conjugate gradient model for mild slope equation. *Coastal Eng.*, 23: 215-225.
- Lie, V. and Tøtøm, A., 1991. Ocean wave over shoals. *Coastal Eng.*, 15: 545-562.
- Liu, P.L.-F. and Tsay T.-K. 1983. On weak reflection of water waves. *J. Fluid Mech.*, 131: 59-71.
- Madsen, P.R. and Larsen, J., 1987. An efficient finite-difference approach to the mild-slope equation. *Coastal Eng.*, 11: 329-351.
- Marschall, R.A., 1993. Aspects of the numerical solution of the Helmholtz equation. Ph.D. Dissertation of The University of Tennessee.
- Massel, S.R., 1993. Extended refraction and diffraction equation for surface waves. *Coastal Eng.*, 19:97-126.
- Mei, C.C., 1985. Resonant reflection of surface waves by periodic sandbars. *J. Fluid Mech.*, 152: 315-335.

- Panchang, V., Pearce, B.R. and Ge, W., 1991. Solution of the mild-slope wave equation by iteration. *Applied Ocean Research*, 13(4): 187-199
- Radder, A.C., 1979. On the parabolic equation method for water-wave propagation, *J. Fluid Mech.* 95, 159-176
- Schiesser, W.E., 1991, *The Numerical Method of Lines: Integration of Partial Differential Equations*, San Diego, Academic Press.
- Smith, G.D., 1985, *Numerical Solution of Partial Differential Equations: Finite Difference Methods*, Oxford, Oxford University Press.
- Sommerfeld, A., 1896. *Mathematische theorie der diffraction.* *Math. Ann.*, 47: 317-374.
- Tsay, T.-K. and Liu, P.L.-F., 1982. Numerical solution of waterwave refraction and diffraction problems in the parabolic approximation. *J. Geophys. Res.*, 87:7932-7940.
- Yu, X., Isobe, M., and Watanebe, A., 1992. *Coastal Eng. in Japan*, 35(1): 21-33.
- Shore Protection Manual, U.S. Army, Coastal engineering Research center. 1977, Vol.1.

VITA

Born in 1962, Changqing Li wasted no time in earning a Bachelor of Science in Physical Oceanography and Marine Meteorology in 1984 from the Shandong College of Oceanography (now Ocean University of Qingdao). He received a Master of Science in Atmospheric Physics in 1987 from the Institute of Atmospheric Physics of Academia Sinica of China. From 1987 to 1990, he spent four years in teaching and research in the University of Science and Technology of China. In 1991, he entered the College of William and Mary, School of Marine Science as a graduate student.